



UNIVERSITY OF
LEICESTER

**DEVELOPMENT OF MOLECULARLY IMPRINTED
POLYMER NANOPARTICLES BASED ASSAY AND
SENSOR FOR FUMONISIN B1**

Thesis submitted for degree of

Master of Philosophy

At the University of Leicester

By

Hasim Munawar

Department of Chemistry

University of Leicester

2018

ABSTRACT

Fumonisin B1 (FB1) is categorised as a human and animal carcinogen produced by *Fusarium* moulds which occur mainly in corn, wheat and other cereals. For decades, immunoassay (ELISA) has been developed as the reference established method for FB1 determination in food and animal feed. Unfortunately, the current assays are inefficient due to factors such as temperature instability of the antibody (recognition element) and enzyme elements in the immunoassay, the presence of natural inhibitors in the samples tested and high levels of non-specific protein binding. Other important factors are the time when results are needed rapidly and the cost of use. This work aims to develop an assay and sensor for FB1 using molecularly imprinted polymer nanoparticles (nanoMIPs) to overcome these limitations.

Firstly, computational modelling was used to identify the best functional monomers that form a complex with FB1. These results were verified by solid phase extraction (SPE) experiments. Ethylene glycol methacrylate phosphate (EGMP) was identified as a suitable functional monomer for FB1. The nanoMIPs for FB1 have been synthesised by solid phase synthesis using the composition based on EGMP. From hot water fraction, the nanoMIPs were collected with concentration 0.06 mg mL^{-1} and particle size $249 \pm 29 \text{ nm}$. The image of nanoMIPs for FB1 was taken by TEM. The phosphate (PO_4^{3-}) and carbonyl (C=O) as functional groups of nanoMIPs were identified by FT-IR Spectrometer. The dissociation constant of nanoMIPs is $0.2 \mu\text{M}$ by SPR (Chapter 3).

Development of molecularly imprinted polymer nanoparticle-based assay (MINA) was started by producing complex conjugate based on horseradish peroxidase (HRP). HRP was complexed with FB1 by carbodiimide reaction using EDC and NHS. After optimisation of the concentration of nanoMIPs (0.06 mg mL^{-1}) and HRP-FB1 conjugate (1:400), MINA was capable producing satisfactory detection of FB1 in concentration range $10 \text{ pM} - 10 \text{ nM}$. The selectivity and cross-reactivity have been tested. The response from commercial monoclonal antibody (mAb) and non-specific imprinted polymer nanoparticles (nanoNIPs) have been lower with the same concentration range ($10 \text{ pM} - 10 \text{ nM}$). Also, the interaction between nanoMIPs and other mycotoxins such as aflatoxin B1 (AFB1), citrinin (CTT), deoxynivalenol (DON), fumonisin B2 (FB2), and zearalenone (ZEA) were shown to be negligible. The application of MINA has been tested in real samples. A total of 18 corn samples has been contaminated by fumonisins with a range from $0.02 - 1.29 \text{ ppm}$. From these results, all samples are safe because the concentration is lower than maximum residue limit of fumonisins (2 ppm). All samples have been further analysed for comparative study with a commercial ELISA kit and HPLC. Statistically, t-test has shown that there is significant similarity of the results obtained by MINA and commercial ELISA kit (AgraQuant, Romer Lab) (Chapter 4).

Development of a molecularly imprinted nanoparticle-based electrochemical sensor (MINES) was fabricated with two types, ferrocyanide-ferricyanide ($[\text{Fe}(\text{CN})_6]^{4-/3-}$) labelled MINES and label free MINES. To gain this technology, the platinum working electrode was electropolymerised by a Zinc(II)porphyrin (ZnP) and pyrrole (Pyr) and immobilised by nanoMIPs using carbodiimide chemicals. The final electrode is nanoMIPs/ZnP/Pyr/Pt. The electrode was tested by differential pulse voltammetry (DPV) using $[\text{Fe}(\text{CN})_6]^{4-/3-}$ for generating the label based MINES and by electrochemical

impedance sensor (EIS) for producing label free MINES. In concentration range of FB1 at 1fM to 10 pM, the linearity and limit detection from EIS ($R^2 = 0.98$, LoD = 0.7 fM) and DPV ($R^2 = 0.96$, LoD = 0.03 fM) show the excellent performance of both methods. The EIS (0.442 k Ω /M) is two times more sensitive than DPV (0.281 μ A/M) (Chapter 5).

In conclusion, the nanoMIPs based assay (MINA) and electrochemical sensor (MINES) are a very promising method for the detection of FB1 in food and animal feed at very low concentrations with no cross-reactivity offering a fast, cost-effective and reliable technique.

Keywords; Fumonisin B1, nanoMIPs, MINA, MINES

ACKNOWLEDGMENT

Firstly, I would like to express my sincere gratitude to my supervisor Prof Sergey A Piletsky and Dr Kal Karim for the continuous support of my MPhil study and related research, for their patience, motivation, and immense knowledge. Also, for sharing their life story and achievement.

Besides that, I would like to thank my examiners, Prof Karl Ryder and Dr Andrew Hall, for their time and efforts for reviewing this thesis.

My sincere thanks also go to Dr Katarzyna Smolinska-Kempton and Dr Alvaro Garcia Cruz for sharing knowledge and discussing troubleshooting during the experiment.

I would also like to thank the collaborators; Prof Wlodzimierz Kutner (ICHF, Poland), Dr Michelangelo Pascale and Dr Annalisa De Girolamo (CNR-ISPA-Italy), Dr Abeer HM Safaryan (Al-Mustansiriyah University, Iraq), Dr Pedro Marote (Université Claude Bernard Lyon, France), Dr Francesco Canfarotta (MIP diagnostic, UK), and Dr Elena Piletska (University of Leicester, UK).

I thank my fellow lab mates for all the fun, discussion, food sharing, and help (Adam, Anca, Antonio, Asma, Bashar, Eman, Fabiana, Javier, Joanna, Julie, Kaseb, Michael, Omar, Thomas, and Todd).

A very special gratitude goes out to IAARD-Ministry of Agriculture, Republic Indonesia for helping and providing the funding for the work. The director of IRCVS (Dr. Drh Hardiman, MM and Dr. Drh. NLP Indi Dharmayanti, M.Si) and head of Toxicology group (Dr. Raphaella Widiastuti) for agreement correspondence. Also thanks for all toxicology's staff and a student group in UK who gets funding from IAARD (April, Ireng, Syahrizal, Luna, Nia, Sandi, Syaiful, Taupik, Vyta) for motivation and fun meeting.

Thanks also to Nawaazers and all Indonesian student in Leicester.

Finally, I must express my very profound gratitude to my parents (Ibu Maemunah dan Bapak Undang Hasim), wife and son (Tania and Haaziq), sisters and a brother (Diah, Ade, Sholehudin) and big family and friends for providing me with unfailing support and continuous encouragement throughout my study and through the process of researching and writing this thesis. This accomplishment would not have been possible without them.

Hasim Munawar

THE LIST OF CONTENT

Abstract.....	i
Acknowledgment	iii
The list of Content	iv
The list of Tables	vii
The list of Figures	viii
The list of Equations	xiii
The list of Abbreviations	xiv
Chapter 1 Introduction	1
1.1 Background	1
1.2 Justification	2
1.3 The aims and objectives of the research	5
Chapter 2 Literature Review	7
2.1 Fumonisin B1	7
2.1.1 Resources, structure, and nomenclature	7
2.1.2 Several experimental studies about the effect of FB1	8
2.1.3 The Toxicity Mechanism of FB1	11
2.2 Molecularly Imprinted Polymers	12
2.2.1 Imprinting Approach	14
2.2.2 Composition	18
2.2.3 Polymerisation	29
Chapter 3 Development of molecularly imprinted polymer nanoparticles for Fumonisin B1	31
3.1 Introduction	31
3.2 Materials and Methods	33
3.2.1 Materials	33
3.2.2 Equipment.....	34
3.2.3 Computational design	34
3.2.4 Testing of polymer binding	35
3.2.5 Synthesis of nanoMIPs for FB1	35
3.2.6 Characterisation of nanoMIPs imprinted with FB1.....	36
3.3 Results and Discussion.....	38

3.3.1	Modelling - minimisation of the energy of FB1	38
3.3.2	Binding energy between FB1 and functional monomers	40
3.3.3	Binding analysis	43
3.3.4	Synthesis and characterisation of nanoMIPs	43
3.4	Conclusion.....	48
Chapter 4 Development of molecularly imprinted polymer nanoparticles-based assay for Fumonisin B1 and its application in corns		
49		
4.1	Introduction	49
4.2	Materials and Methods	51
4.2.1	Materials and Equipment.....	51
4.2.2	Preparation of HRP-FB1	51
4.2.3	Optimisation of HRP-FB1 and nanoMIPs concentration.....	52
4.2.4	Competitive assay.....	52
4.2.5	MINA selectivity and cross-reactivity.....	53
4.2.6	Sample preparation	53
4.2.7	Sample analysis	53
4.2.8	Sample preparation and analysis by commercial kit ELISA.....	54
4.2.9	Sample preparation and analysis by HPLC	54
4.3	Results and discussion.....	54
4.3.1	Optimisation of HRP-FB1 conjugate and nanoMIPs concentration	54
4.3.2	Study of HRP interaction.....	57
4.3.3	MINA calibration curve and its comparison with monoclonal antibody	60
4.3.4	MINA cross-reactivity.....	62
4.3.5	Analyte recovery and limit of detection	64
4.3.6	Sample analysis and comparative study with commercial kit ELISA and HPLC	65
4.4	Conclusion.....	67
Chapter 5 Development of an electrochemical sensor for fumonisin B1 determination based on molecularly imprinted polymer nanoparticles		
68		
5.1	Introduction	68
5.2	Materials and Methods	70
5.2.1	Materials	70
5.2.2	NanoMIPs based sensor fabrication for FB1.....	70
5.2.3	Characterisation of ZnP/Pyr polymer.....	71

5.2.4	Development of labelled sensor using differential pulse voltammetry (DPV)	72
5.2.5	Development of a free label sensor using electrochemical impedance spectroscopy (EIS).....	72
5.3	Results and discussion.....	73
5.3.1	The electropolymerisation of ZnP/Pyr	73
5.3.2	Immobilisation of nanoMIPs on ZnP/Pyr/Pt electrode	75
5.3.3	Determination of FB1 using MINES.....	76
5.4	Conclusion.....	81
Chapter 6	General conclusion and future work.....	83
6.1	Conclusions	83
6.2	Future work	84
	References.....	85
	APPENDIX 1: Publication in support of this thesis	98
	APPENDIX 2 calibration curve for nanoMIPs.....	99

THE LIST OF TABLES

Table 1-1. Distribution of Fumonisin B1 in Indonesia's corn 1990-2017.....	2
Table 1-2. The advantages and disadvantages of HPLC, LC-MS/MS and ELISA for determination of FB1 in corn based on several articles.....	4
Table 2-1. Fumonisin analogues.....	7
Table 2-2. Comparison between Covalent and Non-covalent Imprinting Approach.....	16
Table 3-1. The minimised potential energy of FB1 structure in vacuum and water by molecular mechanics.....	38
Table 3-2. The binding energies of complexes between the monomers and FB1 minimised in water.....	41
Table 3-3 Filtration of Fumonisin B1 in standard polymer-based SPE.....	43
Table 4-1 The Procedure of MINA for FB1.....	56
Table 4-2. The optimisation of comparison between MINA and other competitive direct ELISA or immunoassays for Fumonisin determination.....	57
Table 4-3 The calibration curve procedure of MINA for FB1.....	59
Table 4-4. MINA response comparison and linear equation values for calibration curves for mycotoxins.....	63
Table 4-4. Comparison between MINA and other FB1 determination techniques.....	64
Table 4-5 Recovery test.....	64
Table 4-6. Comparison of sample preparation and analysis from MINA, ELISA, and HPLC.....	65
Table 5-1. NanoMIPs sensor response comparison and linear equation values for DPV calibration curves for mycotoxins.....	79
Table 5-2. FB1 Impedimetric sensor response for EIS measurements.....	81

THE LIST OF FIGURES

Figure 1-1. The total number of publications reporting the application of HPLC, LC-MSMS and immunoassay/ELISA for analysis of fumonisins in corn in 1991–2017.	3
Figure 2-1. Fumonisin backbone (a) and 3-hydroxypyridinium (3HP) (b).....	7
Figure 2-2. The two-dimension structure of Fumonisin B1 and its ten chiral carbons	8
Figure 2-3. Histopathological change of liver (a), kidney (b), spleen (c), gill (d) and brain (e) of <i>O. niloticus</i> after exposure FB1 for six weeks (adapted from Abu-Hassan <i>et al.</i> , 2016) ⁷¹	9
Figure 2-4. Clinical and pathological change in the serum of (a) 9 months-old filly and (b) 14 months old colt dosed FB1 (adapted from Kellerman <i>et al.</i> , 1990) ⁷³	10
Figure 2-5. Liver from a health pig (a) and a pig identified porcine pulmonary oedema (adapted by Hascheck <i>et al.</i> , 2001) ⁷⁵	11
Figure 2-6. Sphingolipid biosynthesis (adapted from Merrill Jr <i>et al.</i> , 2001) ⁷⁶	11
Figure 2-7. Illustration of FB1 interfere to sphingolipid biosynthesis (adapted from Juvala <i>et al.</i> , 2008) ⁷⁷	12
Figure 2-8. Illustration of covalent imprinting approach on mannose imprinted polymer (adapted from Shen and Ren, 2014) ⁸⁰	14
Figure 2-9. Illustration of non-covalent imprinting approach on atrazine imprinted polymer (adapted from Matsui <i>et al.</i> , 1995) ⁸¹	15
Figure 2-10. Illustration of semi-covalent imprinting approach on the 4-chlorophenol imprinted polymer, a. Template synthesis b. Polymer preparation (adapted from Qi <i>et al.</i> , 2010) ⁸²	17
Figure 2-11. Illustration of metal ion mediated imprinting approach on L-histidine imprinted polymer (adapted from Prasad <i>et al.</i> , 2011) ⁸²	18
Figure 2-12 The structure of Fumonisin B1	19
Figure 2-13. Several functional monomers with different types, acid (a) i : methacrylic acid (MAA), ii: <i>p</i> -vinyl benzoic acid , iii: acrylic acid (AA), iv: itaconic acid, v: 2-(trifluoromethyl)-acrylic acid (TFMAA) vi: acrylamide-(2-methyl)-propane sulfonic acid (AMPSA); base (b) i : 4-vinylpyridine (4-VP), ii: 2-vinylpyridine (2-VP), iii : 4-(5)-vinylimidazole, iv: 1-vinylimidazole, v: allylamine, vi : <i>N,N</i> -diethyl aminoethyl methacrylamide (DEAEM); and neutral (c) i : acrylamide, ii : methacrylamide, iii : 2-hydroxyethyl methacrylate (2-HEMA), iv : trans-3-(3-pyridyl)-acrylic acid (adapted from Cormack & Elorza, 2004) ⁹³	20
Figure 2-14. (a) Selectivity (k'_{NIC}/k'_{BIPY}) for nicotine and bipyridyl by different M/T ratio (b) Binding isotherms of 3H-theophylline binding to imprinted polymers prepared with M : T of 4 : 1, 12 : 1, 100 : 1 and 500 : 1. (adapted from Yilmaz <i>et al.</i> , 1999 and Andersson <i>et al.</i> , 1999) ^{87,94}	22
Figure 2-15. (a) Effect of PETRA concentration on the % swelling values of PEO hydrogels (b) SEM images of freeze-dried PEO hydrogels. (A) PEO-	

	PETRA 1% w/w, (B) PEO-PETRA 2.5% w/w, (C) PEO-PETRA 5% w/w, (D) PEO-PETRA 10% w/w (adapted from Wong <i>et al.</i> , 2015) ⁹⁵	23
Figure 2-16.	Selection of crosslinkers used for molecular imprinting. i: <i>p</i> -divinylbenzene (DVB); ii: 1,3-diisopropenyl benzene (DIP); iii: ethylene glycol dimethacrylate (EGDMA); iv: tetramethylene dimethacrylate (TDMA); v: <i>N,O</i> -bisacryloyl-1-phenylalaninol; vi: 2,6-bisacryloylamidopyridine; vii: 1,4-phenylene diacrylamide; viii: <i>N,N</i> -1,3-phenylenebis(2-methyl-2-propenamamide) (PDBMP); ix: 3,5-bisacrylamido benzoic acid; x: 1,4-diacryloyl piperazine (DAP); xi: <i>N,N</i> -methylene bisacrylamide (MDAA); xii: <i>N,N</i> -ethylene bismethacrylamide; xiii: <i>N,N</i> -tetramethylene bismethacrylamide; xiv: <i>N,N</i> -hexamethylene bismethacrylamide; xv: anhydroerythritol dimethacrylate; xvi: 1,4;3,6-dianhydro-d-sorbitol-2,5-dimethacrylate; xvii: isopropylenebis(1,4-phenylene) dimethacrylate; xviii: trimethylpropane trimethacrylate (TRIM); xix: pentaerythritol triacrylate (PETRA); xx: pentaerythritol tetraacrylate (PETEA) (adapted from Cormack & Elorza, 2004) ⁹³	25
Figure 2-17.	Structure of initiators: i: azobisisobutyronitrile (AIBN); ii: azobisdimethylvaleronitrile (ABDV); iii: dimethylacetal of benzil; iv: benzoylperoxide (BPO); v: 4,4_-azo(4-cyanovaleric acid) (adapted from Cormack & Elorza,2004) ⁹³	26
Figure 2-18.	Decomposition of AAC (a) and DMPA (b) (adapted from Mijangos <i>et al.</i> , 2006) ⁹⁰	27
Figure 2-19.	Percentage of binding 100 ppb Ochratoxin (OTA) to Imprinted polymer in buffer (a) and acetonitrile (b) solution (adapted from Turner <i>et al.</i> , 2004) ¹⁰¹	28
Figure 2-20	Mechanism of free radical polymerisation: (1) initiation, (2) propagation, (3) chain transfer, (4) termination via (a) disproportionation and (b) combination (adapted from Belyazit <i>et al.</i> , 2016) ¹⁰⁴	30
Figure 3-1	Illustration of molecular mechanics force field: bond stretching, angle bending, torsion term, and non-bonded interaction (adapted from Leach, 1996) ¹¹⁴	32
Figure 3-2.	The influence of pH or pKa to changing of FB1 structure (adapted from https://chemicalize.com/#/calculation) ¹²⁰	39
Figure 3-3.	Three-dimensional structure of the R enantiomer FB1 in (a) vacuum and in (b) water (hydrogen: cyan, oxygen: red, nitrogen: blue, carbon: white) ...	39
Figure 3-4.	Three-dimensional structure of the S enantiomer FB1 in (a) vacuum and in (b) water (hydrogen: cyan, oxygen: red, nitrogen: blue, carbon: white) ...	40
Figure 3-5.	The structure of three monomers interacted with FB1	40
Figure 3-6.	The illustration of FB1 (minimised in water) complex with DEAEM (+). (hydrogen: cyan, oxygen: red, nitrogen: blue, carbon: white, H-bonds: grey)	42
Figure 3-7.	The illustration of FB1 (minimised in water) complex with EGMP (-). (hydrogen: cyan, oxygen: red, nitrogen: blue, carbon: white, H-bonds: grey)	42

Figure 3-8. Scheme of solid phase synthesis for generating nanoMIPs for FB1. (1) immobilisation of FB1 onto glass beads (2) glass beads based solid phase used for polymerisation (3) initiation by TEMED in APS (4) removal low-affinity nanoMIPs and unreacted monomer by cold water (5) elution high-affinity nanoMIPs by hot water.	44
Figure 3-9 Washing fractions in cold water (blue line) and elution fractions in hot water (red line)	45
Figure 3-10. Diagram of the size distribution by intensity for cold water fraction at 4 °C	46
Figure 3-11. Diagram of the size distribution by intensity for hot water fraction at 60 °C	46
Figure 3-12. TEM image of nanoMIPs for Fumonisin B1 at 500 nm (a) and 200 nm (b) magnification	46
Figure 3-13. FT-IR spectra of nanoMIPs in solid.....	47
Figure 3-14. FT-IR spectra of acetonitrile (red line) and nanoMIPs in acetonitrile (blue line).....	47
Figure 3-15. The binding affinity of nanoMIPs-FB1 complex measured using the BIAcore method. Gradient concentrations (ranging from 0.38 to 12 μM) of nanoMIPs were injected through flow cells with immobilised FB1. The kinetic profiles are shown. The dissociation constant (KD) of the nanoMIPs-FB1 complex was calculated to be 0.2 μM	48
Figure 4-1. Plot HRP-FB1 absorbance at 450 nm against HRP-FB1 concentration. Microplates were coated with a fixed nanoMIPs concentration (0.03 mg mL^{-1}), the blocking solution was incubated for 2 h, TMB substrate was incubated for 5 min, and then quenched with sulfuric acid. The control experiment was performed without nanoMIPs.....	55
Figure 4-2. Optimisation of nanoMIPs concentration. Microplate was coated with nanoMIPs concentration ranging from 0.006 to 0.06 mg mL^{-1} . The HRP-FB1 conjugate was used at 1:800 dilution, the blocking agent was incubated for 2 h, TMB substrate was incubated for 5 min, and reaction quenched with sulfuric acid.	56
Figure 4-3. HRP interference in MINA. (1) Firstly nanoMIPs are deposited for coating of microplates. (2) Then, some wells were added by HPR-FB1 conjugate and others were added by HRP. (3) After that substrate, TMB was added. (4) Afterwards, the stopover solution was added. Finally, absorption was measured at 450 nm using microplate reader.	58
Figure 4-4. Plot of absorbance at 450 nm for HRP and HRP-FB1 concentrations in a binding to.....	58
Figure 4-5. Calibration curve of HRP 0.15 - 1.2 $\mu\text{g mL}^{-1}$	59
Figure 4-6. MINA protocol, (1) firstly nanoMIPs are deposited onto microplates wells. (2) Then, competitive assay between HPR-FB1 conjugate and FB1 standard was performed. (3) After that substrate TMB was added. (4) Afterwards, the stopover solution was added. Finally, absorption was measured at 450 nm using microplate reader.	60

Figure 4-7. Calibration plot for FB1, measured using MINA and the respective control using nanoNIPs. The concentration for nanoMIPs and nanoNIPs was 0.06 mg mL ⁻¹ . All experiments were performed using FB1 standard solutions ranging from 10 pM to 10 nM (in 0.01 M PBS), HRP-FB1 conjugate dilution at 1:400, blocking solution (incubation 2 h), TMB substrate (incubation 5 mins) and then quenched with sulfuric acid.	61
Figure 4-8. Calibration plot for FB1 measured using conventional ELISA, the concentration of mAb used was 0.006 mg mL ⁻¹ . All experiments were performed using FB1 standard solutions ranging from 10 pM to 10 nM (in 0.01 M PBS), HRP-FB1 conjugate dilution at 1:400, blocking solution (incubation 2 h), TMB substrate (incubation 5 mins) and then quenched with sulfuric acid.	61
Figure 4-9. MINA response to FB1, flatoxin B1 (AFB1), citrinin (CTT), deoxynivalenol (DON), and zearalenone (ZEA). For the experiments microplates were coated with nanoMIPs (0.06 mg mL ⁻¹), HRP-FB1 conjugate dilution was 1:400, standard solution concentration ranged from 10 pM to 10 nM.	62
Figure 4-10. MINA and HRP response to other mycotoxins. For the experiments microplates were coated with nanoMIPs (200 ul, 0.03 mg mL ⁻¹), HRP-FB1 and HRP conjugate dilution was 1:800, standard solution concentration ranged for each compound 10 pM.	63
Figure 4-15. MINA protocol, (1) firstly nanoMIPs are deposited in microplates. (2) Then, competitive assay between HPR-FB1 conjugate and sample extracts was performed. (3) Substrate TMB was added. (4) Afterwards, the stopover solution was added. Finally, absorption was measured at 450 nm using a microplate reader.	65
Figure 4-16. The distribution of fumonisins in corn samples by MINA, commercial ELISA kit, and HPLC.	66
Figure 4-17. Correlation sample analysis of MINA-HPLC (a) and ELISA-HPLC (b)..	67
Figure 5-1. Chemical structure of ZnP and Pyr monomers	70
Figure 5-2. FB1 nanoMIPs sensor fabrication: (1) electropolymerization of 5,10,15,20-tetrakis(4-aminophenyl)-porphyrin-Zn(II) and Pyrrole (ZnP/Pyr) in a solution of 0.1 M tetra-(n-butyl)-ammonium tetrafluoroborate (C ₄ H ₉) ₄ NBF ₄ in acetonitrile. (2) Immobilisation of nanoMIPs through carbodiimide chemistry (incubation in 0.7 M EDC and 0.6 M NHS in 0.01 M PBS during 24 h).	71
Figure 5-3. Equivalent circuit employed for EIS fitting. <i>R_s</i> is the solution-phase resistance, <i>R_{et}</i> is the electron transfer resistance, <i>C_{dl}</i> is the double-layer capacitance, and <i>Z_w</i> is the Warburg impedance.	72
Figure 5-4. Cyclic voltammograms from (a) bar electrode at 0.1 M (C ₄ H ₉) ₄ NBF ₄ , acetonitrile, (b) the electropolymerization of 46.84 μM ZnP and 0.14 M Pyr at a potential range of -1.1 to 1.3 V (vs. Ag/Ag ⁺) and a scan rate of 50 mV/s (8 cycles) in 0.1 M (C ₄ H ₉) ₄ NBF ₄ , acetonitrile.	73
Figure 5-5. The surface of bar Pt electrode (left) and ZnP/Pyr polymer deposit on Pt electrode (right).	74

Figure 5-6. Infrared spectrum from ZnP/Pyr polymer. The polymer was electro-deposited on a gold surface.....	74
Figure 5-7. Schematic representation from nanoMIPs immobilisation on ZnP/Pyr/Pt electrode via carbodiimide chemistry.....	75
Figure 5-8. AFM images for (a and a') ZnP/Pyr polymer surface. (b and b') nanoMIPs immobilised on ZnP/Pyr polymer surface. The measured area was $5 \times 5 \mu\text{m}^2$	76
Figure 5-9. DPV reponse for a solution 100 fM FB1 standard in control using as recognition element ZnP/Pyr polymer, nanoNIPs and nanoMIPs. All the measurements were carried out in 0.01 M PBS buffer and 0.005 M $[\text{Fe}(\text{CN})_6]^{4-/3-}$, recorded at the potential range -0.25 to +1.10 V vs. Ag/AgCl and 5 min previous incubation.	77
Figure 5-10. The schematic diagram of redox activity of $[\text{Fe}(\text{CN})_6]^{4-/3-}$ on nanoMIPs/ZnP/Pyr/Pt electrode because of interaction between FB1 and nanoMIPs (modified from Le <i>et al.</i> , 2016 ¹⁸²).....	77
Figure 5-11. Differential pulse voltammetry reponse for (1) 0, (2)1 fM, (3)10 fM, (4) 100 fM, (5) 1 pM, and (6) 10 pM FB1. All the measurements were carried out in 0.01 M PBS and 0.005 M $[\text{Fe}(\text{CN})_6]^{4-/3-}$, recorded at the potential range -0.25 to +1.10 V (vs. Ag/AgCl).....	78
Figure 5-12. DPV calibration curve for FB1 (10 fM, 100 fM and 10 pM) in ZnP/Pyr/Pt (control), nanoNIPs and nanoMIPs. All measurements were carried out in 0.01 M PBS and 0.005 M $[\text{Fe}(\text{CN})_6]^{4-/3-}$	78
Figure 5-13. DPV calibration curve for FB1 and other mycotoxins (FB2, AFB1, CTT, DON and ZEA). All the measurements were carried out using a nanoMIPs sensor in 0.01 M PBS and 0.005 M $[\text{Fe}(\text{CN})_6]^{4-/3-}$ in a mycotoxin concentration range from 1fM – 10 pM.	79
Figure 5-14. Nyquist plot for EIS determination of FB1 using a nanoMIPs sensor for concentrations at (1) 0 M, (2) 1 fM, (3) 10 fM, (4) 100 fM, (5) 1 pM, and (6) 10 pM. All the measurements were carried out in 0.01 M PBS buffer, recorded at the frequency range 400 mHz - 200 kHz and at potential +0.35 V (vs. Ag/AgCl). Inset is the equivalent circuit where R_s is the solution-phase resistance, R_{et} is the electron transfer resistance, C_{dl} is the double-layer capacitance, and Z_w is the Warburg impedance.....	80
Figure 5-15. EIS calibration curve for FB1 and other mycotoxins (FB2, AFB1, CTT, DON and ZEA). All the measurements were carried in 0.01 M PBS buffer, in mycotoxins concentration from 0 – 10 pM, recorded at the frequency range 400 mHz - 200 kHz and at potential +0.35 V (vs. Ag/AgCl).....	81

THE LIST OF EQUATIONS

(3-1) Energy of force field.....	32
(3-2) Gibbs free energy.....	32
(3-3) Binding percentage.....	35

THE LIST OF ABBREVIATIONS

AFB1	Aflatoxin B1
Ag	Silver
CE	counter electrode
CTT	citrinin
CV	cyclic voltammetry
DEAEM	2-(Diethylamino)ethyl methacrylate
DLS	Dynamic Light Scattering
DON	Deoxynivalenol
DPV	differential pulse voltammetry
EGMP	Ethylene glycol methacrylate phosphate
EIS	electrochemical impedance spectroscopy
ELEM	Equine leukoencephalomalacia
ELISA	Enzyme Linked Immunosorbent Assay
FB1	Fumonisin B1
FB2	Fumonisin B2
FTIR	Fourier transfer infrared
HPLC	High Performance Liquid Chromatography
HRP	Horseradish peroxidase
HRP-FB1	Horseradish peroxidase-Fumonisin B1
LC-MS/MS	Liquid Chromatography Mass Spectrophotometry
MINA	nanoMIPs based assay
MINES	nanoMIPs based electrochemical sensor
MIP	Molecularly Imprinted Polymer
MM	Molecular Mechanics
nanoMIPs	Molecularly Imprinted Polymer Nanoparticles
nanoNIPs	Non-specific imprinted polymer nanoparticles
PPE	Porcine Pulmonary Edema
Pt	Platinum
Pyr	Pyrrrole
RE	reference electrode
SPE	Solid Phase Extraction
TEM	Transmission Electron Microscopy
TMB	3,3',5,5'-Tetramethylbenzidine
WE	working electrode
ZEA	Zearalenone
ZnP	5,10,15,20-tetrakis(4-aminophenyl)-porphyrin-Zn(II) atau Zinc(II) porphirin

CHAPTER 1 INTRODUCTION

This work was fully supported and funded by Indonesian Agency for Agriculture Research and Development (IAARD), Ministry of Agriculture, Republic of Indonesia. IAARD and the Toxicology Group, and Indonesian Research Centre for Veterinary Science (IRCVS) are interested in improving food safety throughout Indonesia in development of detection techniques for toxins in food and animal feed.

The research carried out in this thesis is to advance this area by the development of molecularly imprinted polymer nanoparticles-based assays and sensors for detection of fumonisins found Indonesia. The samples investigated and analysed are corn taken randomly from the traditional market in Surabaya, East Java, Indonesia.

It is expected that this would contribute for supporting human and animal health in Indonesia and the rest of the world.

1.1 Background

Fumonisin pose a potential risk to human and animal health being carcinogenic and hepatotoxic.¹⁻³ Because of these implications, these compounds are categorised as group 2B carcinogenic by the International Agency for Research on Cancer (IARC).⁴ Moreover, the maximum level of fumonisins recommended is 2–4 ppm by US Food and Drug Administration (USFDA) and European Commission (EC).^{5,6} The Indonesian Government recommends the regulation for the level of fumonisins contamination at 1–2 ppm.⁷ Fumonisin B1 (FB1), which is the most common type of fumonisins,⁸ is implicated in the aetiology of equine leukoencephalomalacia (ELEM) in horse and porcine pulmonary oedema (PPE) in pig.⁹ Consequently, it is considered that Fumonisin are harmful compounds which governments should be gravely concerned about.

Furthermore, the occurrence of FB1 in Indonesia has been observed by many researchers since 1990s.¹⁰⁻¹⁴ In previous studies, it was confirmed that FB1 was found in corn consumed by humans and animals. The results showed that 58%-100% of all samples of Indonesian corn were contaminated with FB analysed from 1991-2017. This occurrence has varied depending on many factors such as temperature, humidity, and storage

time.^{15,16} The lowest concentration was 0.47 µg/kg, during 1991–1995 and the highest level was 252.310 µg/kg in 2010 – 2017 as can be seen in Table 1-2. For these reasons FB1 contamination of corn could be considered a substantial issue especially in Indonesia.

Table 1-1. Distribution of Fumonisin B1 in Indonesia's corn 1990-2017

Year	Contamination (µg/kg)		Percentage of samples contaminated by FB1 (%)
	Min	Max	
1991 – 1995	226	1,780	58(7/12)
1996 – 2000	0.47	2,440	94(45/48)
2001 – 2005	18	3,306	81(25/31)
2005 – 2010	-*	61,000	-(-/273) *
2011 – 2017	2880	252,310	100(24/24)

*no data

In addition, the analysis of FB1 in contaminated samples (Table 1-1) gave different results depending on the analytical methods used. Mostly, the assessment of FB1 in corn has used chromatography and immunoassay techniques. In this case, advancements in the reliable determination of FB1 is essential for improving food and feed safety in Indonesia. However, the advantages and disadvantages need to consider comprehensively before any technology is developed and approved.

1.2 Justification

An overview of the literature from 1991 to 2017 about the determination of fumonisins in corn highlights the awareness of researchers about this problem. They have developed different advanced techniques specifically to analyse fumonisins in food samples especially corn. Commonly, there are three methods which are widely used for determination of fumonisins in corn such as HPLC, LC-MS/MS, and immunoassay ELISA, as shown in Figure 1-2.

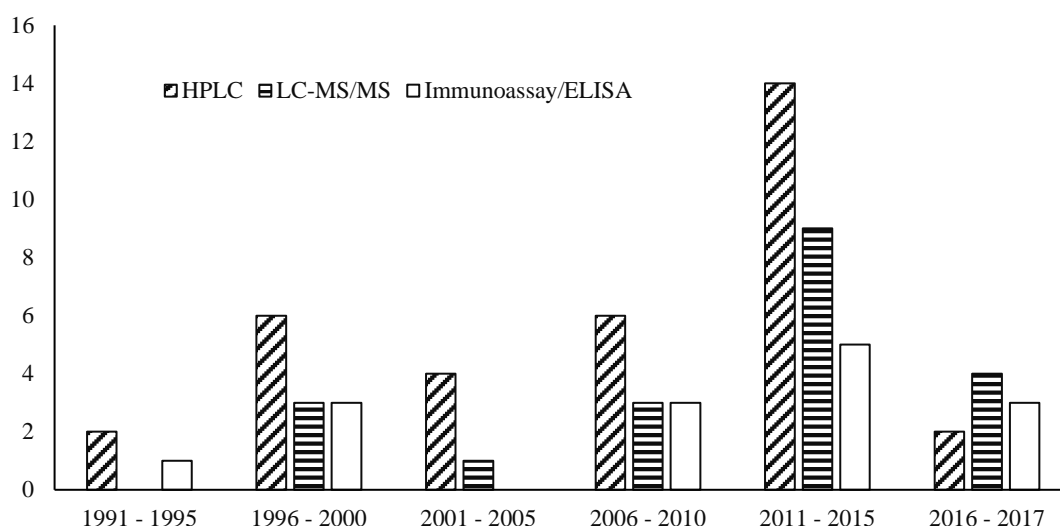


Figure 1-1. The total number of publications reporting the application of HPLC, LC-MSMS and immunoassay/ELISA for analysis of fumonisins in corn in 1991–2017.

Chromatography has been the most widespread method used since the 1990s for determination of Fumonisin in corn. High-Performance Liquid Chromatography (HPLC) is the most common technique applied with a limit of detection of 0.025 – 300 ppb¹⁷⁻³⁴ followed by Liquid Chromatography-Mass Spectroscopy (LC-MS) or tandem Mass Spectroscopy (LC-MS/MS) with a detection limit of 0.002–8 ppb.³⁵⁻⁴⁵ MS can improve the performance of HPLC removing obstacles such as derivatisation, peak interference, and long retention time. Enzyme-Linked Immunosorbent Assay (ELISA) has become a newly popular technique for fumonisin analysis since 1996. The detection limit of ELISA is lower than chromatography methods (0.03 ppt – 50 ppb).⁴⁶⁻⁵⁸ This immunoassay is the preferred technique because its application is more straightforward than HPLC or LC-MS in the analysis of fumonisins.

Furthermore, the sensing technology has been developed and applied for detection of fumonisins in food although this technique has not been widely used. An excellent recent review has covered development of sensors for FB1 since 1996.⁵⁹ Mostly, the methods used in sensors are optical and amperometry. Unlike immunoassays and chromatography techniques, the limit of detection for sensing is approximately 0.5 pg L⁻¹ in the working range 7- 9 ng L⁻¹.⁶⁰

The immunoassays and sensors are more sensitive and show excellent recovery at 80% but they are less reliable than the other analytical methods (Table 1-2). Chromatography techniques use sophisticated instruments that would need trained users because of complicated operation. The immunoassay and sensors use different methods for sample preparation than chromatography that can use not only water but also organic solvents. However, selecting the right solvent for extraction and analysis in chromatography would be time-consuming and costly. For practical reasons, development of immunoassays and sensors will become a favourable and popular direction for research. The focus in this work is the development of robust assays and sensors that can work with much diluted aqueous samples of food and do not require highly skilled personnel to operate them.

Table 1-2. The advantages and disadvantages of HPLC, LC-MS/MS and ELISA for determination of FB1 in corn based on several articles

Methods	Advantages	Disadvantages
HPLC	<ul style="list-style-type: none"> Recovery is higher than 80%, and precision is more top than 95%. 	<ul style="list-style-type: none"> Derivatisation with o-phthalide aldehyde (OPA) and AccQ-Fluor reagent is necessary to increase sensitivity and avoid peak interference. The trained users are required for operating the machine The extraction and cleaning up take more time
LC-MS/MS	<ul style="list-style-type: none"> High selectivity and sensitivity would be achieved because of mass detector Recovery is higher than 80% 	<ul style="list-style-type: none"> The trained expert is needed to operate this instrument. Precision is lower than 90% The extraction and purification of the sample are required, such as ultrasonic extraction (USE), and accelerated solvent extraction (ASE).
ELISA and sensors	<ul style="list-style-type: none"> The amount of sample used is smaller, around 100 μL It can be used for screening method in the field and industry The procedure is relatively simple 	<ul style="list-style-type: none"> Many factors are influencing measurements in ELISA such as reagent materials, the time for incubation, blocking, and washing, and interaction with microplate. The antibody is not stable at room temperature, often due to denaturation process The production of antibody is expensive and takes long times.

Most immunoassays and sensors use monoclonal or polyclonal antibodies for molecular recognition. These substances are expensive because their production uses animals such as mice and rabbits. Also, the procedure for obtaining pure antibodies is lengthy. For this reason the replacement of the antibody is essential step to improve the performance of both, ELISA and sensors, in particular for reducing time and cost of analysis.

Recently, molecularly imprinted polymer nanoparticles (nanoMIPs) have been developed which could be more efficient than monoclonal or polyclonal antibodies in terms of the time of preparation, cost and stability. To generate nanoMIPs, it is not necessary to use animals, such as rabbits. Likewise, the nanoMIPs can be obtained in a short time and have a long shelf life and resistance to elevated temperatures and extreme pHs, where antibody could be easily denatured. NanoMIPs have the potential to replace antibodies in assay and sensor applications for the determination of fumonisins.

1.3 The aims and objectives of the research

The aim of this study is to develop nanoMIPs-based assay and sensor for screening food or animal feed for mycotoxin contamination especially FB1 for supporting human and animal health in Indonesia.

To achieve this aim, the objectives of this research are to:

1. Find the best functional monomers using computational chemistry (molecular modelling) for the synthesis of FB1 imprinted nanoMIPs,
2. Synthesise FB1 imprinted nanoMIPs using solid phase chemistry by immobilisation of FB1 on glass beads,
3. Test for binding affinity of FB1 imprinted nanoMIPs to FB1 using a nanoMIPs based assay (MINA),
4. Compare the performance of MINA with commercial ELISA kit and HPLC in real samples such as corn for detection of FB1,
5. Test FB1 imprinted nanoMIPs using electrochemical sensor (MINES) using differential pulse voltammetry (DPV) and electrochemical impedance spectroscopy (EIS) for detection of FB1,

6. Optimise assay and sensors for binding affinity and selectivity of FB1 and analogues,
7. Disseminate the results of studies through a presentation at international conference and preparation of a paper for submission to peer-reviewed journals.

The thesis includes a literature review (Chapter 2) describing toxicological effects of FB1 and the interference of FB1 with sphingolipid metabolism. The thesis also provides a brief description of nanoMIPs and imprinting approach in general, the composition, and polymerisation methods employing solid phase approach. The experiments and results are reported in the following three chapters. Chapter 3 show how to develop nanoMIPs for FB1, combining simulation and empirical investigations. Chapter 4 and Chapter 5 describe how synthesised nanoMIPs were employed in assay and sensor applications. Chapter 4 shows testing of 18 corn samples in the assay with detail analysis of recovery and limit of detection. Finally, the general conclusion and future research were given in Chapter 6 as the closing remarks on the thesis.

CHAPTER 2 LITERATURE REVIEW

2.1 Fumonisin B1

2.1.1 Resources, structure, and nomenclature

Fumonisin B1 is produced mostly by *Fusarium moniliforme* and *F. proliferatum*. It has been reported that fumonisins have over ten compounds with different functional groups including Fumonisin A, B, C, and P shown in Figure 2-1 and Table 2-1.⁶¹⁻⁶⁴

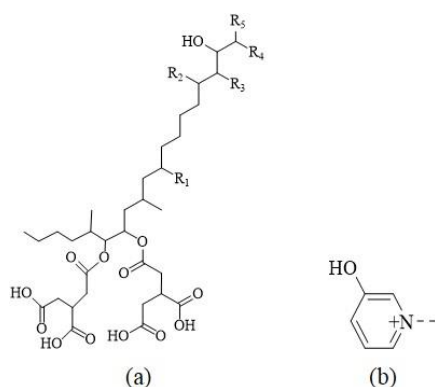


Figure 2-1. Fumonisin backbone (a) and 3-hydroxypyridinium (3HP) (b)

Table 2-1. Fumonisin analogues

Fumonisin	Side chains of Fumonisin backbone				
	R1	R2	R3	R4	R5
A1	OH	OH	H	NHCOCH ₃	CH ₃
A2	H	OH	H	NHCOCH ₃	CH ₃
B1	OH	OH	H	NH ₂	CH ₃
B2	H	OH	H	NH ₂	CH ₃
B3	OH	H	H	NH ₂	CH ₃
B4	H	H	H	NH ₂	CH ₃
C1	OH	OH	H	NH ₂	H
C2	H	OH	H	NH ₂	H
C3	OH	H	H	NH ₂	H
C4	H	H	H	NH ₂	H
P1	OH	OH	H	3HP	CH ₃
P2	H	OH	H	3HP	CH ₃
P3	OH	H	H	3HP	CH ₃

Fumonisin B1 has long IUPAC nomenclature and the structures have ten chiral centres (Figure 2-2).^{65,66} Because of the chirality, FB1 has at least one pair of enantiomers:

- (2R)-2-[2-[(5R,6R,7S,9S,11R,16R,18S,19S)-19-amino-6-[(3R)-3,4-dicarboxybutanoyl]oxy-11,16,18-tri hydroxy-5, 9-dimethylcosan-7-yl]oxy-2-oxoethyl]butanedioic acid
- (2S)-2-[2-[(5S,6R,7R,9R,11S,16R,18S,19S)-19-amino-6-[(3S)-3,4-dicarboxybutanoyl]oxy-11,16,18-trihydroxy-5,9-dimethylcosan-7-yl]oxy-2-oxoethyl] butanedioic acid.^{65,66}

Consequently, drawing structures of FB1 should consider R and S types and these types were used in further experiments.

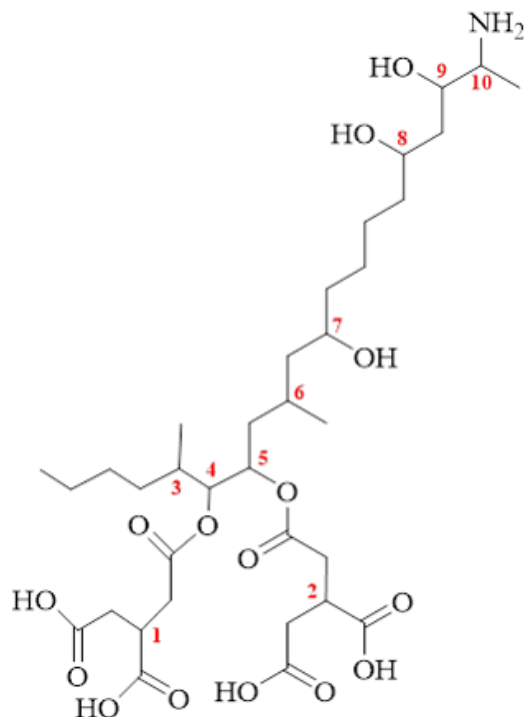


Figure 2-2. The two-dimension structure of Fumonisin B1 and its ten chiral carbons

In addition, a different type of FB1 structure would have similar physical-chemical properties such as melting point, polarity, boiling point, solubility behaviour, chromatographic mobility, and index of refractivity, but it has different on polarised light (optical activity) and chiral reagent.⁶⁷ In previous research, it is reported that the (-)-enantiomer of the insecticide fipronil is less toxic to *Ceriodaphnia dubia* (water flea) than (+)-enantiomer of fipronil. Some experts produce a single enantiomer of fipronil to investigate differing toxicity.⁶⁸ From these reason, probably the enantiomer of FB1 could potentially have different toxicity. However, there is no comprehensive information describing about it. It can be argued that the chirality of FB1 influences not only physical and chemical properties but also toxicity.

2.1.2 Several experimental studies about the effect of FB1

Over the past 28 years, fumonisins have been mentioned because this residue can trigger carcinogenesis, equine leukoencephalomalacia (ELEM), and porcine pulmonary edema (PPE). One experiment stated that the histopathological change of rat's liver specimen (hydroponic generation, single-cell, and few hyaline droplets) after receiving 1% FB1 for 33 days.⁶⁹ A recent experiment on *Oreochromis niloticus* (Nile tilapia), FB1 could

damage liver and kidney, and harm spleen, gill and brain. Figure 2-3 (a) – (e) shows that there are many histological changes in many parts of the body of *O. niloticus*. Having exposure of FB1 for six weeks, liver (Figure 2-3 (a)) showed diffuse hepatocyte degeneration with focal hepatocyte necrosis, while kidney (Figure 2-3 (b)) indicated tubular degeneration and interstitial inflammatory cell infiltration. Likewise, there were many signs found in spleen, gill, and brain such as necrosis in lymphocytes, epithelial hyperplasia, ischemic neuronal injury and demyelination respectively.⁷⁰ Therefore, it could be revealed that FB1 would affect not only carcinogenesis but also damage organs.

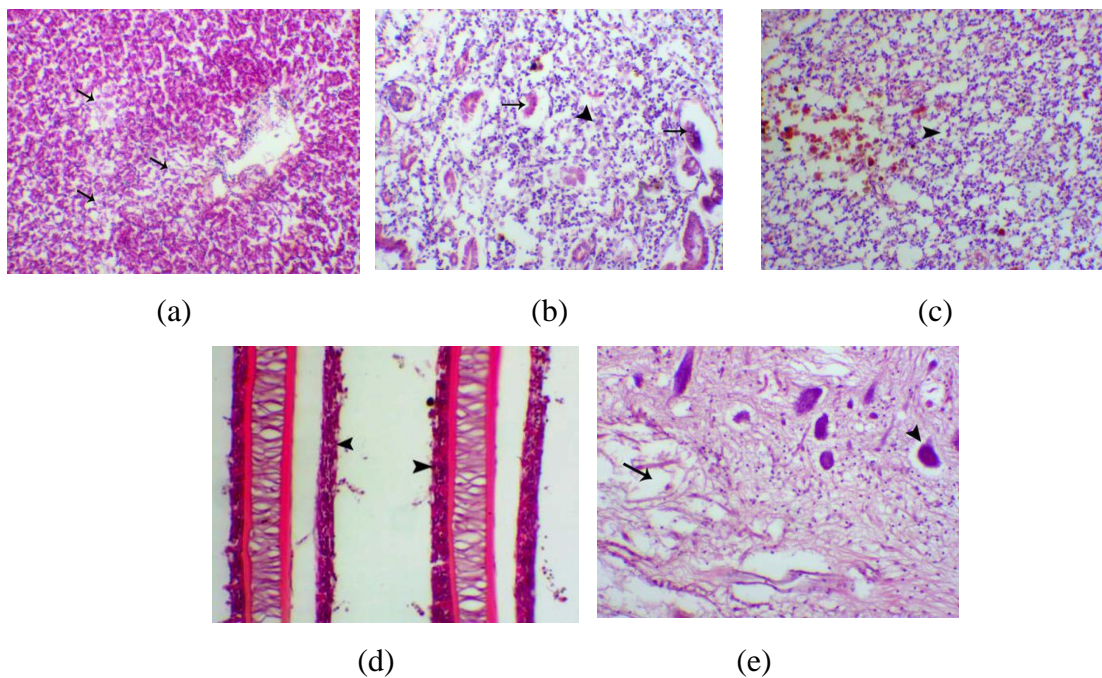


Figure 2-3. Histopathological change of liver (a), kidney (b), spleen (c), gill (d) and brain (e) of *O. niloticus* after exposure FB1 for six weeks (adapted from Abu-Hassan *et al.*, 2016)⁷¹

As indicated previously, ELEM was found in horses that ingested feed contaminated by FB1, with the neurologic symptoms.⁷² The symptoms could be marked by clinical signs such as apathy, docility, tremors, pawing emotions, stupidity, incoordination, walking into an object, and paralysis of lips and tongue.⁷³ These clinical signs were supported by clinical pathology data such as the increase of aspartate transaminase (AST) and glutamyl transferase (GGT). Figure 2-4 (a) showed that the peak of AST on nine month-old-filly (female horse) was between day 22 and 31. Then, Figure 2-4 (b) illustrates the increase of GGT on 14 months-old-colt (male horse) between day 20 to 33.⁷³ Therefore, it is indicated FB1 can cause ELEM shown by clinical signs and pathology.

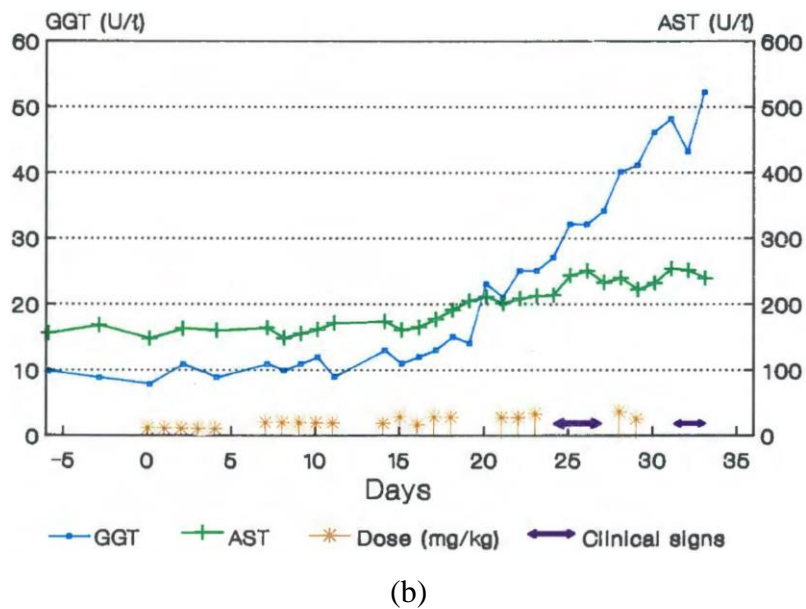
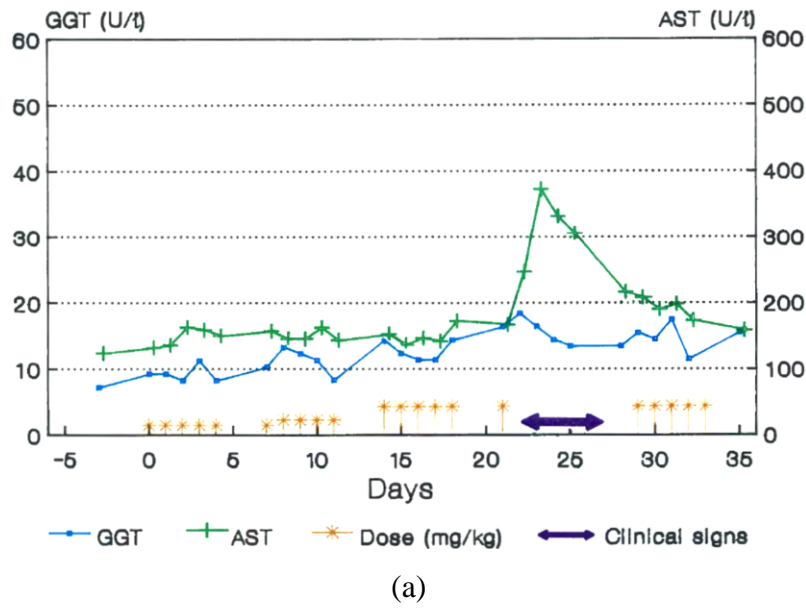
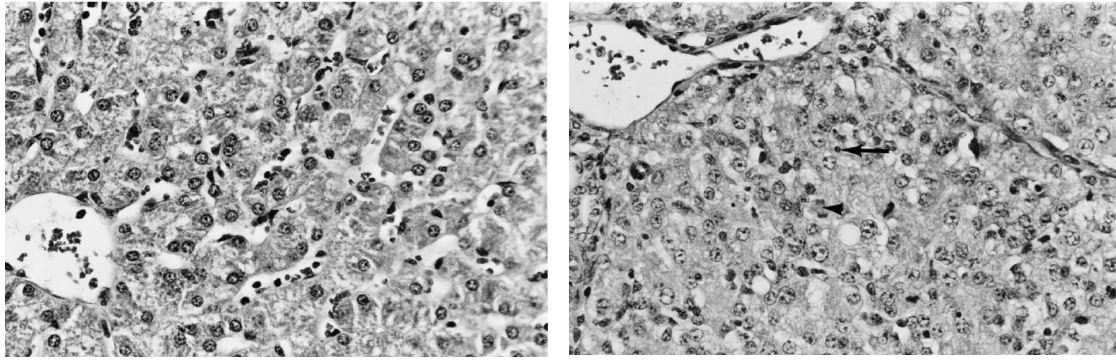


Figure 2-4. Clinical and pathological change in the serum of (a) 9 months-old filly and (b) 14 months old colt dosed FB1 (adapted from Kellerman *et al.*, 1990)⁷³

Unlike ELEM, PPE cases can be found in pig. The onset of clinical signs of PPE is four days in average such as lethargy, dyspnea, cyanosis, posterior weakness, recumbence, mild salivation, and moist rales.⁷⁴ Figure 2-5 demonstrates the change of a healthy pig and pig with PPE after ingesting corn contaminated FM. In healthy pigs (Figure 2-5 (a)), the liver has the central vein (lower left) that is surrounded by hepatocytes ordered in cords separated by sinusoids. On the other hand, the liver of treated pig (Figure 2-5 (b)), has disorganised hepatocytes.⁷⁵ Hence, it seems that the FB1 can affect PPE and damage liver.



(a)

(b)

Figure 2-5. Liver from a health pig (a) and a pig identified porcine pulmonary oedema (adapted by Hascheck *et al.*, 2001)⁷⁵

2.1.3 The Toxicity Mechanism of FB1

FB1 can inhibit the sphingolipid biosynthesis. This lipid mechanism is an imperative part of cells because of many functions such as basic molecule services and regulation of some cell functions. Figure 2-6 illustrates the simplified scheme of sphingolipid synthesis. Initially, sphinganine is formed by serine and palmitoyl-CoA through 3-ketosphinganine. Then, it is acylated by ceramide synthase to be dihydroceramide, and it is finally desaturated to be ceramide.⁷⁶

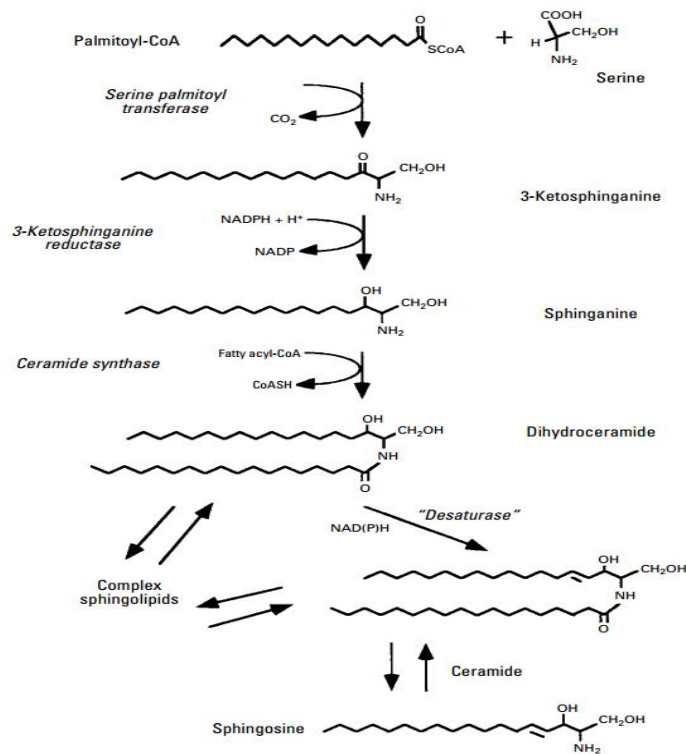


Figure 2-6. Sphingolipid biosynthesis (adapted from Merrill Jr *et al.*, 2001)⁷⁶

Unfortunately, the sphingolipid biosynthesis could be disrupted by FB1. One reason is the backbone structure of sphingosine is similar with FB1. In this case, FB1 could inhibit the acylation reaction between sphinganine and ceramide synthase as shown Figure 2-7. Consequently, its impact is the elevation of sphinganine. It will produce sphinganine and finally phosphatidylethanolamine as well as some fatty acids. Another reason, FB1 could increase ceramide and inhibit sphingosine products. These products, in the same way, could increase phosphatidylethanolamine and fatty acids as signalling the disease and organ damage.

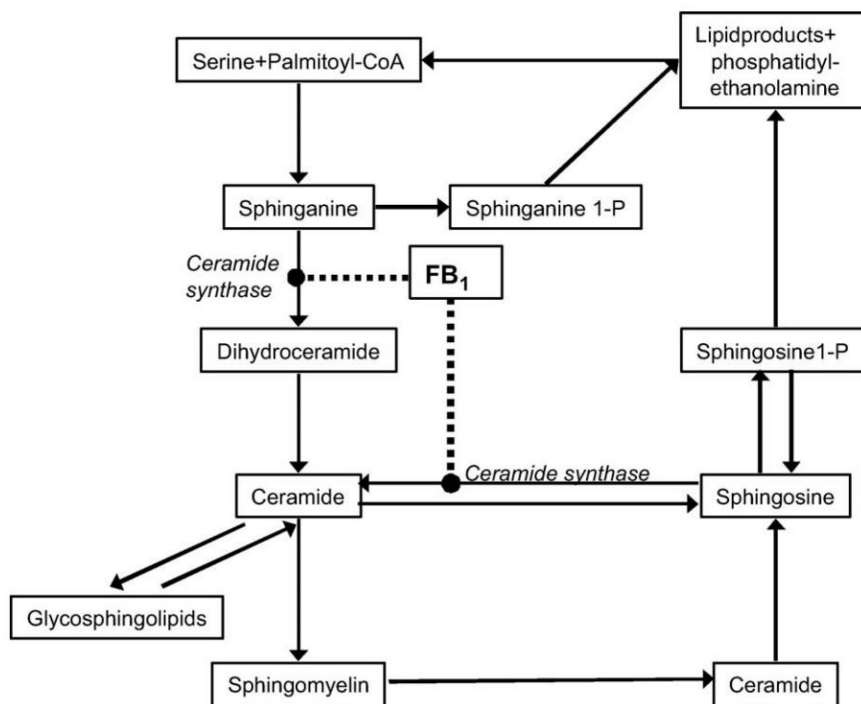


Figure 2-7. Illustration of FB1 interfere to sphingolipid biosynthesis (adapted from Juvala *et al.*, 2008)⁷⁷

2.2 Molecularly Imprinted Polymers

According to Alexander *et al.*, 2006, Molecular imprinted polymer (MIP) can be defined as follows:

“the construction of ligand-selective recognition sites in synthetic polymers where a template (atom, ion, molecule, complex or a molecular, ionic, macromolecular, assembly, including micro-organism) is employed in order to facilitate recognition site formation

*during the covalent assembly of the bulk phase by a polymerisation or polycondensation process, with subsequent removal of some or all of the template being necessary for recognition to occur in the spaces vacated by the templating species”.*⁷⁸

Historically, the research about MIP has been initiated by a Polyakov's article in 1931. This article mentions the silica owning many pores because of the presence of the additive solvent such as benzene, toluene, and xylene.⁷⁸ This finding indicated that the silica might have the capability to uptake the additive agents and this phenomenon would become the first invention of molecular imprinting. From this invention, the research could grow up focusing on biochemical processes and biomolecule structures. The next experiment was later continued by Pauling (1940) even though his objectives were probably different from Polyakov. Pauling used the concept of silica imprinting to describe how to produce antibody through imprinting antigen even though this original thinking was later proven to be wrong.

“An interesting possible method to generate antibodies from serum or globulin solution outside of animal is suggested by the theory. The globulin would be treated with a denaturing agent or condition sufficiently strong to cause the chain ends to uncoil; after which this agent or condition would be removed slowly while antigen or haptin is present in the solution in a considerable concentration. The chain ends would then coil up to assume the configurations stable under these conditions, which would be configurations complementary to those of the antigen or haptin”^{78,79}

The Pauling's theory initially has been supported by the results from Dickey's experiment (1949). These results confirmed that the imprinted silica is mimicking antibody, binding template dyes such as methyl, ethyl, propyl, and butyl orange. Furthermore, the curiosity was extended by conducting imprinting organic polymer and improving the condition of the imprinted polymer.^{78,79}

This section will explain the imprinting approach, the composition of the polymerisation of molecularly imprinting, the computational simulation method, and the polymerisation methods.

2.2.1 Imprinting Approach

The imprinting approach is the principal for the preparation of molecular imprinting. There are two common imprinting approaches namely covalent and non-covalent methods. Each has advantages and disadvantages depending on what kind of molecularly imprinted polymer is made. Also, this stage will explain other imprinting methods such as semi-covalent, metal ion mediated, and mixed imprinting methods.

2.2.1.1 Covalent Imprinting Approach

There are three steps in covalent imprinting method. Firstly, the reaction between the template and functional monomers to result in a covalent linkage is performed. In this stage, it might yield the reversible complex having stability under polymerisation condition. Then, this complex is polymerised with crosslinkers to gain polymer matrix. Finally, the template should be removed from the polymer matrix to produce cavities that can rebind covalently with the previous template. Moreover, this covalent imprinting procedure had been applied in the previous experiment obtaining mannose imprinted polymer as can be seen in Figure 2-8.

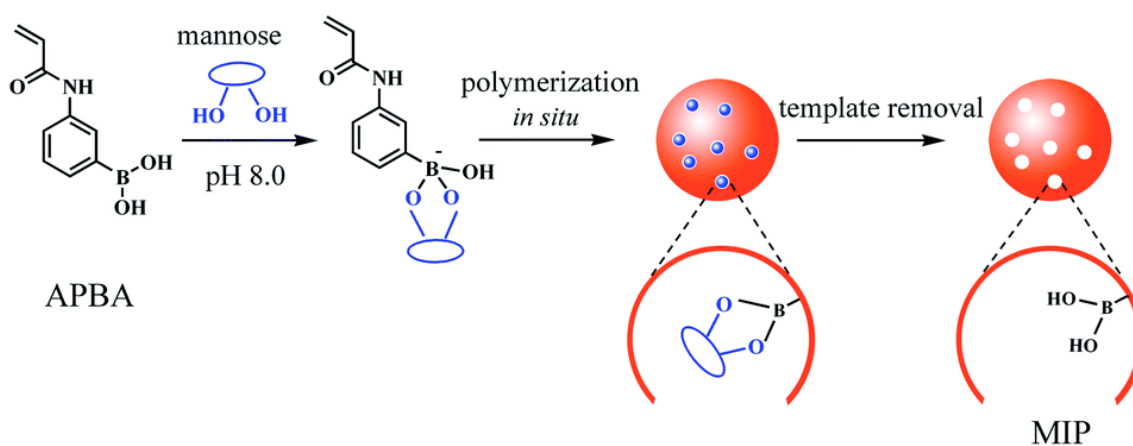


Figure 2-8. Illustration of covalent imprinting approach on mannose imprinted polymer (adapted from Shen and Ren, 2014)⁸⁰

From Figure 2-8 we can see that 3-acrylamidophenylboronic acid (APBA) as a functional monomer and mannose as a template. First is the formation of complex APBA and mannose. Then, the complex is polymerised by precipitation polymerisation with crosslinker and initiator conducted in situ with the essential condition. Lastly, the mannose leaves the polymer resulting cavities.⁸⁰

2.2.1.2 Non-covalent Imprinting Approach

Unlike covalent imprinting, there is no pre-polymerisation in non-covalent imprinting approach. Self-assembly could form the binding between template and monomer during the polymerisation step. It appears that this method is an easy way to produce molecular imprinting so that this approach is frequently used. Non-covalent interactions would happen during polymerisation, including electrostatic, hydrophobic, coordination covalent, and Van der Waals interactions. After polymerisation, the template is finally removed by fixed solvent from the polymer matrix.

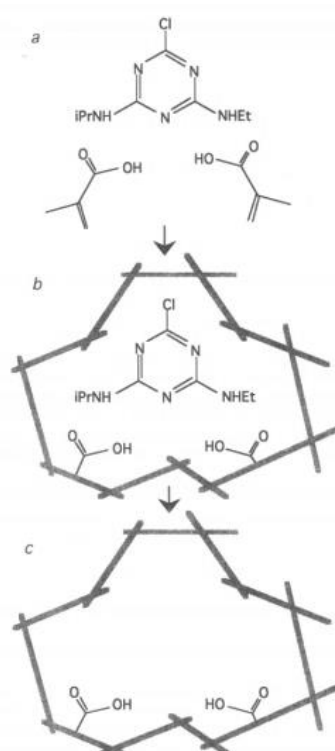


Figure 2-9. Illustration of non-covalent imprinting approach on atrazine imprinted polymer (adapted from Matsui *et al.*, 1995)⁸¹

Figure 2-9 demonstrates how the non-covalent imprinting approach is performed. In the first step, the polymerisation happens between methacrylic acid, and crosslinkers in the presence of atrazine to form the complex between the polymer binding sites and template. Then, the adducts will release atrazine reversibly.

Furthermore, the difference between the covalent and non-covalent imprinting approaches are not the only precondition before polymerisation but also other parameters such as polymerisation conditions, guest binding and guest release, removal of the template after polymerisation and structure of guest binding sites as shown Table 2-2.

Table 2-2. Comparison between Covalent and Non-covalent Imprinting Approach

Factors	Covalent	Non-covalent
Synthesis of monomer-template conjugation	Necessary	Unnecessary
Polymerisation condition (temperature, pH, polarity,)	Wide variety	Restricted
Guest binding and guest release	Slow	Fast
Removal of template after polymerisation	Difficult	easier
Structure of guest binding site	Clearer	Less clear

2.2.1.3 Other Imprinting Approaches

Recently, other imprinting methods have been widely explored such as semi-covalent, metal coordination, and the combination of the methods. The semi-covalent imprinting methods use both covalent and non-covalent binding in producing a MIP. Generally, in this case, covalent binding is used on polymerisation, and non-covalent binding is employed on rebinding the template. Figure 2-10 shows the process of polymerisation of 4-chlorophenol imprinted polymer with two routes. Firstly, the 4-chlorophenyl (4-vinyl) phenyl carbonate (4-CPC), which is a template, was synthesised from 4-vinylphenol, which is from hydrolysis of p-acetoxy styrene, and 4-chlorophenyl chloroformate. Then, 4-CPC and 4-vinylpyridine (4-VP), as a functional monomer, are polymerised by ethylene glycol dimethyl acrylate (*EGDMA*) and 2,2-azobisisobutyronitrile (AIBN) as crosslinker and initiator. Finally, the template was removed by hydrolysis polymer matrix obtaining 4-vinylphenol imprinted polymer completed by binding site for rebinding 4-vinylphenol non-covalently.⁸²

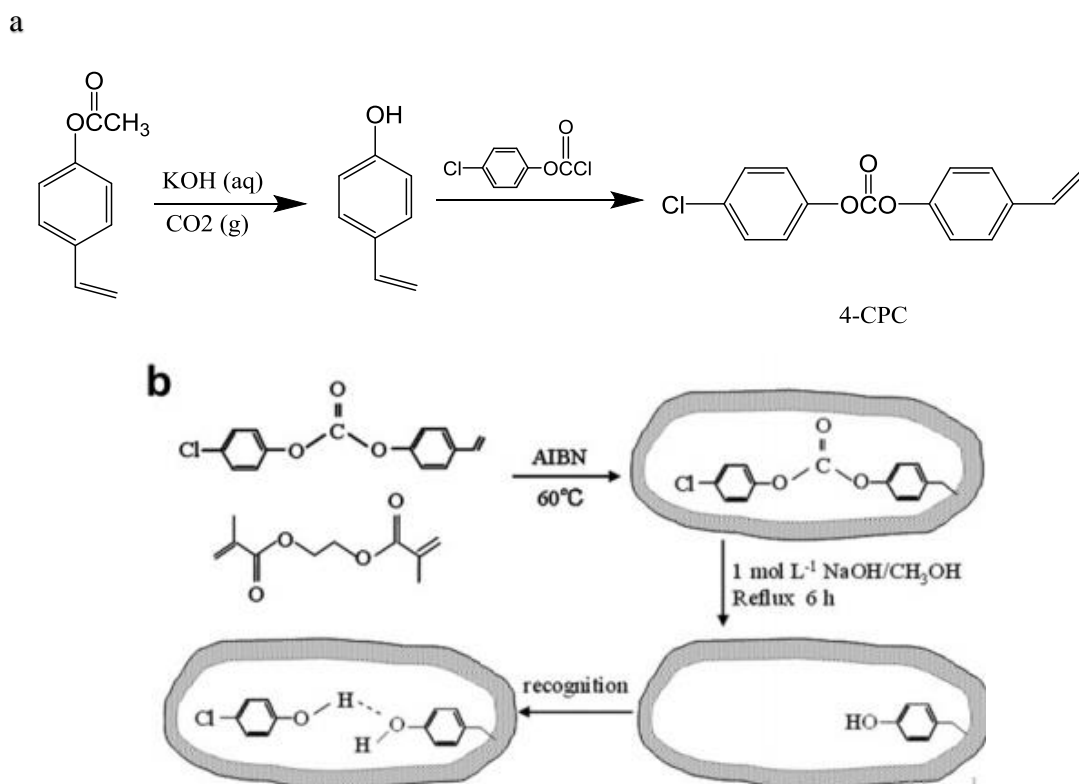


Figure 2-10. Illustration of semi-covalent imprinting approach on the 4-chlorophenol imprinted polymer, a. Template synthesis b. Polymer preparation (adapted from Qi *et al.*, 2010) ⁸²

Also, the metal ion mediated imprinting approach is used in several studies especially to select enantiomer of a compound. Figure 2-11 shows mechanism molecularly imprinted polymer formed to attach L-histidine as a precursor of histamine. Since histidine has enantiomer, L- and D- histidine, preparing complex compound by Cu^{2+} is probably an alternative method to separate them. In the first step, L-histidine as a template is reacted with Cu^{2+} and 2-aminoethyl dihydrogen phosphate (AEDP) as a metal ion and functional monomer to obtain Cu(II) monomer-template complex. Then, the complex is polymerised by adding Ethylene glycol dimethyl acrylate (EGDMA) and multiwalled carbon nanotubes (MWCNTs) under UV light. Finally, L-histidine is removed reversibly from the polymer matrix, but this polymer is not specific on D-histidine.⁸³

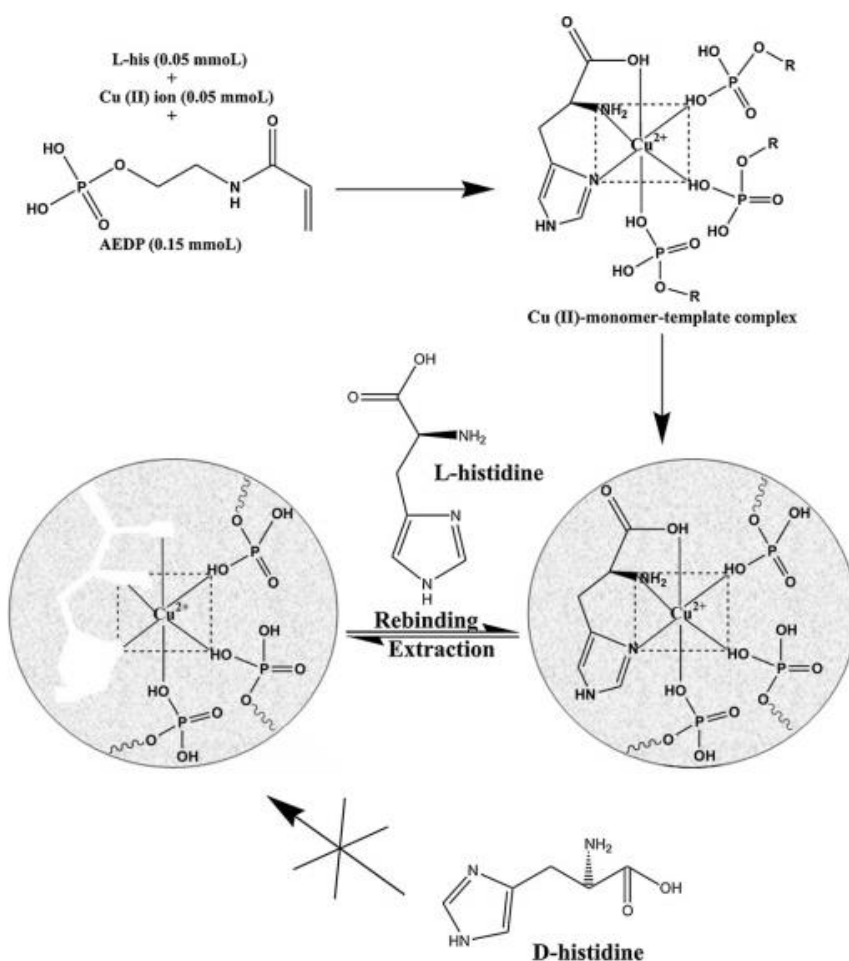


Figure 2-11. Illustration of metal ion mediated imprinting approach on L-histidine imprinted polymer (adapted from Prasad *et al.*, 2011) ⁸²

2.2.2 Composition

Next factor for obtaining MIPs is how to prepare an appropriate composition for it. The effective synthesis of molecular imprinting depends on the template^{84,85} (a target compound), functional monomers^{86,87}, crosslinkers,^{88,89} initiator⁹⁰, and solvent^{91,92}. Therefore, all these components of the MIP will be mentioned in this section because the composition would affect the physical and chemical properties of MIPs, such as particle size, solubility, selectivity, stability and rigidity.

2.2.2.1 Template

Definition of the template could be small or large compounds, metals, proteins, or microorganisms. Besides that, the template could be a synthetic molecule, as Steinke *et*

al., 1995 pointed out.⁸⁵ Unfortunately, not all molecules could be a template depending on their functionality, size and stability.

One of the essential characteristics of the template is its functionalities. These could be the group of hydroxyl, carbonyl, carboxyl, and amide or double bonding. These factors would affect the interaction between the template and functional monomers either covalent or non-covalent interaction. Sometimes, a template has two or more functionalities, as called multiplicity of functional groups. This template could produce molecular imprinting with many active sites. In this research, the template used is FB1 (Figure 2-12) having four carboxyl groups, three hydroxyl groups, and one amino group. Thus, it tends that molecular imprinting obtained would have a cavity with many binding sites.

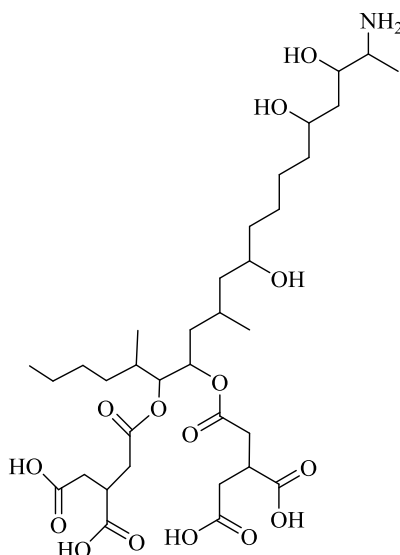


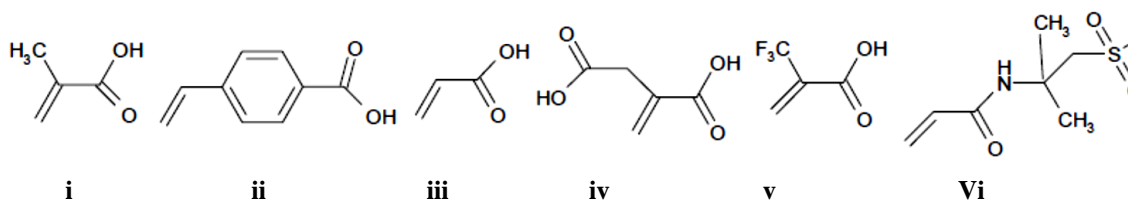
Figure 2-12 The structure of Fumonisin B1

Another significant aspect of the template is its size and stability. The size would have an influence on polymerisation and removal process. Also, the size can affect the size of molecular imprinting. The bigger template would produce the bigger molecular imprinting site. Lastly, the stability is an essential typical of the template in the synthesis of molecularly imprinting. The template is hoped to be inert during polymerisation process. Also, the template can adapt to the environment of polymerisation process. Therefore, although all compounds can be used as a template, the functionalities, size and stability would be a consideration.

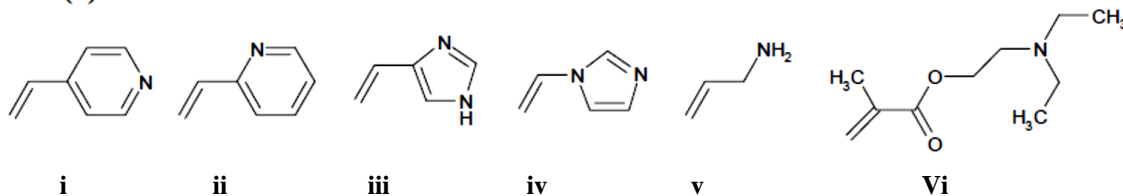
2.2.2.2 Functional Monomers

The interaction between functional monomers and template could be a crucial factor in the preparation of MIPs. This interaction would initiate a cavity in advance. The stronger the template-monomer interaction, the higher the selectivity of the MIPs. The strength of interaction depends probably on the functionalities of functional monomers.

Acidic (a)



Basic (b)



Neutral (c)

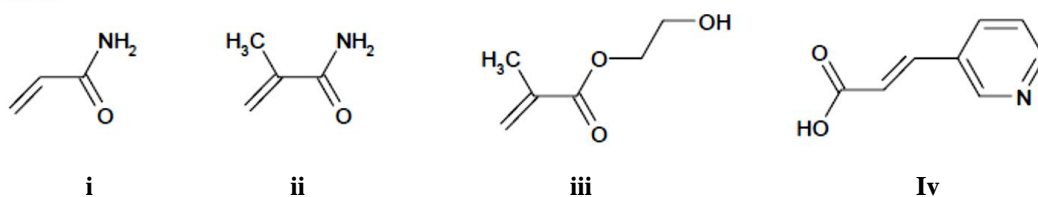


Figure 2-13. Several functional monomers with different types, **acid (a)** i : methacrylic acid (MAA), ii: *p*-vinyl benzoic acid , iii: acrylic acid (AA), iv: itaconic acid, v: 2-(trifluoromethyl)-acrylic acid (TFMAA) vi: acrylamide-(2-methyl)-propane sulfonic acid (AMPSA); **base (b)** i : 4-vinylpyridine (4-VP), ii: 2-vinylpyridine (2-VP), iii : 4-(5)-vinylimidazole, iv: 1-vinylimidazole, v: allylamine, vi : *N,N*-diethyl aminoethyl methacrylamide (DEAEM); and **neutral (c)** i : acrylamide, ii : methacrylamide, iii : 2-hydroxyethyl methacrylate (2-HEMA), iv : *trans*-3-(3-pyridyl)-acrylic acid (adapted from Cormack & Elorza, 2004)⁹³

The functional group could be hydroxyl, carbonyl, carboxyl, and amide that will interact with the template. Because of having different functional groups, the functional monomers are divided into three parts such as acid, base and neutral. Acid monomers have mostly hydroxyl, carbonyl, or carboxyl group whereas base monomers have mostly amide or amine while the neutral monomers have sometimes both of functional groups as can be seen in Figure 2-13.

The type of functional monomers could be negative for acid or positive for the base. This charge cause electrostatic or dipole-dipole interactions with the template. Unlike acid and base functional monomers, neutral type of charge gives Van der Waals interaction. Consequently, the three types of functional monomers could be considered to react with the template.

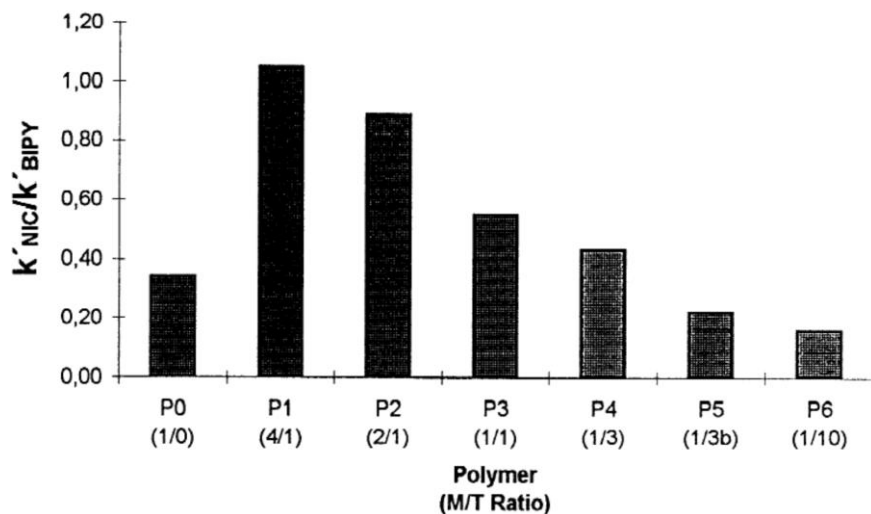
The ratio of functional monomers to the template can affect the selectivity of the imprinted polymer. It is reported that the excess of the template could decrease the selectivity of bipyridyl to nicotine (k'_{NIC}/k'_{BIPY}). Figure 2-14 (a) shows that the ratio of functional monomer and template to the selectivity of molecularly imprinted polymer to nicotine. The composition of P6 shows the lowest selectivity because of the highest concentration of template.⁸⁷ Similarly with the template, the functional monomers should have appropriate composition because it could reduce the selectivity of the imprinted polymer. Figure 2-14 (b) illustrates that the highest concentration of functional monomers could decrease the selectivity of molecularly imprinted polymer to 3H-theophylline.⁹⁴ Hence, the formulation of functional monomers could calculate correctly to obtain the higher selectivity of the imprinted polymer.

2.2.2.3 Crosslinkers

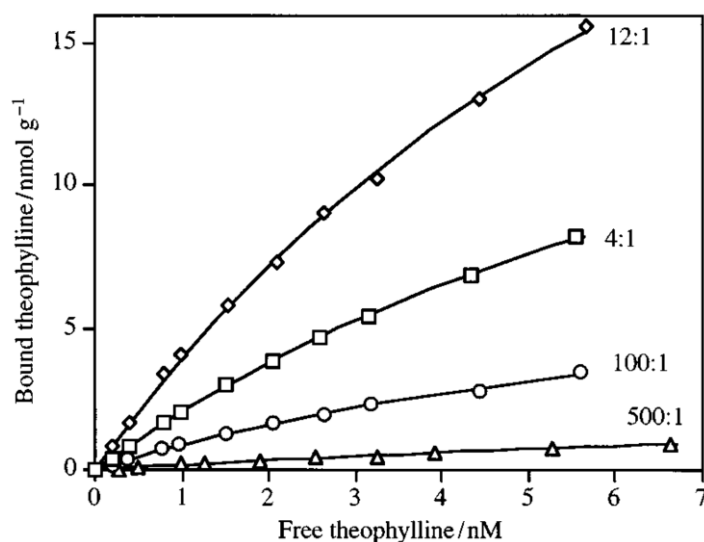
Maintaining the template-functional monomers interaction, the crosslinkers is used to obtain the rigid matrix of the polymer. Some researcher state that the crosslinkers are like the glue that has two or more double bond to form the rigid crosslinked network.

Crosslinkers have at least three functions, controlling the morphology of polymer, stabilising the binding sites of the polymer and conveying the mechanical stability of matrix polymer. Thus, the performance of molecular imprinting could be affected by crosslinkers.

The crosslinkers could be influenced on the morphology of polymer, as Wong *et al.*, 2015 pointed out, such as swelling and mesh size. It is reported that the higher concentration of pentaerythritol tetra acrylate (PETRA), as a cross-linking agent, significantly reduce the percentage of swelling of polyethylene oxide (PEO) hydrogels.



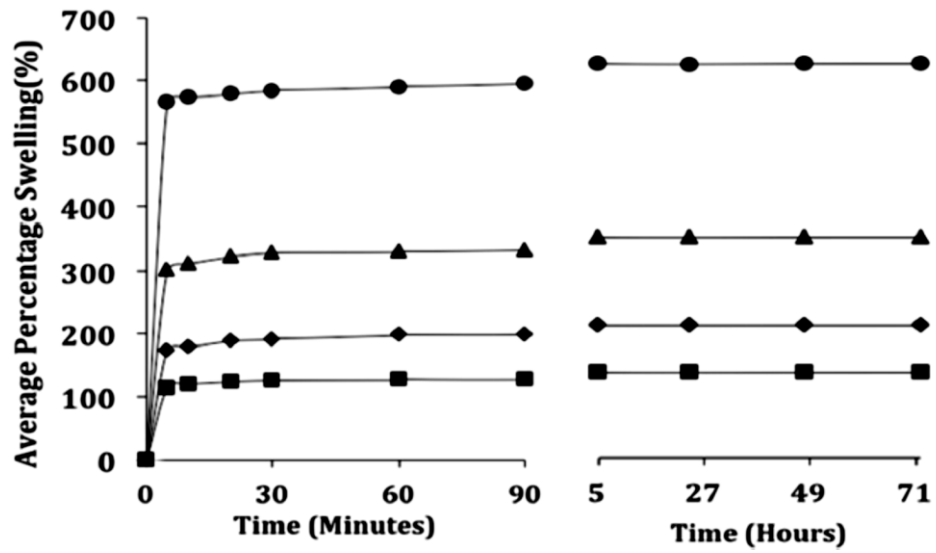
(a)



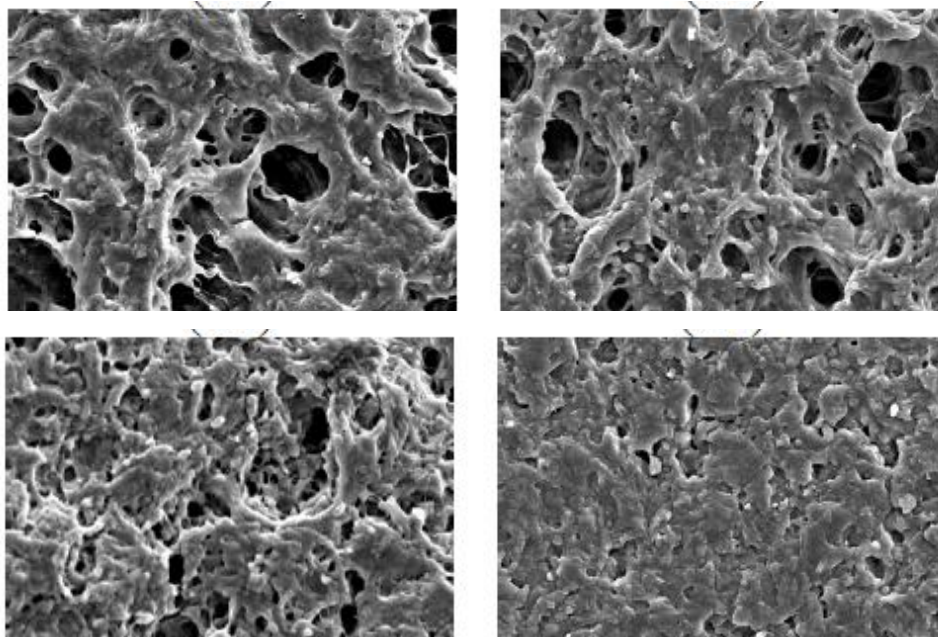
(b)

Figure 2-14. (a) Selectivity (k'_{NIC}/k'_{BIPY}) for nicotine and bipyridyl by different M/T ratio (b) Binding isotherms of 3H-theophylline binding to imprinted polymers prepared with M : T of 4 : 1, 12 : 1, 100 : 1 and 500 : 1. (adapted from Yilmaz *et al.*, 1999 and Andersson *et al.*, 1999)^{87,94}

Figure 2-15 (a) shows that 1% w/w of PETRA imparts the highest proportion of swelling of PEO. These results will be influenced by mesh size of PEO as can be seen in Figure 2-15 (b). The upper concentration of cross-linker reduces the distance between two adjacent crosslinkers.⁹⁵ Therefore, it seems that the pore size of the particle is relatively smaller when adding the less concentration of crosslinkers.



(a)



(b)

Figure 2-15. (a) Effect of PETRA concentration on the % swelling values of PEO hydrogels (b) SEM images of freeze-dried PEO hydrogels. (A) PEO-PETRA 1% w/w, (B) PEO-PETRA 2.5% w/w, (C) PEO-PETRA 5% w/w, (D) PEO-PETRA 10% w/w (adapted from Wong *et al.*, 2015)⁹⁵

Furthermore, the essential function of crosslinkers is to stabilise the binding sites of the polymer. This feature would keep template-functional monomer interaction. In this case, the crosslinker is used for making the matrix of the imprinted polymer. Consequently, the cavity of the polymer could be formed containing the strongly binding site. The variation of crosslinker concentration, called the degree of cross-linking, could influence the interaction with the template. One study stated that around 50 – 75% is the best interval degree of crosslinkers for the synthesis of polymers.(sellergen) Another study claimed that the best range is between 62.5 – 75%.⁹⁶ However, both of results are not ideal formula because the current study obtains that the best result for the degree of cross-linking is around 83.3%.⁸⁸ Hence, the best degree of crosslinkers for the synthesis of the molecularly imprinted polymer could be 50 - 85%.

Besides stability and morphology, the crosslinkers could impart the mechanical stability of the imprinted polymer such as area surface, pore volume, pore size, particle size, thermal gradation, glass translation, and polymer swelling.⁹⁷ Despite that many reports stated about this function, there is less information for supporting connected to the performance of the imprinted polymer directly. In general, it is mentioned that the mechanical stability would be affected by the quality of molecularly imprinted polymer.

Many chemical materials could be a cross-linker. Mostly, crosslinkers have many vinyl groups to prepare matrix. Figure 2-16 demonstrates the commonly crosslinkers used in several previous experiments. However, not all of them can be compatible for generating the imprinted polymer. Thus, using the different type of crosslinkers would obtain the different of the performance of molecular imprinting.

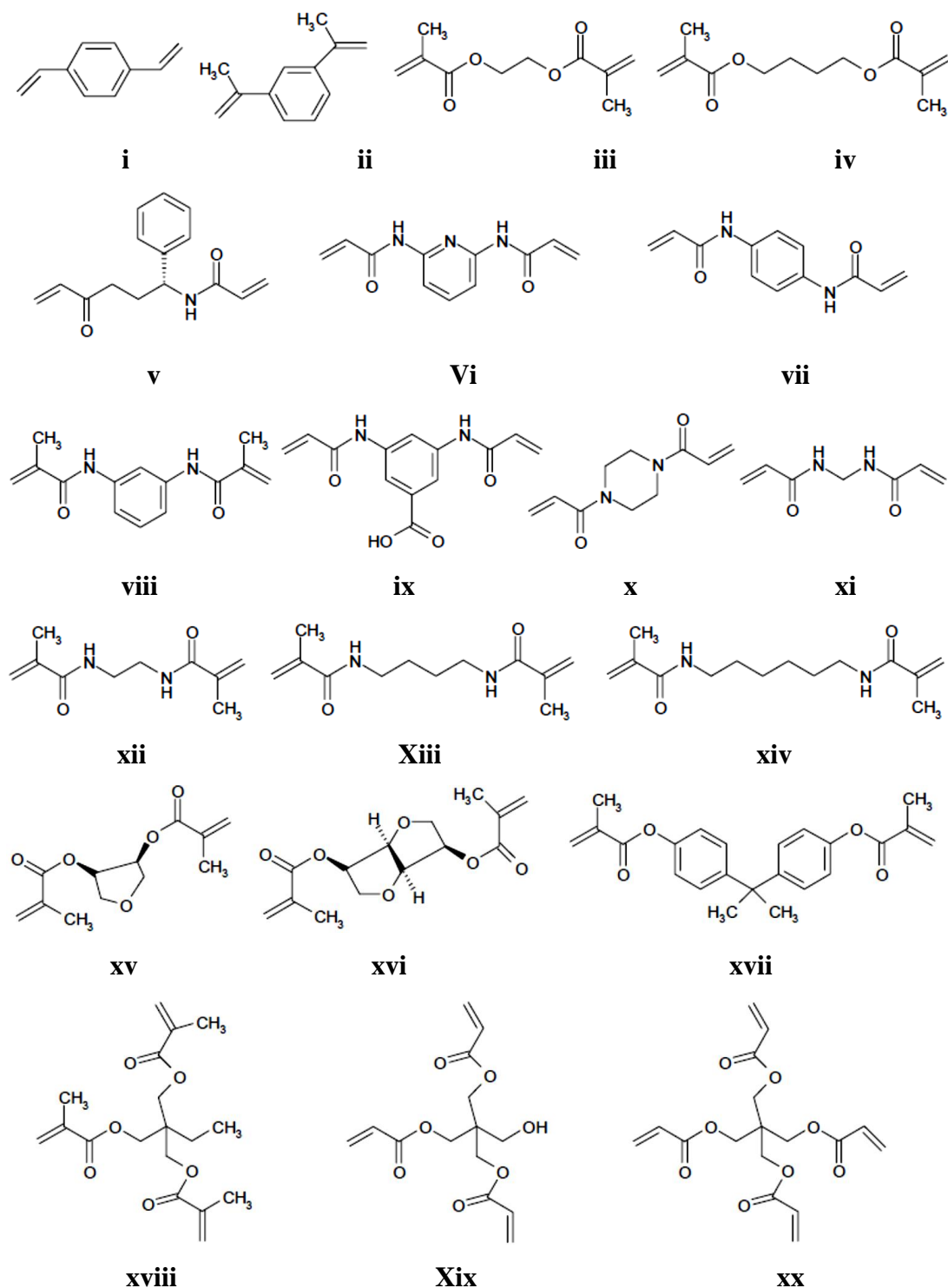


Figure 2-16. Selection of crosslinkers used for molecular imprinting. **i**: *p*-divinylbenzene (DVB); **ii**: 1,3-diisopropenyl benzene (DIP); **iii**: ethylene glycol dimethacrylate (EGDMA); **iv**: tetramethylene dimethacrylate (TDMA); **v**: *N,O*-bisacryloyl-L-phenylalaninol; **vi**: 2,6-bisacryloylamidopyridine; **vii**: 1,4-phenylene diacrylamide; **viii**: *N,N'*-1,3-phenylenebis(2-methyl-2-propenamide) (PDBMP); **ix**: 3,5-bisacrylamido benzoic acid; **x**: 1,4-diacryloyl piperazine (DAP); **xi**: *N,N'*-methylene bisacrylamide (MDAA); **xii**: *N,N'*-ethylene bismethacrylamide; **xiii**: *N,N'*-tetramethylene bismethacrylamide; **xiv**: *N,N'*-hexamethylene bismethacrylamide; **xv**: anhydroerythritol dimethacrylate; **xvi**: 1,4;3,6-dianhydro-D-sorbitol-2,5-dimethacrylate; **xvii**: isopropylenebis(1,4-phenylene) dimethacrylate; **xviii**: trimethylpropane trimethacrylate (TRIM); **xix**: pentaerythritol triacrylate (PETRA); **xx**: pentaerythritol tetraacrylate (PETEA) (adapted from Cormack & Elorza, 2004)⁹³

2.2.2.4 Initiator

The best initiator is an important part of polymerisation composition because there is not reaction without any initiator. The initiator is employed in propagation and termination on polymerisation. These parts are a crucial moment because the polymerisation would be working. Several initiators can be seen in Figure 2-17.

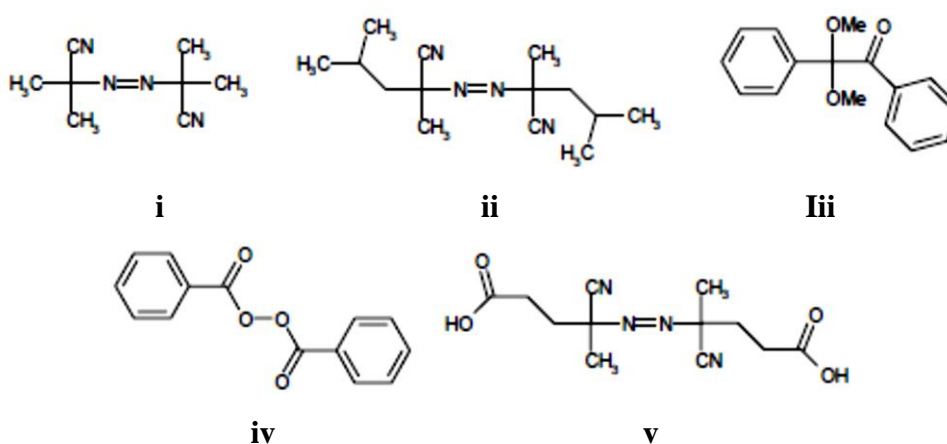


Figure 2-17. Structure of initiators: **i**: azobisisobutyronitrile (AIBN); **ii**: azobisdimethylvaleronitrile (ABDV); **iii**: dimethylacetal of benzil; **iv**: benzoylperoxide (BPO); **v**: 4,4'-azo(4-cyanovaleric acid) (adapted from Cormack & Elorza,2004)⁹³

Commonly, the initiator can be working optimally under light, thermal, or chemical condition and become a free radical component. Figure 2-18 illustrates the example of two initiators in the previous study, 1,1-azobis(cyclohexane-1-carbonitrile) (ACC) and 2,2-dimethoxy-2-phenylacetophenone (DMPA). These initiators have different decomposition process. To be a radical compound, AAC uses the Azo group, -N=N-, to stabilise the radical site under thermal or UV condition. Unlike ACC, DMPA uses benzene ring and oxygen to produce the benzyl ketal radical and the methyl radical under UV condition. Thus, it seems that the initiator could be a radical component by different method depending on the functional group owned.^{90,98,99}

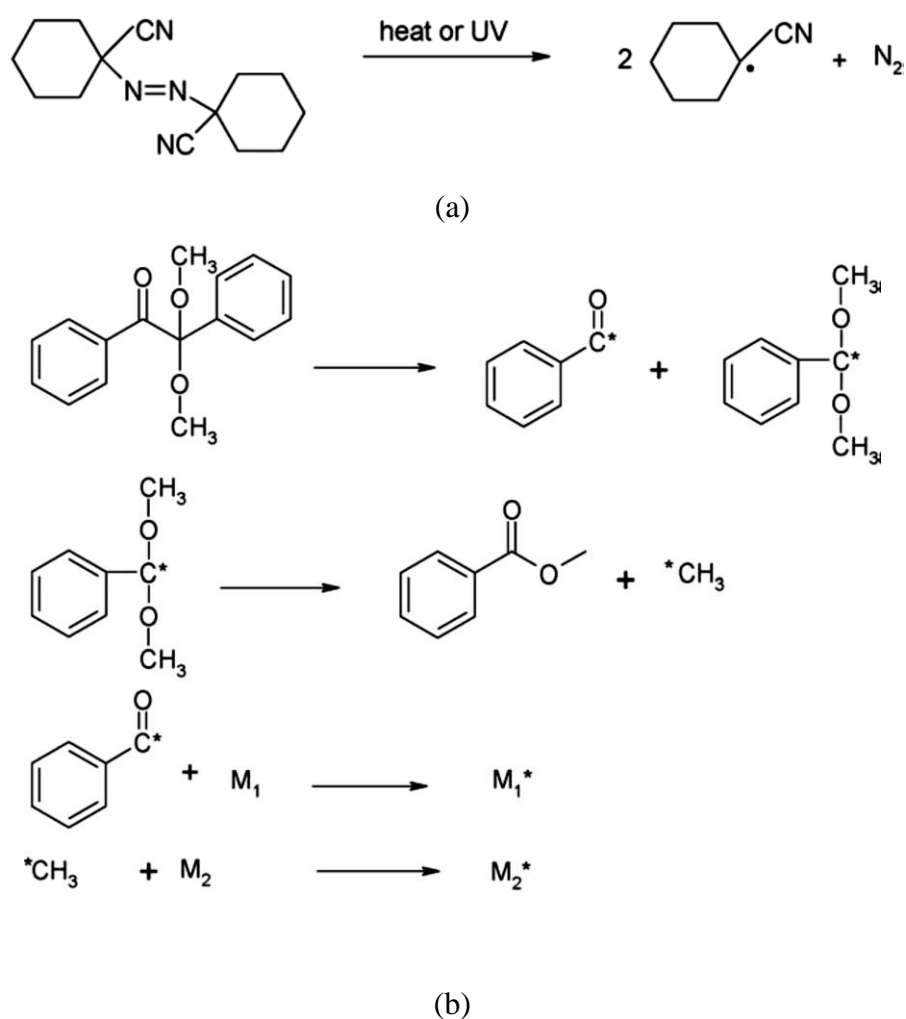
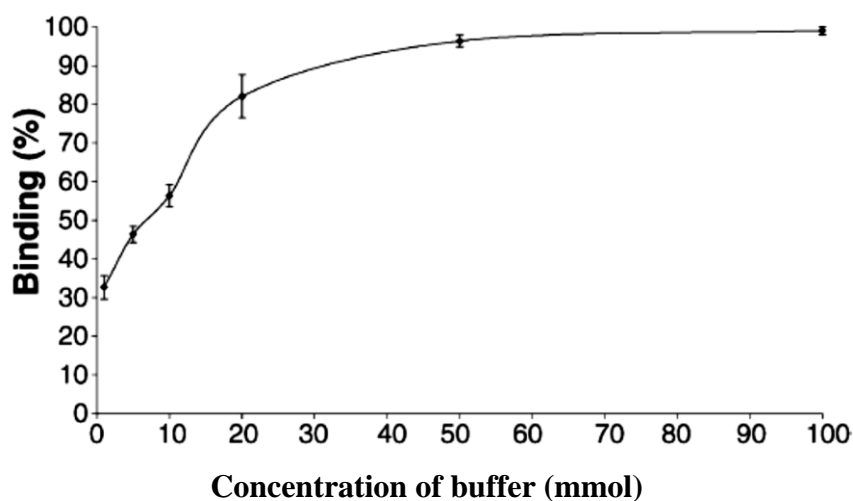


Figure 2-18. Decomposition of AAC (a) and DMPA (b) (adapted from Mijangos *et al.*, 2006)⁹⁰

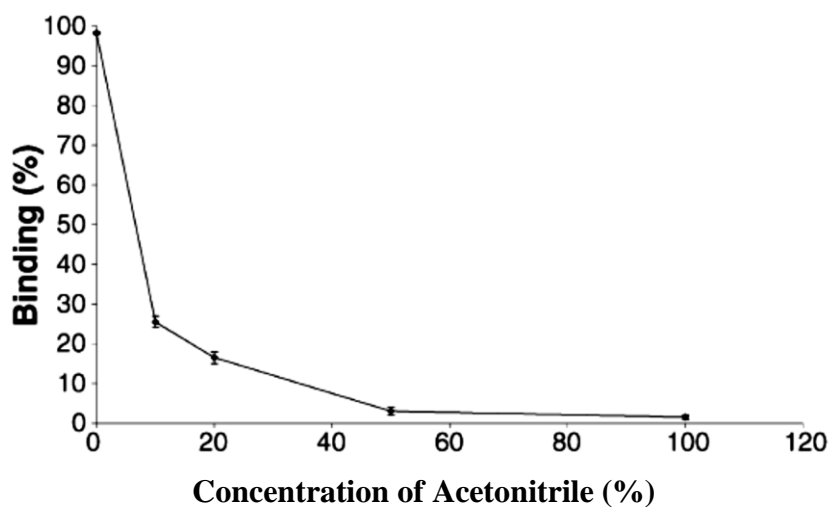
It is said that the thermal initiation is better than photoinitiation to produce a powerful polymer.⁹⁰ However, Piletsky *et al.*, 2004 claimed that low temperature could produce stronger template-functional monomer complex.¹⁰⁰ After that, the concentration of initiator can affect the polymerisation. It is stated that the higher amount of initiator can interfere the template-functional monomer interaction and yield many radicals. other said that the higher concentration of initiator would obtain the imprinted polymer with the large surface.⁹⁰ Therefore, it is possible that the temperature and concentration of initiator are an essential parameter and could control during polymerisation.

2.2.2.5 Solvent

The solvent is the last component to generate the molecularly imprinting successfully. The solvent would facilitate media for polymerisation. According to polarity, the type of solvent could be polar and nonpolar. Then, the polar solvent could be divided into protic and aprotic based on the abundance of O-H and N-H. Protic polar has more O-H and N-H than aprotic polar. This structure will impact to interaction with other components in polymerisation. One effect of this property of solvent is binding capacity or interaction between the template and functional monomer. Figure 2-19 demonstrates the different response of binding OTA to imprinted polymer in a various solvent.



(a)



(b)

Figure 2-19. Percentage of binding 100 ppb Ochratoxin (OTA) to Imprinted polymer in buffer (a) and acetonitrile (b) solution (adapted from Turner *et al.*, 2004)¹⁰¹

The positive results are happened in buffer solution otherwise in acetonitrile medium.¹⁰¹ Unlike the previous experiment; the organic solvent gave the effective response. The reason is that there are many interactions between solvent unpredictable with template-polymer such as electrostatic force, van der Waals force, and hydrogen bonding.^{90,102} Despite that there is less certain data about the effect of solvent accurately and steadily, the solvent will impact the performance of the imprinted polymer.

As previously stated, the solvent also has a contribution to a mesh size of the polymer. It is because of the conformation of polymer to solvent. A study reported that the particle size of polymer in a water medium is larger than in buffer solution.⁹¹ Therefore, the selection of solvent is an important factor to synthesis molecularly imprinted polymer.

2.2.3 Polymerisation

Having discussed the composition of MIP, polymerisation would be mentioned in this section. The MIP is categorised in copolymers based on monomer composition including functional monomers and crosslinkers. Also, since this composition of MIP includes functional groups and double bonds, both condensation and addition polymerisation methods could be used to generate the MIP.¹⁰³

Polymerisation is a process to connect among template, functional monomers, and crosslinkers in a solvent helped by an initiator to be an imprinted polymer. This process could be an important step requesting ideal condition such as temperature. Either low or high temperature would result different the quality of molecular imprinting. Mostly, the polymerisation method used is free radical polymerisation having three steps such as initiation, propagation and termination.

Firstly, free radicals are produced by either thermal, light, electron transfer (redox) processes. This process is called initiation. After generating free radical compound, the functional monomers are attacked. Then, this monomer will react with crosslinkers to form a polymer which attaches the template to form molecular imprinting. Lastly, the polymerisation will be stopped by deactivating the free radical polymerisation. This process is called termination owning three types such as combination, disproportionation,

and radical transfer to the monomer. The illustration of this mechanism can be seen in Figure 2-20.

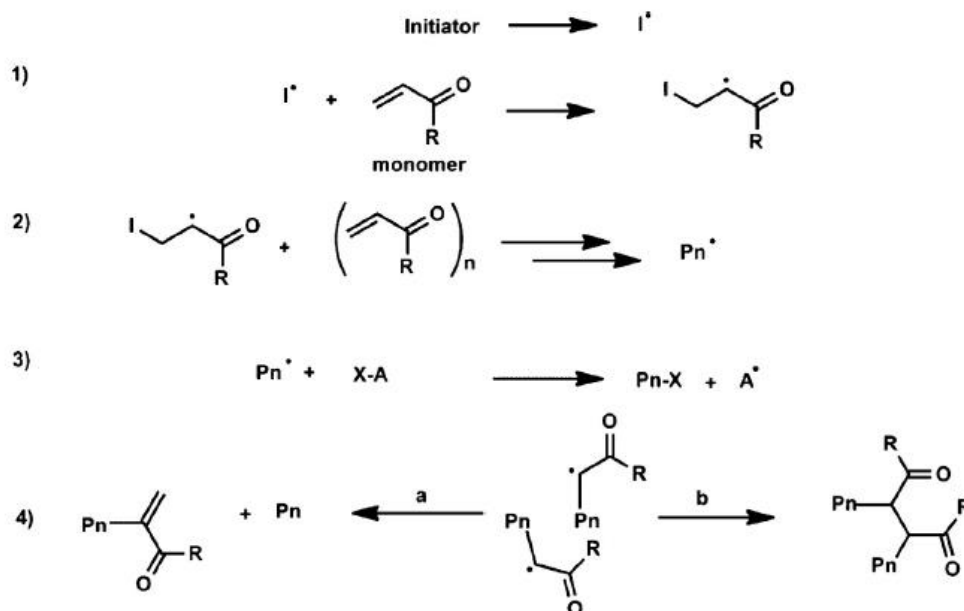


Figure 2-20 Mechanism of free radical polymerisation: (1) initiation, (2) propagation, (3) chain transfer, (4) termination via (a) disproportionation and (b) combination (adapted from Belyazit *et al.*, 2016)¹⁰⁴

2.2.3.1 Solid Phase Method

After defining the polymerisation process, the solid phase protocol for generating molecularly imprinted polymer nanoparticles (nanoMIPs) is discussed. Traditionally, several polymerisation techniques have been applied in many research such as Bulk, solution, suspension, and emulsion for producing a polymer.¹⁰⁵ However, it would be very hard to produce polymer nanoparticles having characteristics as a high selectivity antibody.

Solid phase synthesis use solid materials to immobilise a target compound, such as glass beads, in order to obtain a single particle of polymer specifically to template. By contrast, many traditional methods, such as bulk polymerisation, is not through immobilisation process. As a result, the formed polymers have binding sites heterogeneity.¹⁰⁶ Because of this different technique, it could be argued that polymer synthesised by solid phase method is more selective than by traditional polymerisation.

CHAPTER 3 DEVELOPMENT OF MOLECULARLY IMPRINTED POLYMER NANOPARTICLES FOR FUMONISIN B1

3.1 Introduction

The performance of molecular imprinted nanoparticles (nanoMIPs) depends on the composition of the polymer, especially functional monomers, as mentioned in Section 2.2.2.^{86,87} In previous reports, nanoMIPs for fumonisin B2 (FB2) have been produced from several functional monomers, such as *N*-(3-aminopropyl) methacrylamide hydrochloride (NAPMA), *N*-isopropylacrylamide (NIPAm), acryl amide (AA) and *N*-tert-butylacrylamide (TBAm).¹⁰⁷ This study would be the first study describing the use of nanoMIPs based ELISA for mycotoxins, FB2.

In this chapter, the functional monomers of nanoMIPs for fumonisin B1 (FB1) were identified by combining empirical studies and computational modelling. It was expected that this combination would generate nanoMIPs with enhanced affinity to FB1. Three monomers were taken from a previous study (NAPMA, NIPAm, TBAm)¹⁰⁷, and another monomer was taken from a simulation using molecular mechanics.

Molecular mechanics (MM) is a well-known method for identifying useful monomers for producing molecularly imprinted polymers.¹⁰⁸⁻¹¹¹ This simulation uses the energy potential from empirical data collected from X-ray crystallography and NMR experiments. The empirical evidence is represented by the energy of force field components such as bond stretching, angle bending, torsion term, and non-bonded interactions (electrostatic and van der Waals) as can be seen in Equation 3-1 and Figure 3-1.^{97,112} Furthermore, the binding energy of molecules could be calculated by the change of Gibbs free energy (ΔG) described in Equation 3-2. This equation is the same as previous equation (3-1) but the energy would be represented as the average of Gibbs free energy of molecular mechanics force field of the complex formed by the template and functional monomers. Besides that, MM has been used for many targets.¹¹³ Therefore, it could be concluded that the molecular mechanics can be applied in this study to find the best functional monomer for Fumonisin B1.

$$\mathcal{V}(r^N) = \sum_{\text{bonds}} \frac{k_i}{2} (l_i - l_{i,0})^2 + \sum_{\text{angles}} \frac{k_i}{2} (\theta_i - \theta_{i,0})^2 + \sum_{\text{torsions}} \frac{V_n}{2} (1 + \cos(n\omega - \gamma)) + \sum_{i=1}^N \sum_{j=i+1}^N (4\epsilon_{ij} \left[\left(\frac{\sigma_{ij}}{r_{ij}} \right)^{12} - \left(\frac{\sigma_{ij}}{r_{ij}} \right)^6 \right] + \frac{q_i q_j}{4\pi\epsilon_0 r_{ij}}) \quad (3-1)$$

Where : $\mathcal{V}(r^N)$ = the potential energy, $\sum_{\text{bonds}} \frac{k_i}{2} (l_i - l_{i,0})^2$ = bond energy, $\sum_{\text{angles}} \frac{k_i}{2} (\theta_i - \theta_{i,0})^2$ = angle energy, $\sum_{\text{torsions}} \frac{V_n}{2} (1 + \cos(n\omega - \gamma))$ = torsion energy, and $\sum_{i=1}^N \sum_{j=i+1}^N (4\epsilon_{ij} \left[\left(\frac{\sigma_{ij}}{r_{ij}} \right)^{12} - \left(\frac{\sigma_{ij}}{r_{ij}} \right)^6 \right] + \frac{q_i q_j}{4\pi\epsilon_0 r_{ij}})$ = non bonded interaction

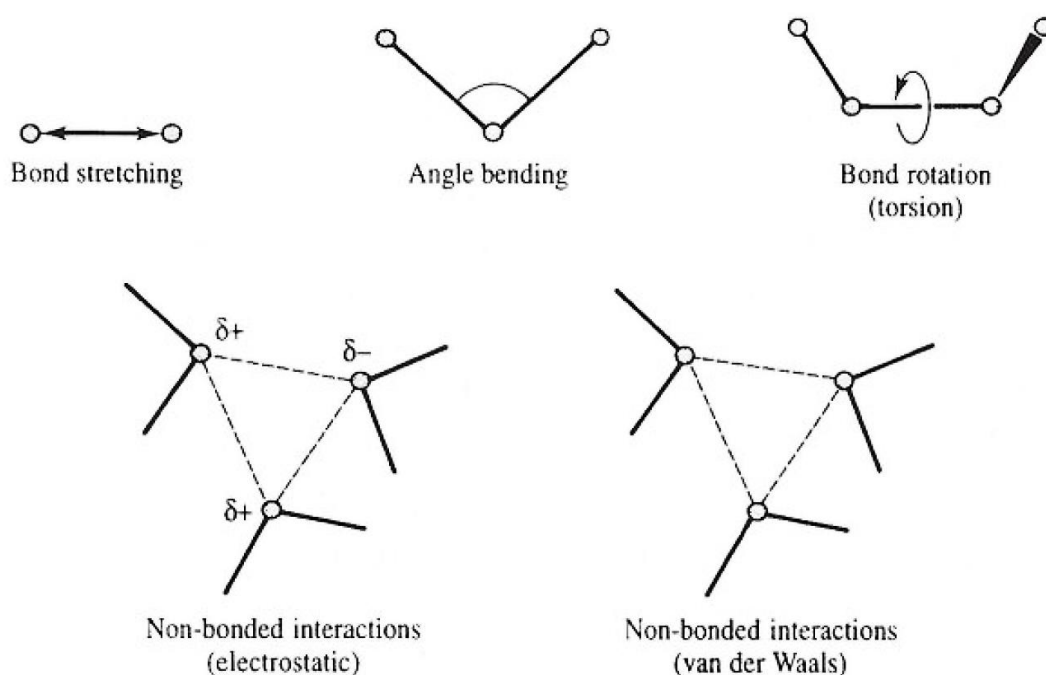


Figure 3-1 Illustration of molecular mechanics force field: bond stretching, angle bending, torsion term, and non-bonded interaction (adapted from Leach, 1996)¹⁴

$$\Delta G_{\text{bind}} = \Delta G_{\text{t+r}} + \Delta G_{\text{r}} + \Delta G_{\text{h}} + \Delta G_{\text{vib}} + \sum \Delta G_{\text{p}} + \Delta G_{\text{conf}} + \Delta G_{\text{vdW}} \quad (3-2)$$

ΔG_{bind} = complex formation, $\Delta G_{\text{t+r}}$ = translational (energy associated with the motion) and rotational (energy associated with rotation); ΔG_{r} = restriction of rotors upon complexation; ΔG_{h} = hydrophobic interactions; ΔG_{vib} = residual soft vibrational modes; $\sum \Delta G_{\text{p}}$ = the sum of interacting polar group contributions; ΔG_{conf} = adverse conformational changes; and ΔG_{vdW} = unfavourable van der Waals interactions.

In this section, the best functional monomer was identified using Sybyl 7.3 software using MM methods and LEAPFROGTM algorithm as used in preceding research by Piletsky's group.¹¹⁵ Furthermore, LEAPFROGTM was used in this work to obtain information of the interactions between template and 26 functional monomers shown by the binding energy score from the calculation of inter and intramolecular binding. In the end, the monomers were ranked based on energy of their complex with the template.

Firstly, the enantiomer of FB1 was drawn. The potential energy of FB1 was then minimised in two conditions (vacuum and water) by using MM to find the most stable energy minimised structure of FB1. The LEAPFROGTM algorithm was employed for obtaining a database of energy interaction between functional monomer and FB1. The two best monomers identified by their high binding score to FB1 were ethylene glycol methacrylate phosphate (EGMP) and *N,N*-diethylamino ethyl methacrylate (DEAEM). These results were confirmed by affinity chromatography using polymer solid phase extraction (SPE). Production of nanoMIPs was achieved using solid phase synthesis method.¹¹⁶ Dynamic light scattering (DLS) was used for identifying size of nanoparticles confirmed by transmission electronic microscopy (TEM), while FT-IR spectrometer was used for identifying functional group, and surface plasmon resonance (SPR) was used for obtaining dissociation constant values. This chapter aims to develop high-affinity nanoMIPs for FB1.

3.2 Materials and Methods

3.2.1 Materials

Fumonisin B1 (FB1) was purchased from ChemCruz, USA. Ethylene glycol methacrylate phosphate (EGMP), *N,N*-diethylamino ethyl methacrylate (DEAEM), *N*-isopropylacrylamide (NIPAm) *N,N'*-methylene-bis-acrylamide (BIS), *N*-tert-butylacrylamide (TBAm), ammonium persulfate (APS), tetramethylethylenediamine (TEMED), Phosphate buffered saline (PBS), sodium hydroxide (NaOH), glutaraldehyde (GA), bovine serum albumin (BSA), horseradish peroxidase (HRP), 3,3',5,5'-tetramethylbenzidine (TMB), Tween 20, 2-[morpholino]ethanesulfonic acid (MES),

acetone, and [3-(2-aminoethyl amino)propyl] trimethoxysilane were purchased from Sigma-Aldrich, UK. N-(3-aminopropyl)methacrylamide hydrochloride > 98% (NAPMA) was purchased from Polyscience Inc., UK. Solid phase cartridges loaded with polymeric ethylene glycol methacrylate phosphate (EGMP) and *N,N*-diethylamino ethyl methacrylate (DEAEM), were synthesised through bulk polymerisation by members of Biotechnology group, Department of Chemistry, University of Leicester. Flat bottom polystyrene 96 well microplates were purchased from Elkay Laboratory Products, UK. Double-distilled ultrapure water (Millipore, UK) was used for the experiments. SPHERIGLASS® A-Glass 2429 (70 – 100 μm diameter, >70% SiO_2) were from Potters Industries LLC. All chemical and solvents were analytical or HPLC grade and used without any purification.

3.2.2 Equipment

Polypropylene solid-phase extraction (SPE) tubes 6 ml, disposable plastic syringes, filter membrane, 0.22 μm , magnetic stirrer hot plates, sintered disc filter funnel, buchner filter flasks, buchner filter cones, flat-bottom glass vessel 200 ml, amicon ultra-15 centrifugal filter units, glass vials, UV-visible spectrophotometer, dynamic light scattering (DLS) from Malvern Instruments Ltd, Biacore 3000 from GE Healthcare Life Sciences, plastic cuvettes 10 \times 10 \times 45 mm, oven, ultra-sonication bath, and vacuum pump, transmission electronic microscopy (TEM) from Gatan and microplate reader from Hidex Sense.

3.2.3 Computational design

There were several steps in finding a suitable monomer capable of interacting with FB1. Initially, an enantiomer of Fumonisin B1 structure was selected from Database PubChem based on its chirality such as R and S types.^{65,66} These structures were then drawn in three-dimension using Sybyl 7.3 and charged by the Gasteiger-Huckel computational procedure. The potential energy of 3D structure of Fumonisin B1 was then minimised to 0.001 Kcal mol⁻¹ and refined by molecular mechanics.^{108,115,117} This procedure was done in two conditions treated in two different dielectrics constant, such as vacuum ($\epsilon = 1$) and water ($\epsilon = 80$). In the last step, a LEAPFROGTM algorithm was used to screen a virtual library of 26 functional monomers and select the two best functional monomers which can interact with FB1 according to high binding energy score.^{108,115,117}

3.2.4 Testing of polymer binding

After modelling, two functional monomers were selected according to their binding scores: EGMP and DEAEM. To verify the affinity of the functional monomers to the template experimentally, we have used chromatography separation. For that, solid phase extraction (SPE) cartridges were loaded with 50 mg of the polymer made of EGMP and DEAEM. After that, FB1 standard solution was loaded and non-bound material eluted from the SPE. The binding was assessed by measuring the absorbance of the solution before (A_{BE}) and after elution (A_{AE}) at 282.5 nm. The binding efficiency was calculated as shown in Equation 1.

$$\text{Binding (\%)} = \frac{A_{BE} - A_{AE}}{A_{BE}} \times 100\% \quad 3-3$$

3.2.5 Synthesis of nanoMIPs for FB1

There are two steps in the synthesis of nanoMIPs using solid phase method: immobilisation of FB1 on glass beads and polymerisation of nanoMIPs. In general, the procedure used here followed Canfarotta *et al.*, 2015.¹¹⁶

(1) Immobilisation of FB1 on glass beads

Before immobilising FB1, 60 g of glass beads were activated by boiling in 1 M NaOH (0.8 ml of solution per g of glass beads) for 15 min. Glass beads were then rinsed by deionized water (eight times with 200 ml) and PBS (300 ml) to neutralise the base, and washed three more times with deionized water to remove salt residues. The glass beads were rinsed with acetone (twice with 200 ml) and dried at 80 °C for 3 h. Dried glass beads were incubated in [3-(2-aminoethylamino)propyl] trimethoxysilane solution 2% (v/v) in anhydrous toluene (0.4 ml of solution per g beads) overnight at room temperature in a bolted container of suitable volume. Next the glass beads were decanted onto a sintered disc filter funnel and rinsed with at least eight volumes of acetone and one volume of methanol. Finally, the activated glass beads were dried under vacuum and moved to a container of suitable volume.

For immobilising FB1, the activated glass beads were then incubated in 7% (vol/vol) GA solution in 0.01 M PBS, pH 7.2 for 2 hours, filtered, and washed with deionized water. These beads were then incubated in 0.01 mg mL⁻¹ FB1 in 0.01 M PBS, pH 7.4, overnight at room temperature. The FB1 functionalised beads were treated with 1 mg mL⁻¹ sodium cyanoborohydride in PBS 0.01 M (0.4 mL of solution per g of glass beads) for 30 min at room temperature. Finally, the FB1-immobilised glass beads were filtered, rinsed with double-distilled ultrapure water, dried, and stored in a glass container of suitable volume.

(2) Synthesis of nanoMIPs

The monomer mixture containing 39 mg NIPAM, 2 mg BIS, 33 mg TBAm dissolved in 2 mL ethanol, 67.2 mg EGMP (selected monomer from molecular modelling), and 2.2 mg NAPMA, was dissolved in 100 mL double-distilled ultrapure water and sonicated for 5 min. This solution (5 mL) was afterwards degassed with nitrogen for 1 hour and added to 6 g glass beads bearing the immobilised FB1. The polymerisation was initiated chemically by adding and shaking gently 0.5 mL APS (60 mg mL⁻¹) containing TEMED (30 µL). The mixture was polymerised at room temperature overnight. After this time, the beads were transferred into an SPE cartridge (5 mL) fitted with a 20 µm porosity PE frit. Unreacted monomers and other low-affinity materials were removed by eluting with cold water at 4 °C (10 x 3 mL). The cartridge was then put in a water bath at 70 °C, and eluted with hot water (10 x 3 mL) producing fraction of high affinity at 60 °C.

3.2.6 Characterisation of nanoMIPs imprinted with FB1

(1) Concentration and particle size

The concentration of nanoMIPs was determined by measuring absorbance at 197 nm and comparing with a standard solution of nanoMIPs prepared (appendix 1). The hydrodynamic size of nanoMIPs for FB1 was then characterised by a ZetaSizer Nano ZS (Malvern Instruments Inc, UK) with dynamic light scattering (DLS). About 2 mL nanoMIPs of FB1 was sonicated homogeny and analysed by DLS.

(2) Image

Transmission Electron Microscopy (TEM) images of nanoMIPs were taken using a JEOL JEM 1010, 100 kV high contrast TEM equipped with a Gatan SC1000 Orius CCD camera (Gatan, Abingdon Oxon, UK). Samples for the analysis were prepared by depositing a drop of the nanoMIPs dispersion, previously filtered through a 1.2 μm PES syringe filter, on a carbon-coated TEM copper grid (400 mesh), and leaving them to dry at room temperature.

(3) Functional groups

The nanoMIPs in solid and solution phase were prepared and measured by Spectrum One FT-IR Spectrometer, PerkinElmer at 4000-500 cm^{-1} .

(4) Dissociation constant

The experiments were performed on SIA Au SPR gold chips (GE Healthcare) modified with mercaptoundecanoic acid. Bare gold chips were first cleaned by hydrogen plasma at 50 W for five minutes with an Emitech K1050X Plasma Cleaner (Emitech) and then placed in ethanol containing 2.2 mg/ml mercaptoundecanoic acid, overnight in a sealed vial. After surface modification, chips were rinsed with ethanol and dried under a stream of N_2 , assembled in the holder following the manufacturer instructions and docked in the SPR instrument (Biacore 3000, GE Healthcare). For ligand coupling, the chips were activated by injection of 50 μl EDC 0.2 M and NHS 0.05 M in water at 5 $\mu\text{l}/\text{min}$, followed by 1 injection of FB1 (at 0.1 mg/ml) in phosphate buffer at 5 $\mu\text{l}/\text{min}$ until around 1000 RU were reached. Remaining NHS esters were deactivated by injection of 100 μl of ethanolamine hydrochloride (0.1 M) at 10 $\mu\text{l}/\text{min}$ in PBS. The nanoMIPs were then separately injected onto the FB1-modified chip in concentrations ranging from 378 nM to 12 μM . A control channel passivated with ethanolamine was used as a control. The analysis was performed in 1 \times PBS at pH 7.4. Kinetic analysis of the sensorgram was performed with the BiaEvaluation software v4.1 assuming a 1:1 Langmuir binding model.

3.3 Results and Discussion

3.3.1 Modelling - minimisation of the energy of FB1

The minimisation of energy was conducted for enantiomer, R and S. Thus, both R and S type were drawn as 3D structure in two conditions: vacuum and water, and their energy refined by a molecular mechanics.¹¹⁵ This would be interesting to check whether FB1 has different minimised energy according to its chirality in a different environment.

Table 3-1. The minimised potential energy of FB1 structure in vacuum and water by molecular mechanics

Condition	Type	Energy (kcal mol ⁻¹)								
		BS	A	T	OPB	1-4vdW	vdW	1-4 Elec	Elec	Total
Vacuum	R	3.68	18.40	13.17	0.07	9.62	-12.70	-26.37	-21.61	-15.74
	S	3.56	16.16	10.84	0.10	8.90	-13.68	-24.79	-20.60	-19.51
Water	R	3.47	16.28	16.61	0.04	5.61	-12.34	-0.33	-0.55	+28.79
	S	3.54	16.19	15.57	0.08	6.50	-23.75	-0.32	-0.26	+17.56

BS: Bond Stretching Energy; A: Angle Bending Energy; T: Torsional Energy; OPB: Out of Plane Bending Energy; 1-4 vdW: 1-4 van der Waals Energy; vdW: van der Waals Energy; 1-4Elec:1-4 Electrostatic Energy; Elec: Electrostatic Energy

Table 3-1 shows that R and S enantiomer of FB1 in vacuum have slightly different potential energy especially in part related to angle bending, torsional, and electrostatic energy. The energy total of S enantiomer (-19.51 kcal mol⁻¹) is lower than R type (-15.74 kcal mol⁻¹). Unlike in vacuum, the potential energy of FB1 is hugely different in water (Table 3-1). These results are similar to these observed earlier for alanine.^{118,119} Moreover, the structure of FB1 could change to zwitterionic at pH 7 (Figure 3-2) and reduce intramolecular interactions.¹²⁰

Despite that FB1 is charged in water, the trend for total energy of FB1 in water is similar to vacuum. The energy for S enantiomer (+17.56 kcal mol⁻¹) is lower than for R enantiomer (+28.79 kcal mol⁻¹) (see Table 3-1). It suggests that S type is more stable than R type in both conditions. Accordingly, the S type was used for the next experiment to observe its interaction with the functional monomer in water (see in Section 3.3.2). Also, the water was employed for next experiment because the synthesis of nanoMIPs for FB1 was in aqueous conditions (see Section 3.3.4).

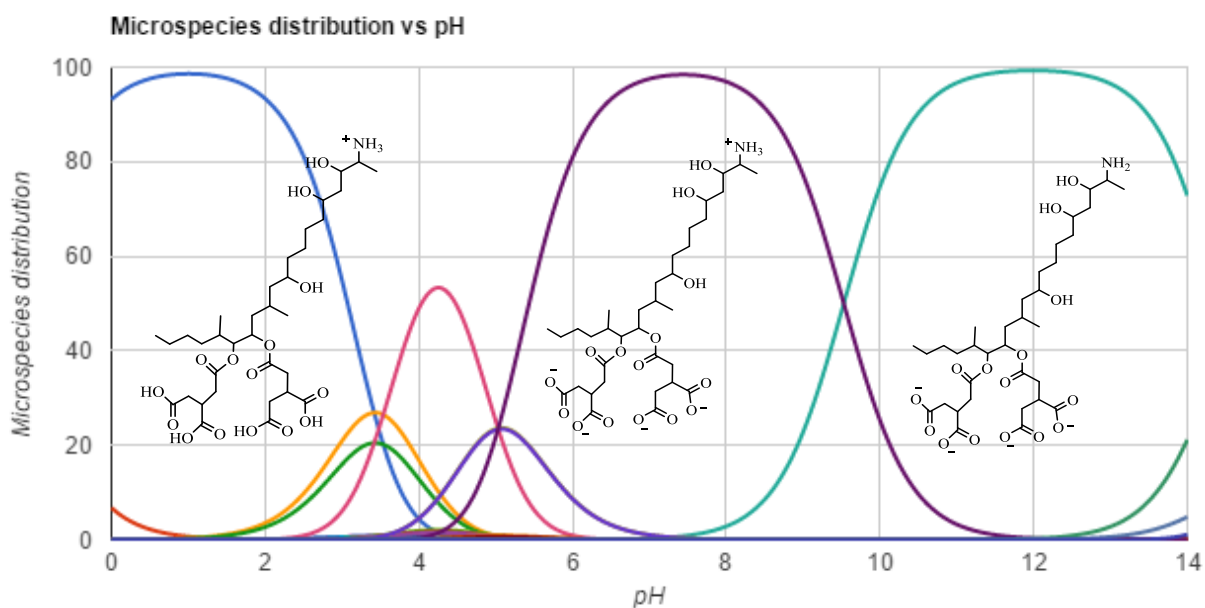


Figure 3-2. The influence of pH or pKa to changing of FB1 structure (adapted from <https://chemicalize.com/#/calculation>)¹²⁰

The 3D structure of each enantiomer is presented in Figure 3-3 and 3-4. As discussed earlier modelling results show that R and S enantiomers have different energy and different appearance in 3D images. It is unclear whether this difference is real and whether it would affect to design of nanoMIPs. For obvious reasons, it would be necessary to test it by synthesising corresponding nanoMIPs and testing its binding properties.

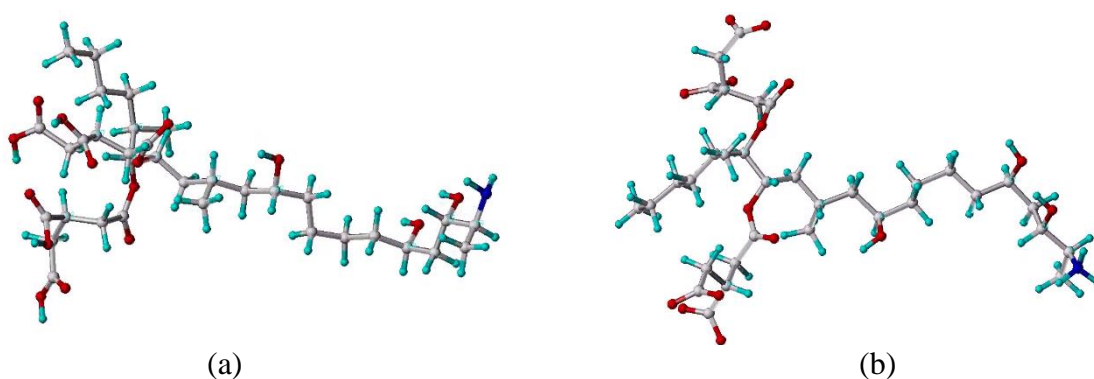


Figure 3-3. Three-dimensional structure of the R enantiomer FB1 in (a) vacuum and in (b) water (hydrogen: cyan, oxygen: red, nitrogen: blue, carbon: white)

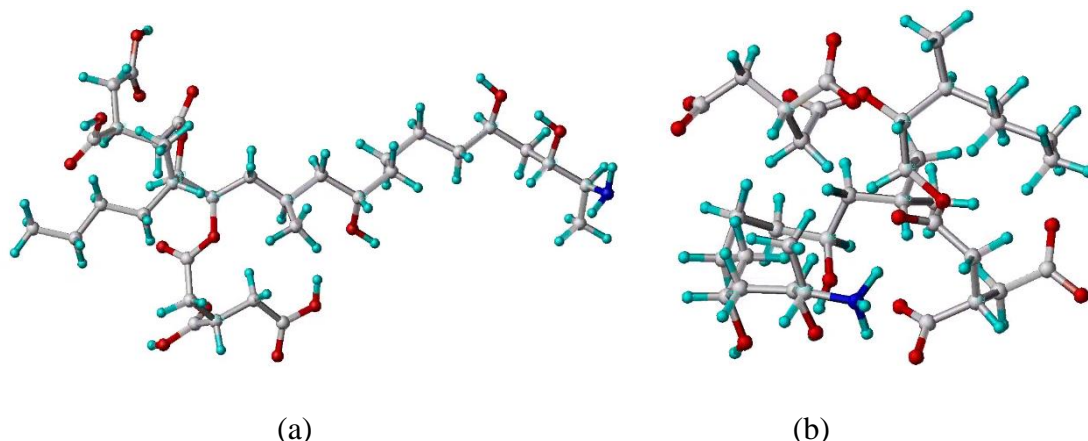


Figure 3-4. Three-dimensional structure of the S enantiomer FB1 in (a) vacuum and in (b) water (hydrogen: cyan, oxygen: red, nitrogen: blue, carbon: white)

3.3.2 Binding energy between FB1 and functional monomers

LEAPFROGTM algorithm is straightforward tool used to find a monomer with high affinity to FB1 (Table 3-2). According to Table 3-2, DEAEM (+) has the lowest binding energy followed by EGMP (-) and AMPSA (-) (Figure 3-5). The binding energy between DEAEM and FB1 in water is $-69.94 \text{ kcal mol}^{-1}$. This energy proves that DEAEM should have excellent binding to FB1. Experimentally, DEAEM has been used in solid phase extraction of fumonisins with great results.¹²¹ The binding energy of DEAEM is similar to EGMP ($-60.93 \text{ kcal mol}^{-1}$). It means that both DEAEM and EGMP have similar chance to bind FB1. Because of these, the binding polymer testing is an essential to step for deciding which of the functional monomers is the best for generating nanoMIPs for FB1 (see Section 3.3.3).

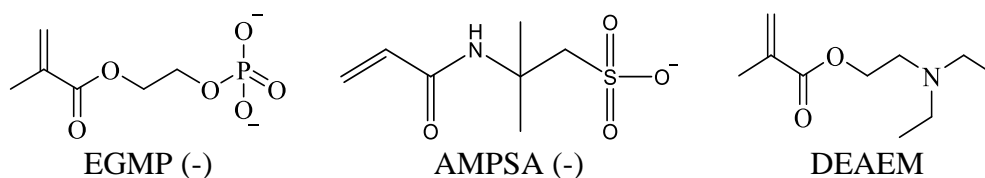


Figure 3-5. The structure of three monomers interacted with FB1

Table 3-2. The binding energies of complexes between the monomers and FB1 minimised in water

Rank	Monomer	Binding energy (kcal mol ⁻¹)
1	DEAEM (+)	-69.94
2	EGMP (-)	-60.93
3	AMPSA (-)	-49.77
4	Trifluoromethacrylic acid (-)	-42.36
5	Itaconic acid	-40.68
6	NN'-Methylene bis acrylamide	-40.49
7	4-Vinylpyridine (+)	-38.24
8	Acrylamide	-37.82
9	EGMP	-36.55
10	Itaconic acid (-)	-36.40
11	NPEDMA	-34.70
12	2- Vinylpyridine (+)	-30.83
13	Acrylic acid	-29.94
14	2-(Diethylamino)ethyl methacrylate	-29.83
15	Acrylamine	-28.59
16	Trifluoromethacrylic acid	-25.73
17	Ethylene glycol dimethacrylate(EGDMA)	-24.20
18	1-Vinylimidazole	-23.83
19	Acrylic acid	-23.78
20	2-Hydroxyethyl methylacrylate	-22.90
21	1-Vinylimidazole (+)	-20.12
22	4-Vinylpyridine	-8.05
23	2- Vinylpyridine	-7.97
24	m-Divinylbenzene	-6.94
25	Styrene	-6.88
26	p-Divinylbenzene	-6.76

DEAEM and EGMP interact with FB1 differently. DEAEM (+) interacts with carboxyl group of FB1, while EGMP (-) forms bond with amine group of FB1 as demonstrated in Figure 3-6 and 3-7. Therefore, this information is justification for conducting binding study to find an appropriate monomer for synthesis of FB (see Section 3.3.3).

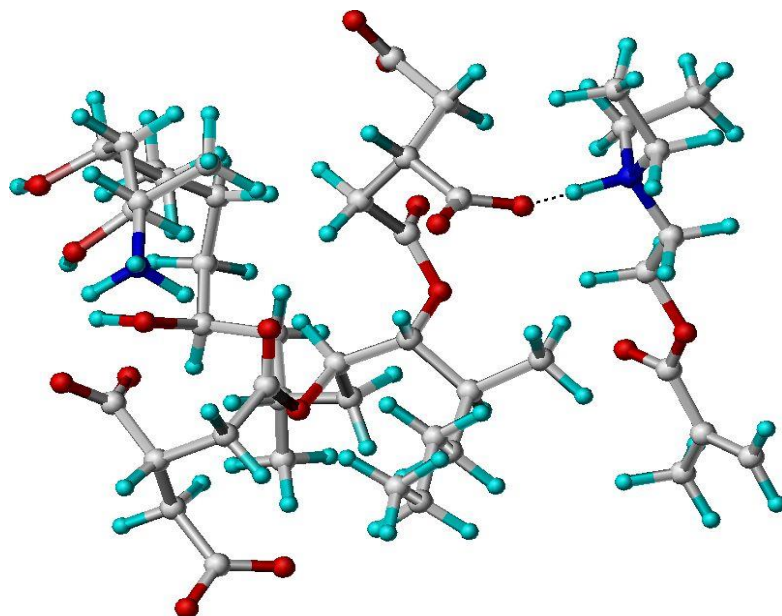


Figure 3-6. The illustration of FB1 (minimised in water) complex with DEAEM (+). (hydrogen: cyan, oxygen: red, nitrogen: blue, carbon: white, H-bonds: grey)

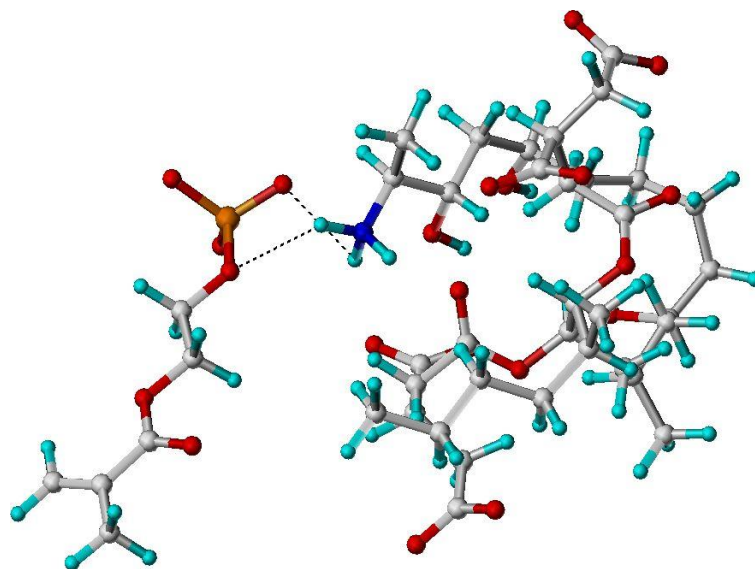


Figure 3-7. The illustration of FB1 (minimised in water) complex with EGMP (-). (hydrogen: cyan, oxygen: red, nitrogen: blue, carbon: white, H-bonds: grey)

3.3.3 Binding analysis

The binding experiments showed that polymers containing both monomers demonstrate binding of FB1 higher than 80%. As can be seen from Table 3-3, EGMP based SPE shows slightly higher binding than DEAEM based SPE. It turns out that interaction of EGMP to FB1 is slightly stronger than DEAEM.

Table 3-3 Filtration of Fumonisin B1 in standard polymer-based SPE

SPE	Binding Energy kcal mol ⁻¹	Before (B)	After (A)	B-A	Percentage Binding
<i>Filtration 1</i>					
DEAEM	-69.94	0.0133	0.0018	0.0115	86.47 %
EGMP	-60.93	0.0171	0.0014	0.0157	91.81 %
<i>Filtration 2</i>					
DEAEM	-69.94	0.0135	0.0019	0.0116	85.92 %
EGMP	-60.93	0.0131	0.0005	0.0126	96.18 %

Surprisingly, this result is contrary to Section 3.3.2 where DEAEM shows lower binding energy. These results prove that there is not precise correlation between the simulation and experimental study as concluded earlier.¹²⁴ Presumably, it is possible to conclude that the results from LEAPFROGTM show only single interaction of functional monomer to a single site of FB1. In experimental studies, monomer can form more than one interaction point with the template which is not accounted in standard LEAPFROGTM protocol. Therefore, due to data obtained in practical tests, EGMP was selected as monomer for preparation of nanoMIPs for FB1.

3.3.4 Synthesis and characterisation of nanoMIPs

The schematic description of nanoMIPs synthesis can be seen in Figure 3-8. The procedure followed Canfarotta and colleagues with several modifications in particular on the amount of chemicals used due to their costs and availability.¹¹⁸ Two steps, immobilisation of FB1 on glass beads and polymerisation of nanoMIPs, are essential in nanoMIP preparation as explained in Section 3.2.5.

The silanol groups on the surface of glass beads were activated by NaOH. The activated glass beads were then linked to [3-(2-aminoethylamino) propyl] trimethoxysilane to produce amine derivatised glass beads. This step is vital for connecting with FB1 helped by glutaraldehyde. This part would determine how many nanoMIPs would be produced.

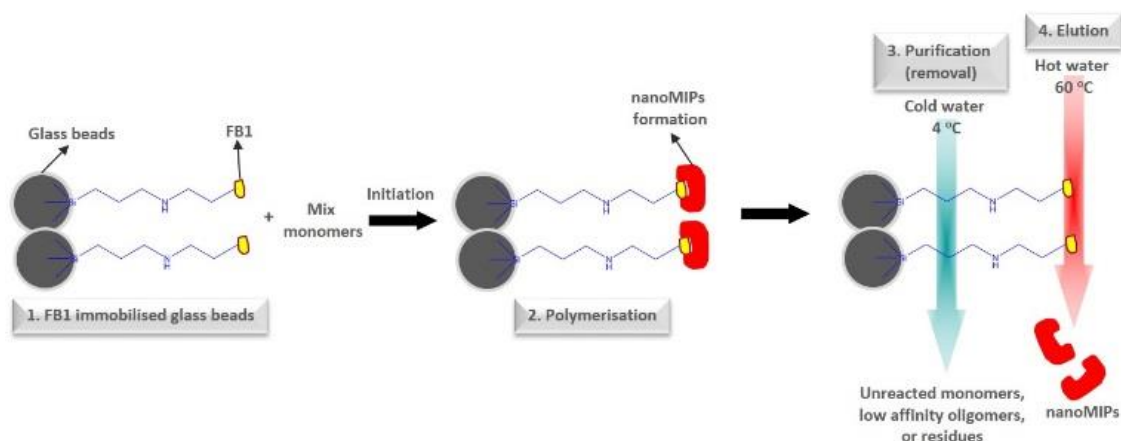


Figure 3-8. Scheme of solid phase synthesis for generating nanoMIPs for FB1. (1) immobilisation of FB1 onto glass beads (2) glass beads based solid phase used for polymerisation (3) initiation by TEMED in APS (4) removal low-affinity nanoMIPs and unreacted monomer by cold water (5) elution high-affinity nanoMIPs by hot water.

Moreover, the nanoMIPs were synthesised by adding the solution of functional monomers and cross-linkers to a solid phase and initiating polymerisation chemically by TEMED in APS. The selected monomer EGMP was used to replace acrylic acid (AA) in the previous experiment.¹¹⁰ EGMP was mixed with the other functional monomers, such as N-isopropylacrylamide (NIPAm) and N-(3-aminopropyl) methacrylamide (NAPMA). This way, we expected to obtain nanoMIPs with high specificity for FB1. Also, the nanoMIPs were created by a non-covalent approach exploring electrostatic, hydrophobic, and Van der Waals interactions. It could be considered that the nanoMIPs would interact with FB1 structure in many ways and the interaction cannot be mentioned obviously because it still needs more explanation theoretically and empirically.

Furthermore, not only high-affinity nanoMIPs would be produced during polymerisation but also the low-affinity nanoparticles. In addition, some quantity of unreacted monomers would remain in solution. Thus, to remove these particles, we have used cold water (4 °C). The hot water (60 °C) was used to disrupt the interaction of nanoMIPs and FB1 and obtain fraction of high-affinity nanoMIPs. Although the temperature of water is 60 °C,

there would not be degradation of FB1 since FB1 is resistant to high temperature of up to 100 °C.¹²⁵

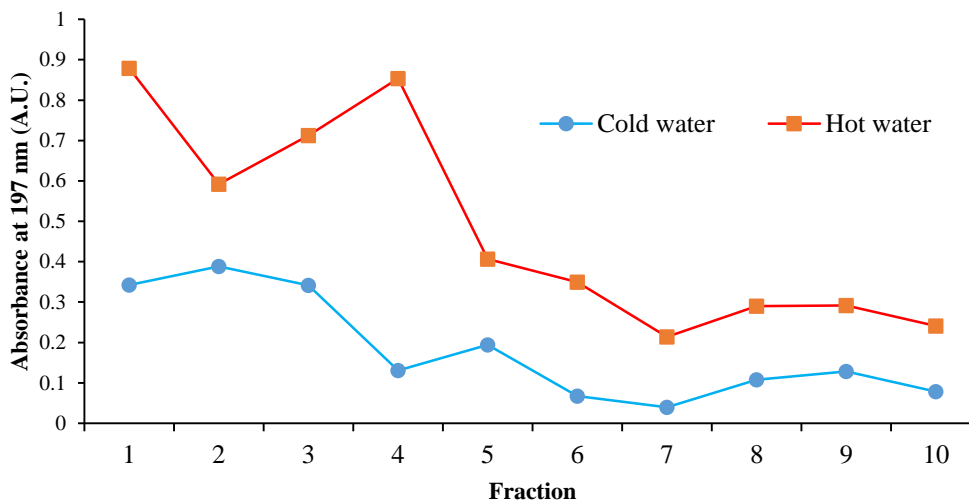


Figure 3-9 Washing fractions in cold water (blue line) and elution fractions in hot water (red line)

Unlike the preceding study, in this experiment, fractions eluted with cold water and hot water were divided into ten fractions and every fraction was measured by UV spectrophotometer at 197 nm. As expected not only hot water fractions but also cold water fractions showed some absorption (Figure 3-9). Also, since the distribution of nanoMIPs in every fraction is not the same, it would be easy to choose which fraction would be collected. However, the performance of nanoMIPs from all fraction would be same.

Deciding from results shown in Figure 3-9, the nanoMIPs are present in fraction one to seven. These nanoMIPs were measured spectrophotometrically at 197 nm and analysed by DLS. As results, the concentration of nanoMIPs obtained from this experiment is 0.06 mg mL⁻¹ and the particle size is 249 ± 29 nm with PDI 0.692 (Figure 3-11). The DLS analysis of cold water fraction shows multi-peaks and the long interval particle size, 179 ± 33 to 482 ± 69 nm (Figure 3-10). The image of nanoMIPS taken by TEM can be seen in Figure 3-12.

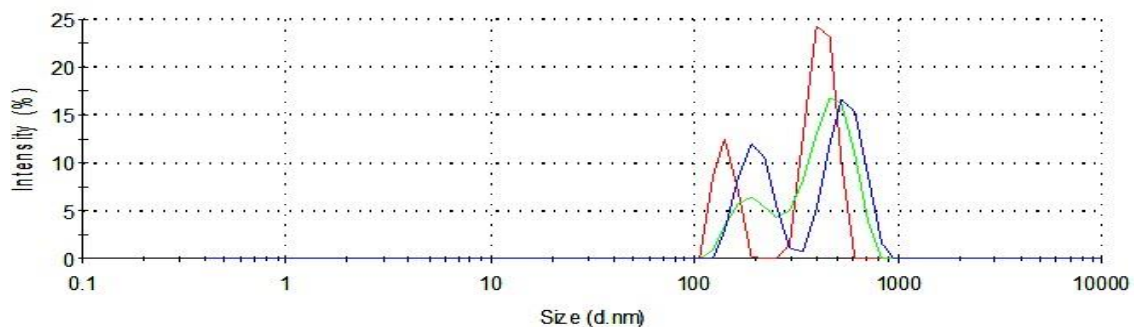


Figure 3-10. Diagram of the size distribution by intensity for cold water fraction at 4 °C

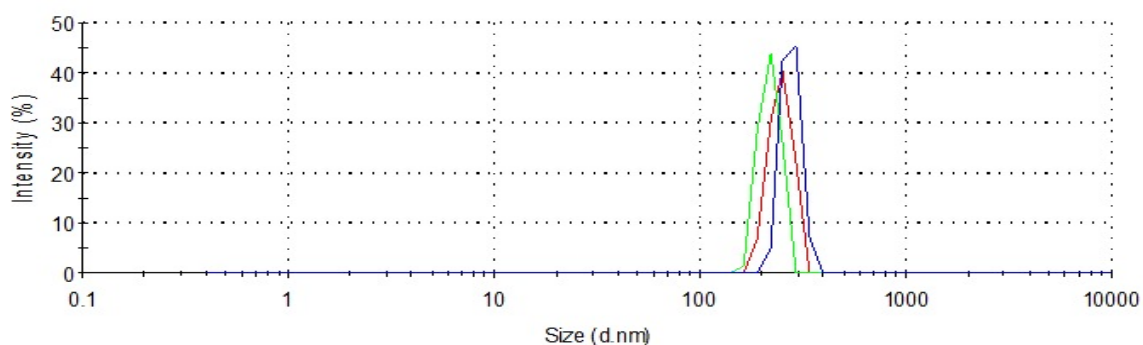


Figure 3-11. Diagram of the size distribution by intensity for hot water fraction at 60 °C

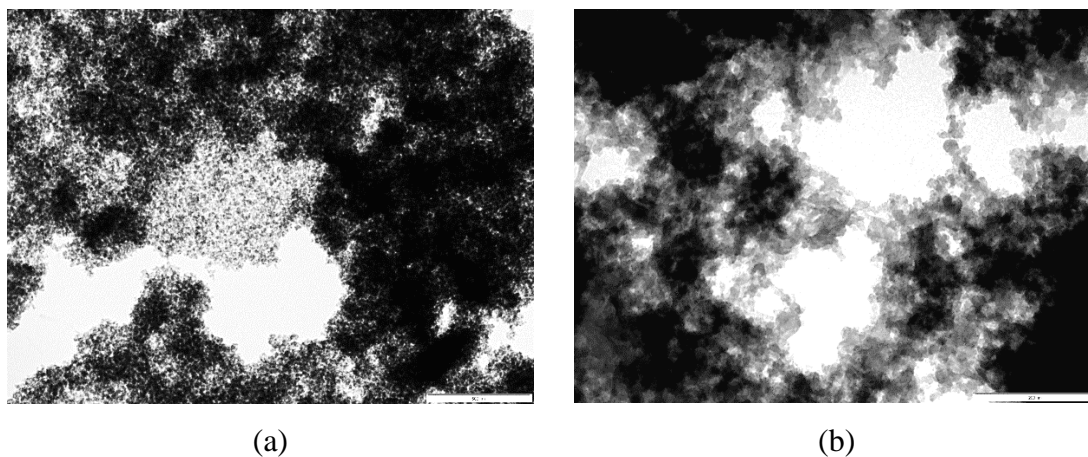


Figure 3-12. TEM image of nanoMIPs for Fumonisin B1 at 500 nm (a) and 200 nm (b) magnification

The FT-IR spectrogram of nanoMIPs in the range 4000 to 500 cm^{-1} can be seen in Figure 3-13 and Figure 3-14. Figure 3-13 showed the spectra of nanoMIPs on a solid phase. The phosphate group (PO_4^{3-}) has been found by observing bands of absorption of symmetric vibration 784 and 956 cm^{-1} and asymmetric vibration 1050 cm^{-1} .¹²⁶ Furthermore, the IR

spectra of nanoMIPs in acetonitrile can be seen in Figure 3-14. The strong band peaked at 1633 cm^{-1} is predicted to stretching vibration of carbonyl (C=O) in amide group.¹²⁷

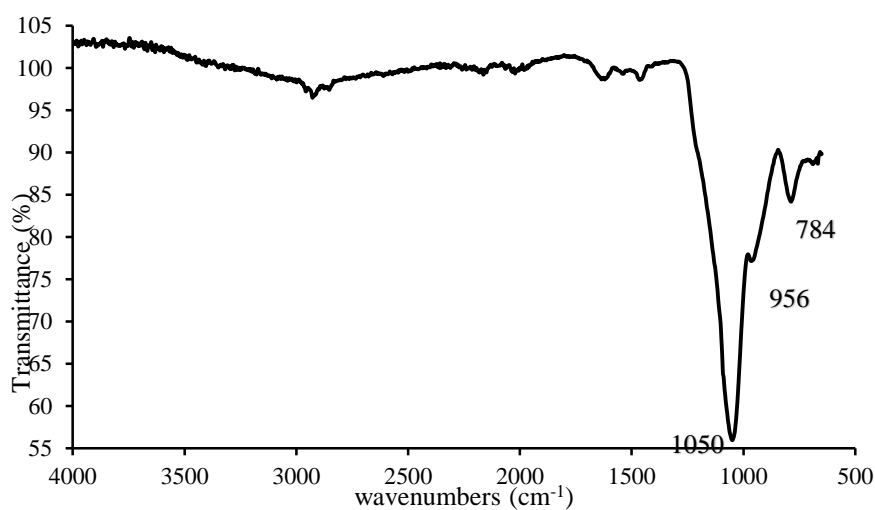


Figure 3-13. FT-IR spectra of nanoMIPs in solid

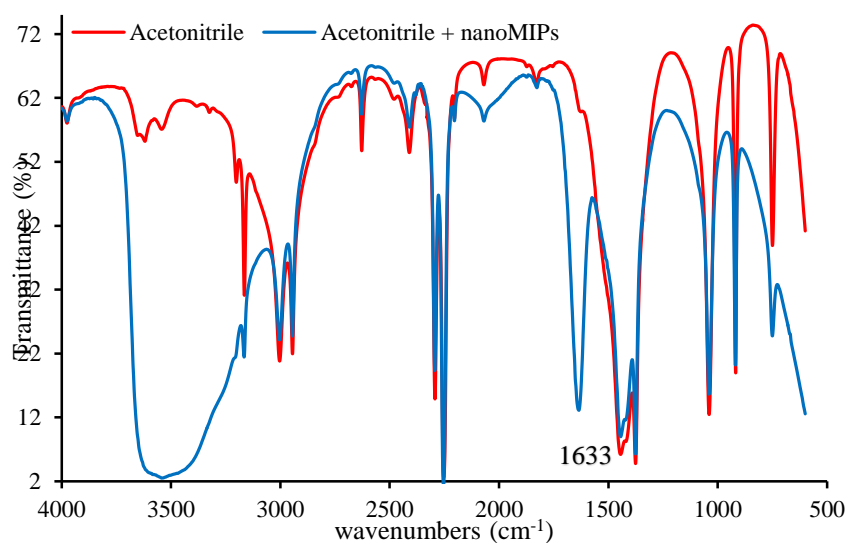


Figure 3-14. FT-IR spectra of acetonitrile (red line) and nanoMIPs in acetonitrile (blue line)

The interaction between nanoMIPs and FB1 specifically can be assessed by the value of a dissociation constant (K_d). In this work, the K_d for nanoMIPs of FB1 is $0.2\ \mu\text{M}$ calculated from the Biacore data using SPR (Figure 3-15). This K_d is higher than K_d measured in prior study.^{108,128}

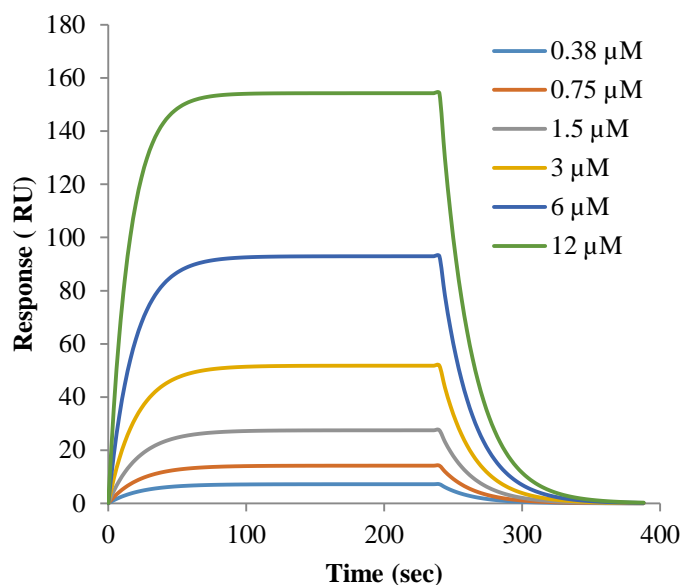


Figure 3-15. The binding affinity of nanoMIPs-FB1 complex measured using the BIAcore method. Gradient concentrations (ranging from 0.38 to 12 μM) of nanoMIPs were injected through flow cells with immobilised FB1. The kinetic profiles are shown. The dissociation constant (KD) of the nanoMIPs-FB1 complex was calculated to be 0.2 μM

3.4 Conclusion

In this work, the molecular imprinting of FB1 has been achieved successfully. By computer simulation and experimental study, EGMP was identified as suitable functional monomer for FB1. The nanoMIPs for FB1 have been synthesised by solid phase synthesis using the composition based on EGMP. From hot water fractions, the nanoMIPs were collected with concentration of nanoMIPs 0.06 mg mL^{-1} and particle size $249 \pm 29 \text{ nm}$. The image of nanoMIPs for FB1 is taken by TEM. The phosphate (PO_4^{3-}) and carbonyl (C=O) as functional groups of nanoMIPs were identified by FT-IR spectrometer. The dissociation constant of nanoMIPs is 0.2 μM . In further experiment, the performance of nanoMIPs will be tested by immunoassay technique as described in Chapter 4 including determination FB1 in corn samples. Several attempts to develop electrochemical sensor using different pulse voltammetry (DPV) and electrochemical impedance spectroscopy (EIS) will be described in Chapter 5.

CHAPTER 4 DEVELOPMENT OF MOLECULARLY IMPRINTED POLYMER NANOPOLYMERS-BASED ASSAY FOR FUMONISIN B1 AND ITS APPLICATION IN CORNS

4.1 Introduction

Historically, several applications for molecularly imprinted polymers (MIP) were reported near the end of 1980s. Thus, MIPs were applied for enantiomer separation of amino acid derivatives,^{129,130} and recognising template or target in assay and sensor techniques.¹³¹⁻¹³⁴ However, the production of MIP could be time-consuming, produces significant wastes and it is costly.¹³⁵ These drawbacks encourage many researchers to improve the performance of the MIP on nanoscale level. The molecularly imprinted polymer nanoparticles (nanoMIPs) have been introduced since 2000s. Unlike MIPs, the nanoMIPs were used not only for assay and sensor approaches and separation purposes, but also for biological purposes such as drug delivery, clinical diagnostic, and biomedical imaging.^{109,136-140}

In this study, the interactions between nanoMIPs (produced in Chapter 3) and fumonisin B1 (FB1) were tested using enzyme-linked immunosorbent assay (ELISA) technique. Herein, the nanoMIPs replaced monoclonal or polyclonal antibody as molecular recognition tools for FB1. Most conventional steps in ELISA such as immobilisation of antibody in a microplate, blocking and washing step, and the addition of substrate and stop solution, were still used with some modifications.¹⁴¹ For instance, the immobilisation of the nanoMIPs was conducted at 40 °C by evaporating water suspension of nanoparticles. Otherwise, antibodies could not survive at high temperature.¹⁴² Therefore, this application is named molecularly imprinted polymer nanoparticles-based assay (MINA).

Preparing MINA needs an enzyme conjugate. Horseradish peroxidase (HRP) has been applied for many experiments as an enzyme conjugate.¹⁴³ In this section, FB1 was conjugated with HRP to obtain an HRP-FB1 conjugate through carbodiimide reaction using 1-ethyl-3-(3-dimethylaminopropyl)-carbodiimide hydrochloride (EDC) and N-hydroxy succinimide (NHS). The conjugate was reacted with substrate - 3,3',5,5'-tetramethyl benzidine (TMB). The colourimetric reaction between conjugate and

substrate play important role for investigating interactions between FB1 and nanoMIPs. Moreover, HRP interference testing was investigated to anticipate the side reaction between HRP and nanoMIPs.

The optimisation of condition of MINA is an essential factor in order to create a trustworthy MINA assay. In this study, the concentration of HRP-FB1 and nanoMIPs were optimised. The other parameters such as the solution and incubation time of blocking, washing, and substrate addition followed preceding research.^{109,110,144,145} From Chapter 3, the concentration of nanoMIPs obtained was 0.06 mg mL⁻¹ and this nanoMIPs was diluted two times until 0.006 mg mL⁻¹ being four series concentration of nanoMIPs (0.006 - 0.06 mg mL⁻¹). The HRP-FB1 conjugate was used in the dilution interval 1:12800 – 1:400. From these results, one optimum concentration of nanoMIPs and HRP-FB1 conjugate was selected. Eventually, the protocol MINA for FB1 was set for determination of FB1 in standard solution and sample extracts.

The performance of MINA was tested by interacting nanoMIPs between FB1 standard and HRP-FB1 conjugate competitively. The concentration range of FB1 used was 10 pM to 10 nM and the dilution of HRP-FB1 conjugate employed was 1:400 based on optimisation results. The results showed that the MINA is very sensitive because the concentration range used here allowed detection of FB1 at levels lower than required 2 ppm.⁵⁻⁷ The comparison study was conducted by replacing nanoMIPs with monoclonal antibody (mAb) and unspecific imprinted polymer nanoparticles (nanoNIPs). These studies proved that the selectivity of nanoMIPs to FB1 is higher than mAb and nanoNIPs. Moreover, the other mycotoxins, such as fumonisin B2 (FB2), aflatoxin B1 (AFB1), citrinin (CTT), deoxynivalenol (DON), and zearalenone (ZEA) were employed for identifying the cross-reaction of MINA. Finally, the MINA was applied in 18 samples of corn taken randomly in the traditional markets). Also, the similar samples were analysed by commercial ELISA kit and HPLC. The results of sample analysis from MINA, ELISA kit and HPLC were compared statistically by t-test at the end. Therefore, the objection of this chapter is to develop MINA for determination of FB1 and its application in corn samples.

4.2 Materials and Methods

4.2.1 Materials and Equipment

Bovine serum albumin (BSA), 1-ethyl-3-(3-dimethylaminopropyl)-carbodiimide hydrochloride (EDC), horseradish peroxidase (HRP), sodium hydroxide (NaOH), *N*-hydroxysuccinimide (NHS), phosphate buffered saline (PBS), 3,3',5,5'-tetramethyl benzidine (TMB), tween 20, 2-[morpholino]ethanesulfonic acid (MES), aflatoxin B1 (AFB1), deoxynivalenol (DON), citrinin (CTT), zearalenone (ZEA), sulfuric acid (H₂SO₄), and methanol were purchased from Sigma-Aldrich, UK. Fumonisin B1 (FB1) and fumonisin B2 (FB2) were purchased from ChemCruz, USA. Monoclonal antibody for FB1 from BioTeZ Berlin Buch GmbH, German. AgraQuant total fumonisins test kit (0.25 – 5 ppm) from Romer Labs, Austria. Double-distilled ultrapure water (Millipore, UK) was used for the experiments. Polystyrene 96 well, flat bottom plate were purchased from Elkay Laboratory Products, UK. All corns were used as samples in this study. All corn samples (18 samples) were taken from traditional markets randomly. All chemicals and solvents were analytical or HPLC grade and used without any purification.

Magnetic stirrer, hot plates, Sigma 3-16 centrifuge, filter paper (Whatmann 1, 4 and GF/A), immunoaffinity column (IMA) for fumonisin B1, filter funnel, flat-bottom glass vessel 200 ml, amicon Ultra-15 centrifugal filter units, Polystyrene 96 well, flat bottom plate were purchased from Elkay Laboratory Products, UK and microplate reader.

4.2.2 Preparation of HRP-FB1

10 mg HRP were diluted in 1 mL MES buffer 0.1M (pH 6) and added 0.4 mg EDC and 0.6 mg NHS for 15 minutes. This solution was then filtered by ultrafiltration on a millipore amicon ultra centrifugal filter unit (30 kDa MWCO). The activated HRP was then accumulated and instantly incubated with 5 mg FB1 in 10 mL PBS buffer 0.01 M at pH 7.4 for 2 hours. The HRP–FB1 conjugate was then washed to remove free FB1 on a millipore amicon ultra centrifugal filter unit (30 kDa MWCO). For this procedure, 10 washes with 5 mL PBS were performed. After that, the conjugate was dissolved in 2 mL

deionised water, calculated its concentration by comparison with the enzymatic activity of the free enzyme, and stored in the fridge at $-18\text{ }^{\circ}\text{C}$ until further used. The HRP-FB1 conjugate was employed as the stock solution and used in optimum dilution.

4.2.3 Optimisation of HRP-FB1 and nanoMIPs concentration

The concentrations of nanoMIPs and HRP-FB1 conjugate were optimised, while others such as blocking, washing, TMB and stop solution were carried out based on previous protocols.^{109,110,144,145}

The concentration of HRP-FB1 conjugate. 40 μL nanoMIPs (0.03 mg mL^{-1}) were added to microplate and evaporated at $40\text{ }^{\circ}\text{C}$, for 24 h. Wells were washed with 3 x 250 μL PBS, blocked with 250 μL PBS including 0.1% BSA and 1% Tween 20, and washed with 3 x 250 μL PBS. 100 μL HRP-FB1 conjugate were added at different dilutions : 1: 12800 – 1:400, washed with 3 x 250 μL PBS, added 100 μL TMB substrate, were added following added stop solution (by 50 μL H_2SO_4 0.05M), and measured the absorbance of each well at 450 nm using a microplate reader.

The concentration of nanoMIPs. 40 μL nanoMIPs with variation concentrations from 0.006 to 0.06 mg mL^{-1} were added to a microplate, followed by evaporating the solvent from nanoMIPs at $40\text{ }^{\circ}\text{C}$, 24 h, washing with 3 x 250 μL PBS, blocking with 250 μL PBS including 0.1% BSA and 1% Tween 20, washing with 3 x 250 μL PBS, adding 100 μL HRP-FB1 conjugate 1:800, washing 3 x 250 μL PBS, adding 100 μL TMB substrate, adding stop solution by 50 μL H_2SO_4 0.05M, and measuring the absorbance of each well at 450 nm using a microplate reader.

4.2.4 Competitive assay

The protocol for analysis of FB1 using the nanoMIPs based assay was prepared for constructing a calibration curve of standard solution and analysing corn samples. In general, the step of the protocol of MINA comprised: coating 100 μL nanoMIPs (0.06 mg mL^{-1}) into microplate, evaporating the solvent from nanoMIPs at $40\text{ }^{\circ}\text{C}$, 24 h, washing with 3 x 250 μL PBS, blocking with 250 μL PBS including 0.1% BSA and 1% Tween 20, washing with 3 x 250 μL PBS, adding 100 μL HRP-FB1 conjugate 1:400 and the FB1

standard solution with concentration range 10pM – 10nM, washing 3 x 250 μ L PBS, adding 100 μ L TMB substrate, adding stop solution by 50 μ L H₂SO₄ (0.05M), measuring the absorbance of each well at 450 nm using a microplate reader, and finally preparation the calibration curve and linearity.

4.2.5 MINA selectivity and cross-reactivity

The selectivity of nanoMIPs-based assay for FB1 was evaluated by replacing nanoMIPs to nonimprinted polymer nanoparticles (nanoNIPs) into a microplate. The nanoNIPs was produced by using the same composition of nanoMIPs in Section 3.2.5. However, the template of nanoNIPs was melamine instead of FB1. The nanoNIPs was used as a control for nanoMIPs. Also, the assay was tested for other mycotoxins such as aflatoxin B1 (AFB1), citrinin (CTT), deoxynivalenol (DON), fumonisin B2 (FB2), and zearalenone (ZEA), for cross reactivity test.

4.2.6 Sample preparation

The protocol of sample preparation followed AOAC Official Method 2001.06.¹⁴⁶ Corn (25 g) was weighed into a blender, added 125 mL extraction solvent, methanol 70% (v/v) in water, blended 2 min at high speed, and filtered through Whatman No. 1 filter paper. Then, 100 μ L of the filtrate was diluted in 790 μ L PBS solution (1:80 dilution). Finally, the sample solution was analysed by MINA.

4.2.7 Sample analysis

The protocol of MINA for sample analysis comprised : coating 100 μ L nanoMIPs (0.06 mg mL⁻¹) into a microplate, evaporating the solvent from nanoMIPs at 40 °C, 24 h, washing with 3 x 250 μ L PBS, blocking with 250 μ L PBS including 0.1% BSA and 1% Tween 20, washing with 3 x 250 μ L PBS, adding 100 μ L mix solution of HRP-FB1 conjugate and the corn extraction, washing 3 x 250 μ L PBS, adding 100 μ L TMB substrate, adding stop solution by 50 μ L H₂SO₄ (0.05M), measuring the absorbance of each well at 450 nm using a microplate reader, and finally plotting the absorbance to calibration curve for obtaining the cocentration of sample solution.

4.2.8 Sample preparation and analysis by commercial kit ELISA

The procedure for sample analysis followed the manual of the AgraQuant total fumonisin test kit (0.25 – 5 ppm) from Romer Labs. Corn 25 g was weighed into a blender and added 125 mL of extraction solvent, methanol 70% (v/v), blended 2 min at high speed, and filtered by Whatman No. 1. Afterwards, 100 μ L of the filtrate was diluted in 1.9 mL water (1:20 dilution), and analysed by kit and read by microplate reader at 450 nm.

4.2.9 Sample preparation and analysis by HPLC

The procedure followed AOAC Official Method 2001.04.¹⁴⁷ 10 g of corn were extracted with 50 mL of acetonitrile:methanol:water (25:25:50), shaken by blender for 1 hour and filtered by Whatman no 4. 10 mL of extraction solution was diluted with 40 mL of PBS and filtered through glass microfibre filter Whatman GF/A. 10 mL of diluted extract was purified through IMA column. Afterwards, the IMA column was washed with 10 mL of water and eluted with 2 mL methanol and followed by 2 mL water. Then, the eluted sample was dried and reconstituted with 800 μ L of acetonitrile: water (30:70). Finally, 50 μ L of the extract solution was injected to HPLC and compared with a calibration curve of FB1.^{147,148}

4.3 Results and discussion

4.3.1 Optimisation of HRP-FB1 conjugate and nanoMIPs concentration

The optimisation of HRP-FB1 conjugate used variation of conjugate concentration as follows: 1:400; 1:800; 1:1600; 1:3200; 1:6400 and 1:12800, in 0.01 M PBS solution. This concentration range was similar to previous research.¹⁰⁹ The fixed concentration of nanoMIPs was prepared at 0.03 mg mL⁻¹ and used in coating the microplates in three replications. The certain HRP-FB1 conjugate concentration giving the highest response was used in the MINA protocol.

The HRP-FB1 absorbance at 450 nm against HRP-FB1 concentration was shown in Figure 4-1. The results showed that the interaction of nanoMIPs with concentration 0.03

mg mL⁻¹ would produce good results with HRP-FB1 conjugate. Moreover, the testing of the blank well with HRP-FB1 conjugate was conducted in order to analyse the systematic error from non-specific response. Figure 4-1 showed that the response of HRP-FB1 conjugate to blank well as quite modest for dilutions 1:12800 to 1:400. These responses would come from the non-specific binding which could potentially be observed for MINA. From these results, we can see that there is no significant interaction between conjugate and microplate. Therefore, it is believed that the absorbance obtained comes from the interaction between the HRP-FB1 conjugate and nanoMIPs.

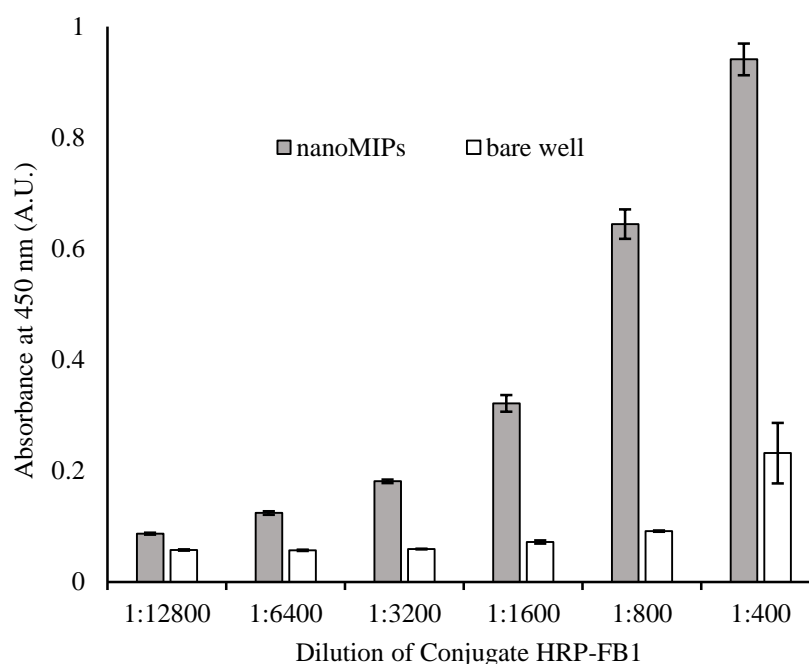


Figure 4-1. Plot HRP-FB1 absorbance at 450 nm against HRP-FB1 concentration. Microplates were coated with a fixed nanoMIPs concentration (0.03 mg mL⁻¹), the blocking solution was incubated for 2 h, TMB substrate was incubated for 5 min, and then quenched with sulfuric acid. The control experiment was performed without nanoMIPs.

The comparison between nanoMIPs coated well and bare well was used to choose the optimal concentration of HRP-FB1 for further experiments. The highest ratio was 1:800 dilution with ratio 1:7 followed by 1:1600 and 1:400 dilution with 1:5 and 1:4 respectively. However, the 1:400 dilution was selected for MINA protocol because the absorbance was approximately one. Interestingly, the 1:400 dilution used in this study was more efficient than the previous study using the 1:200 dilution.¹⁰⁹

Thereafter, the concentration of nanoMIPs was optimised by testing the different amounts of nanoMIPs added to microplate from 0.006 to 0.06 mg mL⁻¹ (Figure 4-2). Similar to optimisation of HRP-FB1 conjugate, each concentration was measured in a microplate in three replications. Figure 4-2 demonstrated that concentrations 0.015 and 0.03 mg mL⁻¹ had slightly different responses. However, the responses for those concentrations were too low. Therefore, the concentration of nanoMIPs selected was 0.06 mg mL⁻¹ for MINA protocol.

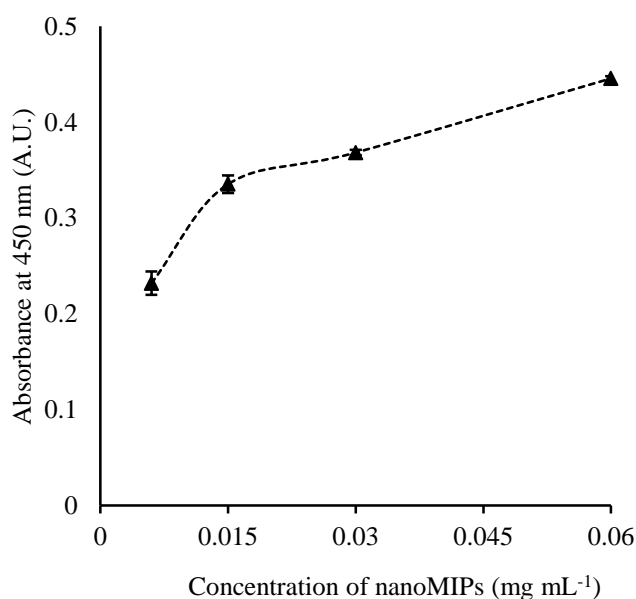


Figure 4-2. Optimisation of nanoMIPs concentration. Microplate was coated with nanoMIPs concentration ranging from 0.006 to 0.06 mg mL⁻¹. The HRP-FB1 conjugate was used at 1:800 dilution, the blocking agent was incubated for 2 h, TMB substrate was incubated for 5 min, and reaction quenched with sulfuric acid.

Table 4-1 The Procedure of MINA for FB1

Step	Solution
1. NanoMIPs immobilisation	100 μ L nanoMIPs 0.06 mg mL ⁻¹ (24 h at 40°C)
2. Washing with buffer solution	0.01 M PBS (3 times \times 250 μ L) at pH 7.4
3. Addition of blocking agent	0.1% BSA, 1% Tween 20 in 0.01 M PBS (250 μ L, 2 h)
4. Washing with buffer solution	0.01 M PBS (3 times \times 250 μ L) at pH 7.4
5. Addition of target and conjugate	100 μ L of the HRP-FB1 conjugate (1:400 dilution, 1 h)
6. Washing with buffer solution	0.01 M PBS (3 times \times 250 μ L) at pH 7.4
7. Addition of substrate	100 μ L of commercial TMB solution, 5 mins.
8. Addition of stopover solution	50 μ L of 0.05 M H ₂ SO ₄ , 10 s.

The protocol for MINA is shown Table 4-1. The protocol relied on the concentration of HRP-FB1 conjugate (1:400) and nanoMIPs (0.06 mg mL⁻¹) optimised as described earlier. Overall, the optimisation of MINA is straightforward and reproducible. The washing and blocking steps followed protocols described earlier.^{109,110,144,145} The optimisation of assay is an important stage for each analytical protocol. Unfortunately, many published articles omit the details of assay optimisation and assay conditions (Table 4-2). The use of concentration of HRP-FB1 conjugate in MINA seems to be more efficient than the conventional competitive direct ELISA. However, the concentration of nanoMIPs used in MINA is higher than the antibodies used in traditional ELISA. This is most likely due to the difference in size or affinity between antibody and nanoMIPs.¹⁴⁹

Table 4-2. The optimisation of comparison between MINA and other competitive direct ELISA or immunoassays for Fumonisin determination

Molecular recognition	Concentration (µg mL⁻¹)	Conjugate	Concentration (µg mL⁻¹) (dilution)	Ref.
mAb	50-150	HRP-FB1	2 (-)	Azcona-Olivera <i>et al</i> , 1992 ¹⁵⁰
mAb	-	HRP-HFB1	-	Maragos&Miklaz, 1996 ¹⁵¹
pAb	10	HRP-FB3	0.8 (1:500)	Christensen <i>et al</i> , 2000 ¹⁵²
mAb	3	HRP-FB1	0.25 (1:500)	Savard <i>et al</i> , 2003 ¹⁵³
nanoMIPs	60	HRP-FB1	0.22 (1:400)	This study

mAb: monoclonal antibody, pAb: polyclonal antibody, nanoMIPs: molecularly imprinted polymer nanoparticles, HFB1: hydrolysed fumonisin B1, FB3: fumonisin B3

4.3.2 Study of HRP interaction

The HRP has been widely used for signal amplification in fumonisin assays for two decades.¹⁵⁴⁻¹⁵⁶ The HRP reacts enzymatically with TMB as a substrate. This reaction changes the colour to be yellow obtained by reducing TMB. For measurement accuracy the reaction is terminated by adding sulfuric acid. The colour represents the concentration of FB1 in standard solution and sample extraction.

Unfortunately, the interference of HRP in the binding of HRP-FB1 conjugate could be substantial. This problem was not stated explicitly in preceding reports.¹⁰⁹ To understand this, the binding of HRP-FB1 conjugate to nanoMIPs was compared with HRP (Figure

4-3). The dilutions of HRP and HRP-FB1 were used from 1:12800 to 1:400 in PBS 0.01 M.

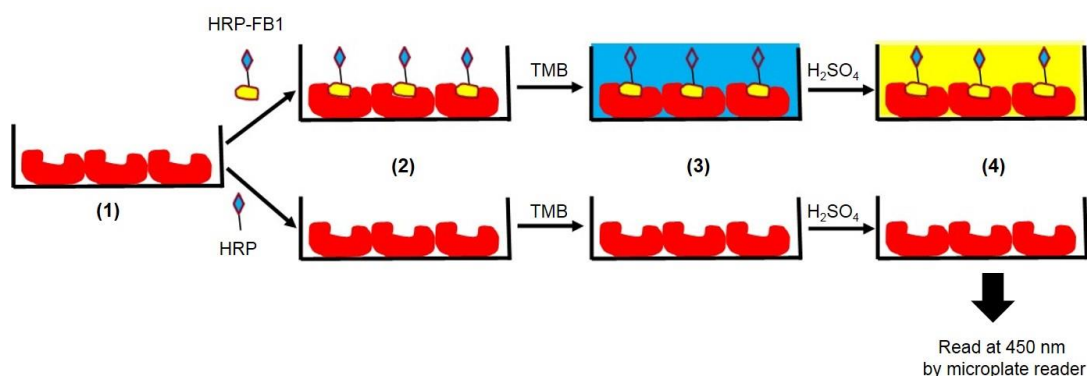


Figure 4-3. HRP interference in MINA. (1) Firstly nanoMIPs are deposited for coating of microplates. (2) Then, some wells were added by HPR-FB1 conjugate and others were added by HRP. (3) After that substrate, TMB was added. (4) Afterwards, the stopover solution was added. Finally, absorption was measured at 450 nm using microplate reader.

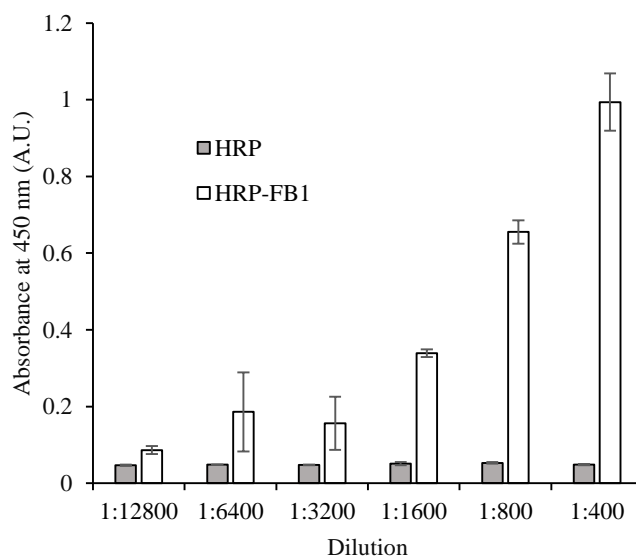


Figure 4-4. Plot of absorbance at 450 nm for HRP and HRP-FB1 concentrations in a binding to nanoMIPs. The concentration used of HRP and HRP-FB1 were dilutions from 1:12800 to 1:400. Microplates were coated with a fixed nanoMIPs concentration (0.06 mg mL⁻¹), the blocking solution was incubated for 1 h, TMB substrate was incubated for 5 min and the reaction quenched with sulfuric acid.

The results showed that the absorbance of HRP-FB1 conjugate increased gradually from 1:12800 to 1:400 dilution. Nevertheless, the HRP showed similar absorbance for all concentrations (Figure 4-4). It could be argued that the interference of HRP is small compared to the absorbance of HRP-FB1 conjugate. Therefore, the interaction between

HRP and nanoMIPs is negligible and nanoMIPs only reacted with FB1. Unfortunately, there is no more explanation about it and further experiment is needed to a structure changing of HRP during complex reaction with FB1.

In this study, the concentration of HRP-FB1 conjugate produced was calculated by comparing signal with calibration curve of HRP (Figure 4-5). As a result, the concentration of HRP-FB1 produced is 0.09 mg mL^{-1} and used in the MINA protocol is $0.22 \text{ }\mu\text{g mL}^{-1}$ (1:400) concentration.

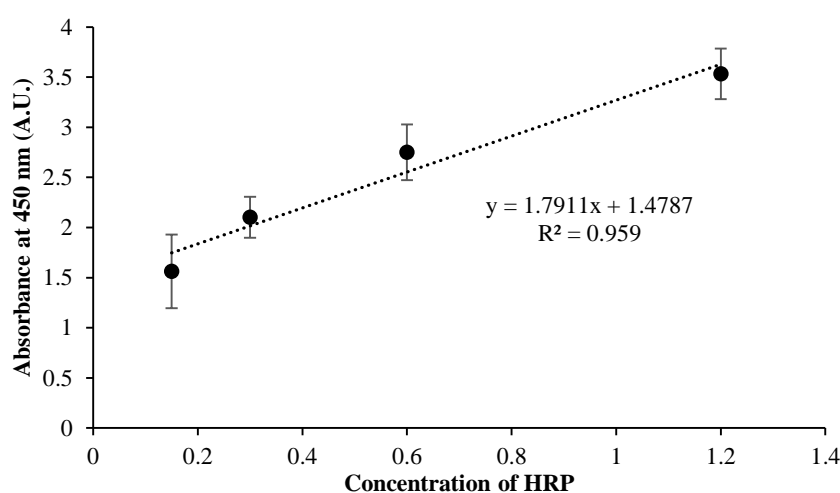


Figure 4-5. Calibration curve of HRP $0.15 - 1.2 \text{ }\mu\text{g mL}^{-1}$

Table 4-3 The calibration curve procedure of MINA for FB1

Step	Solution
1. Immobilisation of nanoMIPs	100 μL nanoMIPs 0.06 mg/mL (24 h at 40°C)
2. Washing with buffer solution	0.01 M PBS (2 times $\times 250 \text{ }\mu\text{L}$) at pH 7.4
3. Addition of blocking agent	0.1% BSA, 1% Tween 20 in 0.01 M PBS (250 μL , 2 h)
4. Washing with buffer solution	0.01 M PBS (3 times $\times 250 \text{ }\mu\text{L}$) at pH 7.4
5. Addition of target and conjugate	100 μL mix solution between 1:400 diluted HRP-FB1 conjugate and FB1 standard solution (10 pM – 10nM)
6. Washing with buffer solution	0.01 M PBS (3 times $\times 250 \text{ }\mu\text{L}$) at pH 7.4
7. Addition of substrate	100 μL of commercial TMB solution, 5 min.
8. Addition of stopover solution	50 μL of 50 mM H_2SO_4 , 10 s.

4.3.3 MINA calibration curve and its comparison with monoclonal antibody

The performance of competitive assay followed the protocol in Table 4-3 and Figure 4-6. The procedure is more efficient because the use of HRP-FB1 is 100 times smaller than in the previous study.¹⁵⁷ The calibration curve (Figure 4-7, top line) showed better fit indicating the reliable competitive binding to FB1 at 10 pM – 10 nM (0.007 – 7.22 ng mL⁻¹) concentrations when plotted on logarithmic scale. The sensitivity achieved is similar to the previous study.¹⁰⁹

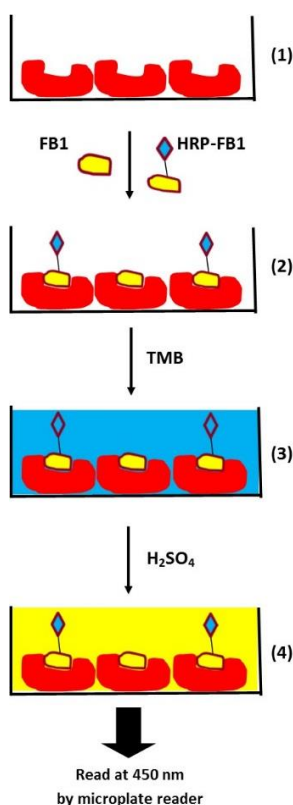


Figure 4-6. MINA protocol, (1) firstly nanoMIPs are deposited onto microplates wells. (2) Then, competitive assay between HPR-FB1 conjugate and FB1 standard was performed. (3) After that substrate TMB was added. (4) Afterwards, the stopover solution was added. Finally, absorption was measured at 450 nm using microplate reader.

In the same way, the non-specific imprinted nanoparticles (nanoNIPs) were tested with FB1 as a control for comparing with nanoMIPs. Despite that the composition of nanoNIPs was the same as the composition for nanoMIPs, their responses to the HRP-FB1 conjugate was different (Figure 4-7, bottom line). Therefore, it can be argued that the nanoMIPs have high affinity to FB1. Furthermore, the calibration curve was compared to that of commercial monoclonal antibody (mAb) for Fumonisin. The response of mAb used was

lower than nanoMIPs (Figure 4-8). Apparently, the nanoMIPs have higher affinity to FB1 than mAb and nanoNIPs.

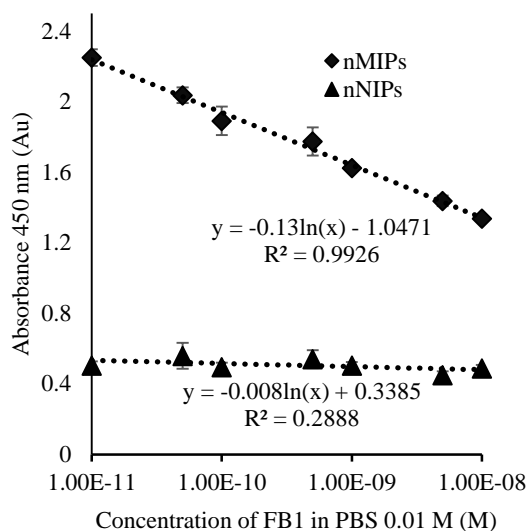


Figure 4-7. Calibration plot for FB1, measured using MINA and the respective control using nanoNIPs. The concentration for nanoMIPs and nanoNIPs was 0.06 mg mL^{-1} . All experiments were performed using FB1 standard solutions ranging from 10 pM to 10 nM (in 0.01 M PBS), HRP-FB1 conjugate dilution at 1:400, blocking solution (incubation 2 h), TMB substrate (incubation 5 mins) and then quenched with sulfuric acid.

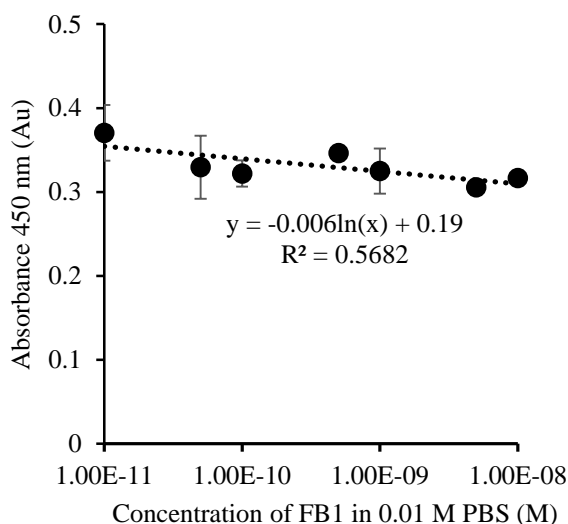


Figure 4-8. Calibration plot for FB1 measured using conventional ELISA, the concentration of mAb used was 0.006 mg mL^{-1} . All experiments were performed using FB1 standard solutions ranging from 10 pM to 10 nM (in 0.01 M PBS), HRP-FB1 conjugate dilution at 1:400, blocking solution (incubation 2 h), TMB substrate (incubation 5 mins) and then quenched with sulfuric acid.

4.3.4 MINA cross-reactivity

The cross-reactivity of MINA was also investigated to other mycotoxins. Fumonisin B2 (FB2) generated signal in MINA with regression linear 0.568 compared to other targets (Figure 4-9). This result is not surprising because the backbone structure of FB2 is relatively the same as FB1¹⁵⁸⁻¹⁶². However, the cross-reactivity in MINA is low for this compound. Unlike FB2, aflatoxin B1 (AFB1), citrinin (CTT), deoxynivalenol (DON), and zearalenone (ZEA) showed no interaction with nanoMIPs (Figure 4-9). Coherently, it could be argued that the binding of nanoMIPs to other mycotoxins are inconsequential.

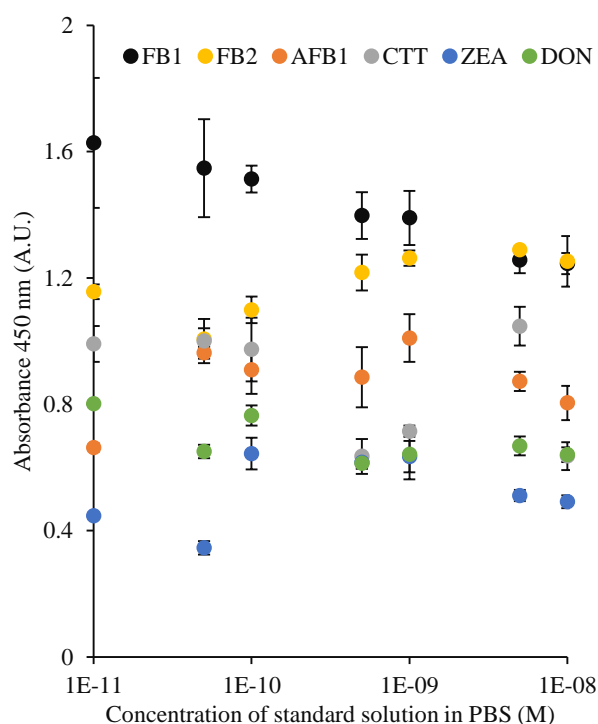


Figure 4-9. MINA response to FB1, flatoxin B1 (AFB1), citrinin (CTT), deoxynivalenol (DON), and zearalenone (ZEA). For the experiments microplates were coated with nanoMIPs (0.06 mg mL^{-1}), HRP-FB1 conjugate dilution was 1:400, standard solution concentration ranged from 10 pM to 10 nM.

Table 4-4. MINA response comparison and linear equation values for calibration curves for mycotoxins

Target compounds	$Absorbance = slope \times Ln C (Molar) + intercept$		
	Slope	Intercept	R ²
FB1	-0.058	0.173	0.990
FB2	0.031	1.852	0.568
AFB1	0.012	1.128	0.068
CTT	-0.036	0.067	0.240
DON	-0.019	0.271	0.444
ZEA	0.013	0.800	0.081

The response for other mycotoxins is much smaller than for FB1 (Figure 4-9). Figure 4-10 proved that the nanoMIPs are only selective to FB1 but not to other mycotoxins.

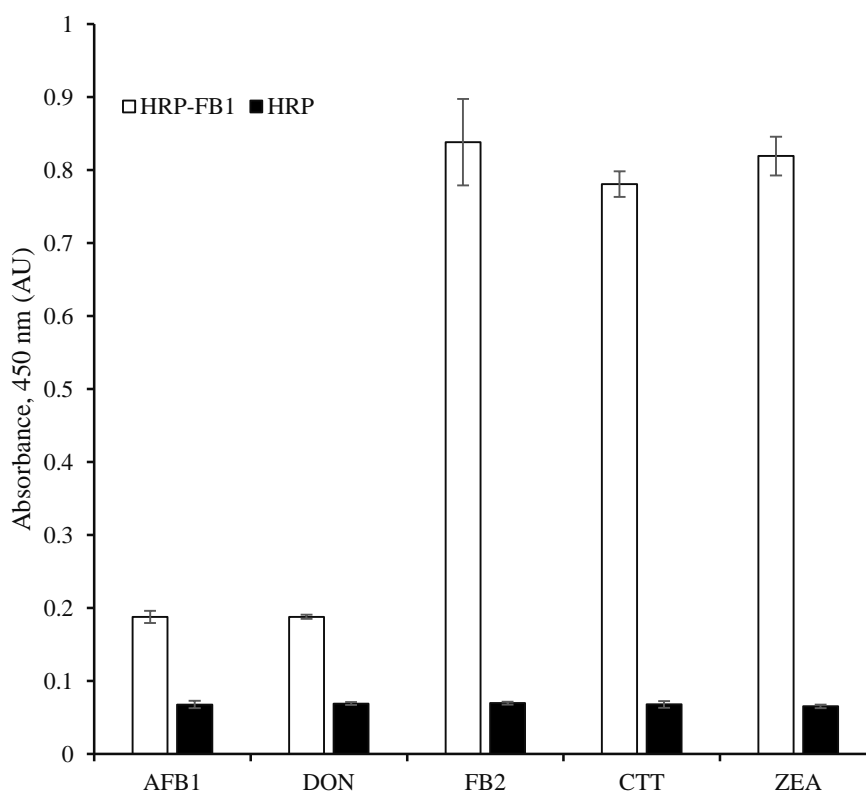


Figure 4-10. MINA and HRP response to other mycotoxins. For the experiments microplates were coated with nanoMIPs (200 μ l, 0.03 mg mL^{-1}), HRP-FB1 and HRP conjugate dilution was 1:800, standard solution concentration ranged for each compound 10 μM .

4.3.5 Analyte recovery and limit of detection

For sample analysis MINA should be validated against several parameters. In this work, recovery test and limit of detection were analysed. The limit of detection could be obtained through interpolation of three-time value of the blank response against a calibration curve of MINA. The blank response was obtained measuring STD for zero concentration of FB1. The calculated limit of detection (LoD) of MINA is 1.9 pM (0.001 ng mL⁻¹). This LoD is almost ten times lower than standard analytical methods (Table 4-4).

Table 4-5. Comparison between MINA and other FB1 determination techniques

Molecular recognition	Method	Linear range (ng mL⁻¹)	Limit of detection (LOD) (ng mL⁻¹)	Ref.
Polyclonal Antibody	Immuno-chromatographic	-	8	Urusov <i>et al</i> , 2017 ¹⁶³
Polyclonal Antibody	ELISA	0.1 – 100	0.6	Urusov <i>et al</i> , 2017 ¹⁶³
Peptide	Microarray-based immunoassay	17.3 – 79.6	11.1	Peltomaa <i>et al</i> , 2017 ⁵¹
Monoclonal Antibody	ELISA	0.08–1.38	0.32	Tang <i>et al</i> , 2017
Monoclonal Antibody	Immunostrip	15 – 500	11.24	Yao <i>et al</i> , 2017 ¹⁶⁴
Molecularly imprinted polymer nanoparticles	MINA	0.007 - 7.22	0.001	This study

Table 4-6 Recovery test

Samples	Concentration in spiked samples	Concentration determined with MINA	Recovery
Sample 1	55 nM	59.47 ± 0.1 nM	108.13%
Sample 2	55 µM	62.57 ± 0.2 µM	113.76%

Furthermore, the reliability of the MINA analysis could be proven by recovery test. In this part, the corn samples were spiked with FB1 (55 nM and 55 µM). The corn was then

extracted by the standard method as described in AOAC 2001.06.¹⁴⁶ The recovery test showed that the MINA could attain the FB1 in real sample from 108.13 to 113.76 % (Table 4-5). It could be argued that the MINA is able to analyse FB1 accurately in corn.

4.3.6 Sample analysis and comparative study with commercial kit ELISA and HPLC

For samples analysed by MINA and ELISA, all corns (18 samples) were extracted by methanol 70% as described in AOAC Official Method 2001.06.¹⁴⁶ Extraction solvent for samples which were analysed by HPLC methods used acetonitrile: methanol: water (1:1:2) [AOAC Official Method 2001.04].¹⁴⁸ MINA and HPLC has similarity on dilution factor (80) whereas dilution factor for ELISA is 20. Moreover, the protocol of sample analysis for HPLC are totally different with MINA and ELISA using microplate (Figure 4-15). Extraction solvent, dilution factor, and sample analysis procedure probably influence in the sample analysis obtained from among MINA, ELISA and HPLC (Table 4-6).

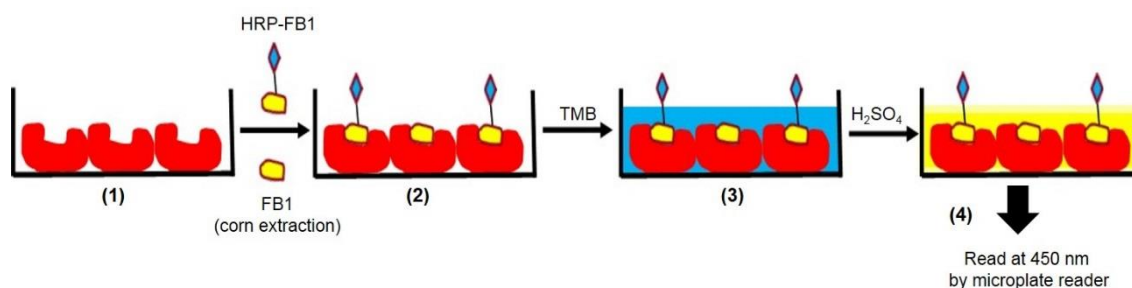


Figure 4-11. MINA protocol, (1) firstly nanoMIPs are deposited in microplates. (2) Then, competitive assay between HPR-FB1 conjugate and sample extracts was performed. (3) Substrate TMB was added. (4) Afterwards, the stopover solution was added. Finally, absorption was measured at 450 nm using a microplate reader.

Table 4-7. Comparison of sample preparation and analysis from MINA, ELISA, and HPLC

Methods	Sample preparation		Sample analysis			
	Solvent	Dilution factor (times)	Concentration range (ppm)	Mean (ppm)	Toxicity (%)	
MINA	M:W (7:3)	80	0.26 - 1.29	0.60	0 (0/18)	
ELISA	M:W (7:3)	20	0.18 - 3.30	0.53	5.6 (1/18)	
HPLC	A:M:W(1:1:2)	80	0.05 - 1.29	0.34	0 (0/18)	

A = acetonitrile, M = methanol, W = water

The results of samples analysis (Table 4-6) showed that the lowest concentration of sample can be found in HPLC method (0.05 ppm) and the highest concentration of sample can be found in ELISA method (3.30 ppm). It can be argued that the concentration of all samples examined by MINA (0.26 – 1.29 ppm) can be observed in the concentration range both ELISA and HPLC. Furthermore, MINA and ELISA has slightly different average of concentration. There was no toxicity detected sample in MINA and HPLC. While, ELISA method obtained one sample (C13) which higher concentration than the level of maximum residue limit of fumonisins (> 2 ppm) as shown in Figure 4-16.

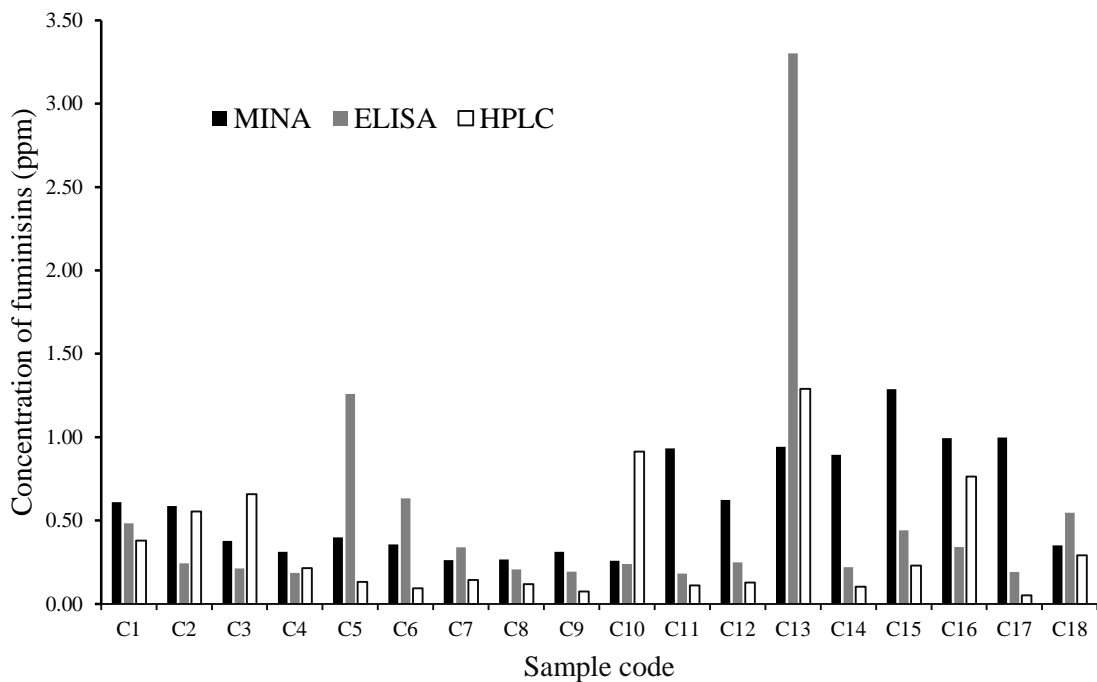


Figure 4-12. The distribution of fumonisins in corn samples by MINA, commercial ELISA kit, and HPLC.

Distribution of fumonisins in corn samples in Figure 4-16 showed most samples have concentration lower than 2 ppm. It seems that all methods provide similar results. Most samples are safe to be consumed. In addition, 50% of sample analysed by MINA is correlated with HPLC, $R^2 = 0.93$ (Figure 4-17 (a)). This percentage of sample is higher than ELISA results which is 30% of sample correlated with HPLC results, $R^2 = 0.96$ (Figure 4-17 (b)). Despite the correlation between MINA and ELISA showed different percentage of sample correlated with HPLC, t-test showed that the MINA results ($t = 1.36$, $P = 0.056$) is significant with ELISA results ($t = 0.67$, $P = 0.25$). It can be argued that both MINA and commercial ELISA kit have the same accuracy.

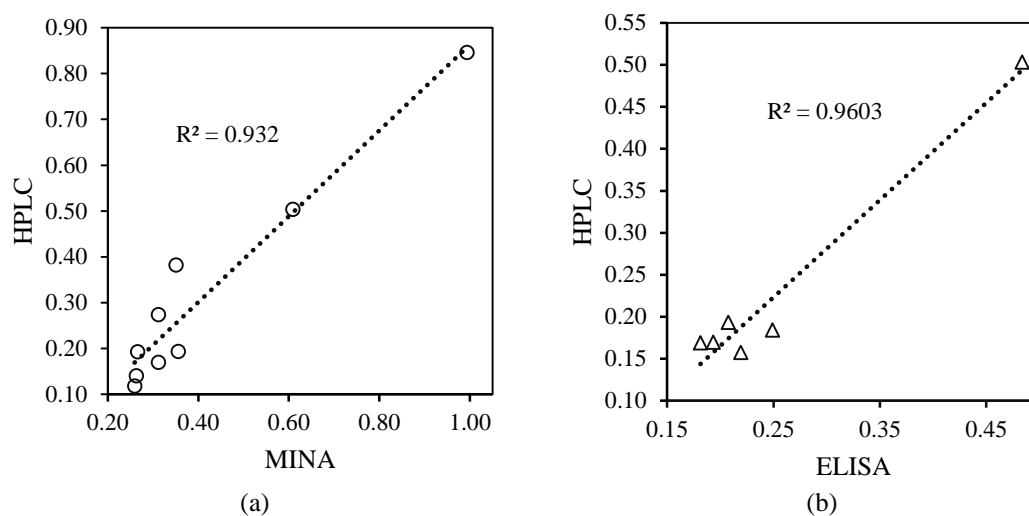


Figure 4-13. Correlation sample analysis of MINA-HPLC (a) and ELISA-HPLC (b)

4.4 Conclusion

Development of molecularly imprinted polymer nanoparticle-based assay (MINA) has proved that the molecularly imprinted polymer nanoparticle (nanoMIPs) are able to replace antibodies as molecular recognition tools for FB1. After optimisation of the concentration of nanoMIPs (0.06 mg mL^{-1}) and HRP-FB1 conjugate (1:400), MINA was capable producing satisfactory detection of toxin in the concentration range $10 \text{ pM} - 10 \text{ nM}$.

The selectivity and cross-reactivity have been tested. The response from commercial monoclonal antibody (mAb) and non-specific imprinted polymer nanoparticles (nanoNIPs) was not significant. Also, the interaction between nanoMIPs and other mycotoxins such as aflatoxin B1 (AFB1), citrinin (CTT), deoxynivalenol (DON), fumonisin B2 (FB2), and zearalenone (ZEA), was negligible.

The application of MINA has been tested in real samples. The total of 18 corn samples have contaminated fumonisin with a range from 0.26 ppm to 1.29 ppm. Afterwards, several samples have been selected for further analysis by commercial kit ELISA and HPLC for comparative study. Statistically, t-test has shown that there is significant similarity of the results obtained by MINA and commercial kit ELISA and 50% sample analysed by MINA correlating positively with HPLC.

CHAPTER 5 DEVELOPMENT OF AN ELECTROCHEMICAL SENSOR FOR FUMONISIN B1 DETERMINATION BASED ON MOLECULARLY IMPRINTED POLYMER NANOPARTICLES

5.1 Introduction

Previously in Chapter 4, replacing monoclonal and polyclonal antibodies to molecularly imprinted polymer nanoparticle (nanoMIPs) in assay application for was described. The technique is called nanoMIPs based assay (MINA). MINA has been applied for determination of fumonisin B1 (FB1). The results revealed that limit of detection (LoD) for MINA is lower than conventional ELISA.^{51,162-164} Additionally, MINA uses fewer chemicals and reagents, resulting in a more efficient assay than immunoassays.¹⁵⁰⁻¹⁵³ Currently, MINA presents several advantages compared to conventional ELISA, such as sensitivity, selectivity and efficiency. Besides, MINA offers high reliability due to nanoMIPs. NanoMIPs can survive on harsh conditions, and they are simple to fabricate, thus allowing low-cost assays due to the antibody replacement. Unfortunately, MINA is still time-consuming and tedious because the MINA protocol involves more steps as ELISA (e.g. washing, blocking, and stop reaction steps). Moreover, some chemical reagents used in MINA are similar to ELISA such as TMB and HRP. Therefore, a method that does not require sample preparation and tedious steps is required for mycotoxin analysis. To overcome these problems, the electrochemical sensor method was also tested.

Herein, Chapter 5, the performance of nanoMIPs was studied in electrochemical sensors. The main advantages of electrochemical sensors are easier on preparation and application, lower of cost production, more portable and faster.¹⁶³⁻¹⁶⁶ The electrochemical sensor combines a molecular recogniser (antibody, aptamer, nanoMIPs) and transducer system (amperometric, potentiometric, conductometric, impedimetric) transforming from chemical to electroanalytical signal.^{167,168} The mechanism how electrochemical sensor works comes from electron transfer contribution. The migration of electron is occurred on solution trough three electrode surfaces used: working, counter and reference. From these pathway, the chemical responses can be translated to analytical signals.

In this work, the nanoMIPs was used as recognition element in an electrochemical sensor for fumonisin B1 (FB1) determination using different pulse votammety (DPV) and electrochemical impedance spectroscopy (EIS) methods. Thus, the technique is named nanoMIPs based electrochemical sensors (MINES).

MINES were prepared on platinum electrode surfaces. The nanoMIPs were attached to the electrode surface using an anchoring electro-conducting polymer. For that, the electroconducting polymer was synthesised by electro-polymerisation of pyrrole (Pyr) and a Zinc (II) porphyrin (ZnP). Afterwards, nanoMIPs were immobilised on the electrode using carbodiimide chemistry. For FB1 determination, MINES used two electrochemical methods: electrochemical impedance spectroscopy (EIS) and differential pulse voltammetry (DPV). For the EIS technique, redox labelling is not needed. Conversely, a redox couple such as ferricyanide ($[\text{Fe}(\text{CN})_6]^{3-}$) and ferrocyanide ($[\text{Fe}(\text{CN})_6]^{4-}$) is needed for DPV analysis.

The main advantages of MINES are the reduction of time for analysis, easier for fabrication, the simplicity on application and reduction of chemical reagents, such as blocking solution, washing solution, enzymatic conjugate (HRP complex), the enzymatic substrate (TMB) and stop solution (sulfuric acid). In that sense, MINES technology is more efficient than MINA.

The performance of MINES was evaluated in an FB1 concentration range from 1 fM to 10 pM. Notably, the concentration range for analysis is lower than MINA (10 pM – 10nM). Moreover, the cross-reactivity was evaluated by evaluating the MINES response to other mycotoxins such as aflatoxin B1 (AFB1), citrinin (CTT), deoxynivalenol (DON), fumonisin B2 (FB2), and zearalenone (ZEA). Hence, in this chapter the development of an electrochemical sensor based on molecularly imprinted polymer nanoparticles (MINES) for FB1 is presented.

5.2 Materials and Methods

5.2.1 Materials

5,10,15,20-tetrakis(4-aminophenyl)-porphyrin-Zn(II) was provided by Porphyrin Systems (Germany). Tetra-(n-butyl)-ammonium tetrafluoroborate ($(C_4H_9)_4NBF_4$), acetonitrile (ACN), 1-ethyl-3-(3-dimethylaminopropyl) carbodiimide hydrochloride (EDC), N-hydroxysuccinimide (NHS), phosphate buffer saline (PBS), potassium ferrocyanide ($K_4[Fe(CN)_6] \cdot 3H_2O$), potassium ferricyanide ($K_3[Fe(CN)_6]$) and pyrrole were procured from Sigma-Aldrich (Poland). Platinum (Pt) electrode was used as a working electrode (WE) and counter electrode (CE). A silver chloride electrode (Ag/AgCl) was used as a reference (RE).

5.2.2 NanoMIPs based sensor fabrication for FB1

Firstly, platinum working electrode was polished with 0.3 and 0.05 micron alumina powder, then rinsed with distilled water. Afterwards, the electrode was cleaned by piranha solution $H_2O_2 : H_2SO_4$ (1:3,v/v) for 3 min and then rinsed with distilled water and acetone. Subsequently, the electro-conducting polymer ZnP/Pyr was deposited on the platinum surface (WE) by electro-polymerization of pyrrole (0.14 M) and Zinc (II) porphyrin ($46.84 \mu M$) in 0.1 M $(C_4H_9)_4NBF_4$ acetonitrile using cyclic voltammetry (CV) at the potential range of -1.1 to 1.3 V (vs Ag/Ag⁺), scan rate of 50 mV s^{-1} and 8 cycles. The structure of pyrrole and Zinc (II) porphyrin can be seen in Figure 5-1.

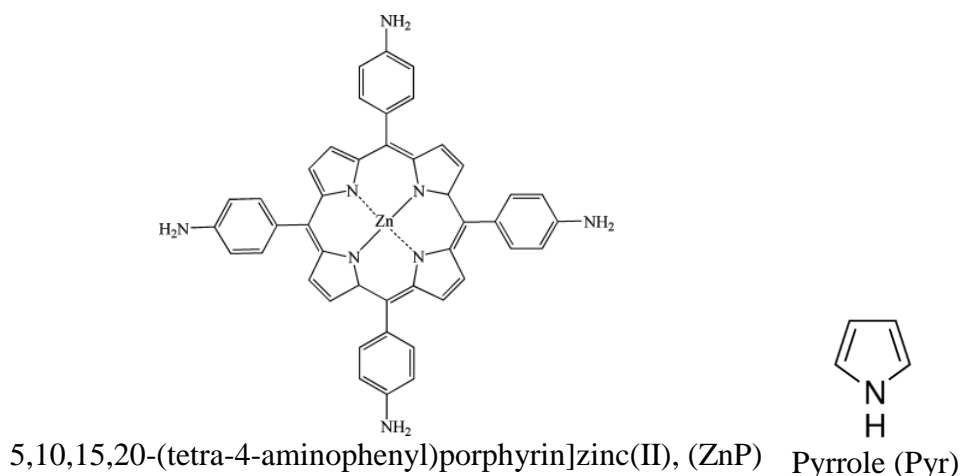


Figure 5-1. Chemical structure of ZnP and Pyr monomers

NanoMIPs were successively covalently immobilised in two steps: (1) the electropolymerization of ZnP/Pyr on the platinum electrode surface (WE) and the (2) immobilisation of nanoMIPs on the ZnP/Pyr polymer (Figure 5-2). For that, nanoMIPs (0.06 mg mL^{-1}) were incubated in 0.7 M EDC and 0.01 M PBS for 5 min . Then, 0.6 M NHS was added and incubated for 5 min . Subsequently, the ZnP/Pyr polymer was immersed in the solution containing nanoMIPs (0.06 mg mL^{-1}), 0.7 M EDC and 0.6 M NHS in 0.01 M PBS for 24 h . Lastly, the obtained sensor was washed with distilled water.

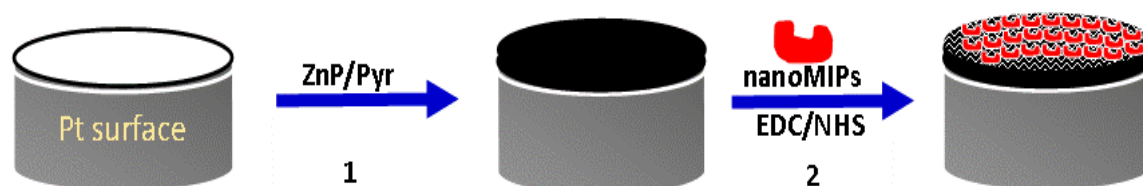


Figure 5-2. FB1 nanoMIPs sensor fabrication: (1) electropolymerization of 5,10,15,20-tetrakis(4-aminophenyl)-porphyrin-Zn(II) and Pyrrole (ZnP/Pyr) in a solution of 0.1 M tetra-(n-butyl)-ammonium tetrafluoroborate ($(\text{C}_4\text{H}_9)_4\text{NBF}_4$) in acetonitrile. (2) Immobilisation of nanoMIPs through carbodiimide chemistry (incubation in 0.7 M EDC and 0.6 M NHS in 0.01 M PBS during 24 h).

5.2.3 Characterisation of ZnP/Pyr polymer

(1) Image

Additionally, the polymer was imaged by Atomic force microscopy (AFM), MultiMode 8 AFM microscope operated by the Nanoscope V Bruker controller (Germany). Images were obtained in a Scan Asyst mode using a probe hq-nsc35 with a cantilever B with nominal spring const. $k = 16 \text{ N/m}$.

(2) Functional groups

Infrared spectra were obtained using Fourier-transform infrared (FTIR) spectroscopy imaging in ATR (Attenuated Total Reflection) mode measured using a Spectrum One FT-IR Spectrometer, PerkinElmer at $4000\text{-}500 \text{ cm}^{-1}$.

5.2.4 Development of labelled sensor using differential pulse voltammetry (DPV)

DPV was applied using a μ Autolab potentiostat Type II (Eco Chem B.V, Utrecht, Netherland) controlled by General Purpose Electrochemical System software (GPES) software, system version 4.9. The potential range employed was -0.25 to +1.10 V and modulation amplitude at 0.05 V. The measurement was carried out in 0.01 M PBS (pH \sim 7) and 0.005 M $[\text{Fe}(\text{CN})_6]^{3-/4-}$.¹⁷⁰

5.2.5 Development of a free label sensor using electrochemical impedance spectroscopy (EIS)

EIS determination experiments were recorded using a Potentiostat EC-lab VMP3 instruments version 9.9 and controlled and modelled using EC-Lab software V10.39, 2014 by Bio-Logic-Science Instruments. The experiments were conducted at Institute of Physical Chemistry of the Polish Academy of Sciences, Warsaw, Poland and at the Department of Chemistry, University of Leicester, UK.

The EIS applied conditions (potential, AC amplitude, and frequency) were +0.5 V (vs Ag/AgCl), 25 mV, 50 mHz to 200 kHz, respectively (35s/scans). Nyquist plots displayed impedance data. The impedance data were then fitted (Z-fit) to an equivalent circuit (Figure 5-3) by using EC-Lab software. For the Z-fit, Nyquist plots were fitted using a randomise method, stopped on 10,000 iterations and the fit stopped on 5,000 iterations. The fitting was dependent on the form of the semi-circle curves obtained in the Nyquist plot. The selection of the equivalent circuit was dependent upon the interfaces of the Nyquist plot to produce the smallest error that was expressed in the standard deviation (X^2).

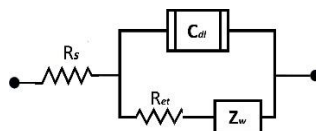


Figure 5-3. Equivalent circuit employed for EIS fitting. R_s is the solution-phase resistance, R_{et} is the electron transfer resistance, C_{dl} is the double-layer capacitance, and Z_w is the Warburg impedance.

5.3 Results and discussion

5.3.1 The electropolymerisation of ZnP/Pyr

The ZnP/Pyr polymer was electropolymerised using cyclic voltammetry at the potential range from -1.1 to +1.3 V, (starting from 0 V). This range results to be higher than preceding studies.¹⁷¹⁻¹⁷³ The potential range variance occurred because different conditions have been employed, such as reference (Ag/Ag^+), solvent, electrolyte and monomer concentration employed. The polymer synthesis was inspired by Ferreira *et al.* work concerning the pyrrole polymerisation in organic solvents.¹⁷⁴ The electropolymerisation parameters were optimised in the present work including the appropriate electrolyte ($(\text{C}_4\text{H}_9)_4\text{NBF}_4$) and organic solvent (acetonitrile).

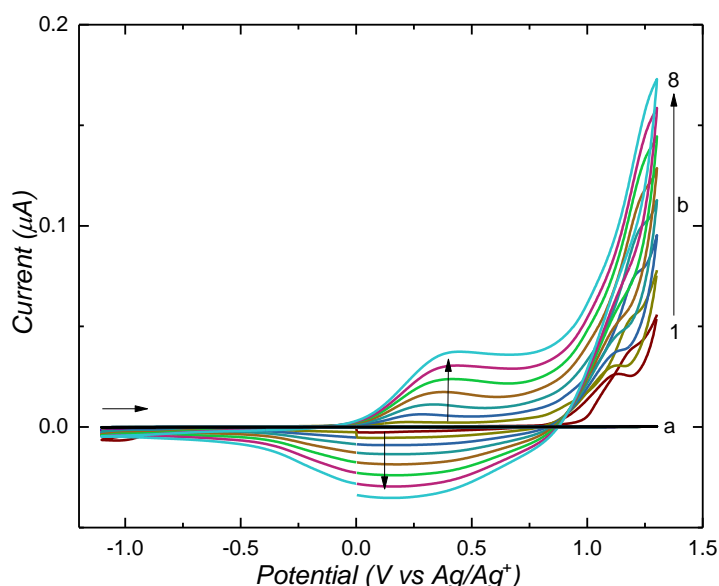


Figure 5-4. Cyclic voltammograms from (a) bar electrode at 0.1 M $(\text{C}_4\text{H}_9)_4\text{NBF}_4$, acetonitrile, (b) the electropolymerization of 46.84 μM ZnP and 0.14 M Pyr at a potential range of -1.1 to 1.3 V (vs. Ag/Ag^+) and a scan rate of 50 mV/s (8 cycles) in 0.1 M $(\text{C}_4\text{H}_9)_4\text{NBF}_4$, acetonitrile.

The cyclic voltammogram for ZnP/Pyr electropolymerisation showed an oxidation peak at +0.80 V (Figure 5-4), characteristic for pyrrole.¹⁷⁴ From the first to the eighth cycle, the current continuously grows indicating deposition of a conducting polymer. The ZnP/Pyr polymerisation results in a deposition of a black thin polymer layer. (Figure 5-5). After polymerisation, the electro-activity of the polymer was observed from -0.25 to +1 V. This potential range was used in the further electrochemical analysis. The blank

signal from the platinum bar electrode was recorded using cyclic voltammetry under the same conditions (0.1 M $(C_4H_9)_4NBF_4$, acetonitrile) and used as a baseline.

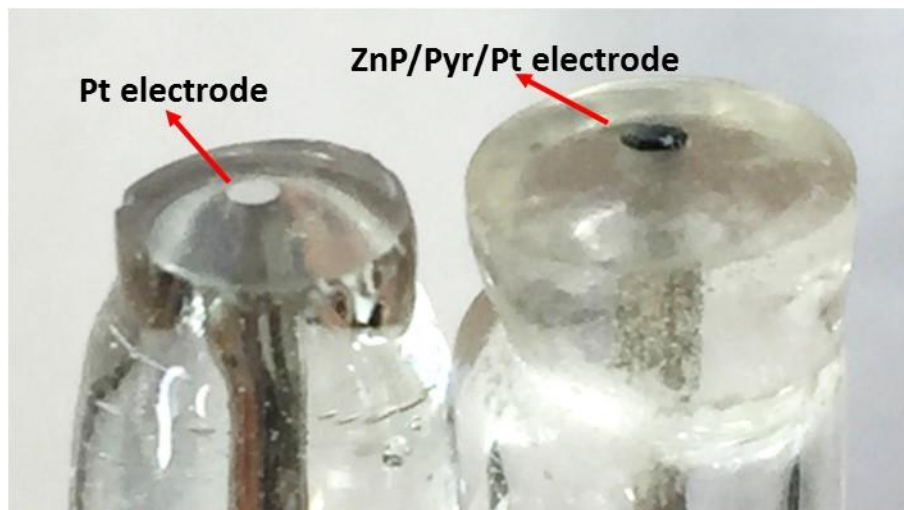


Figure 5-5. The surface of bar Pt electrode (left) and ZnP/Pyr polymer deposit on Pt electrode (right).

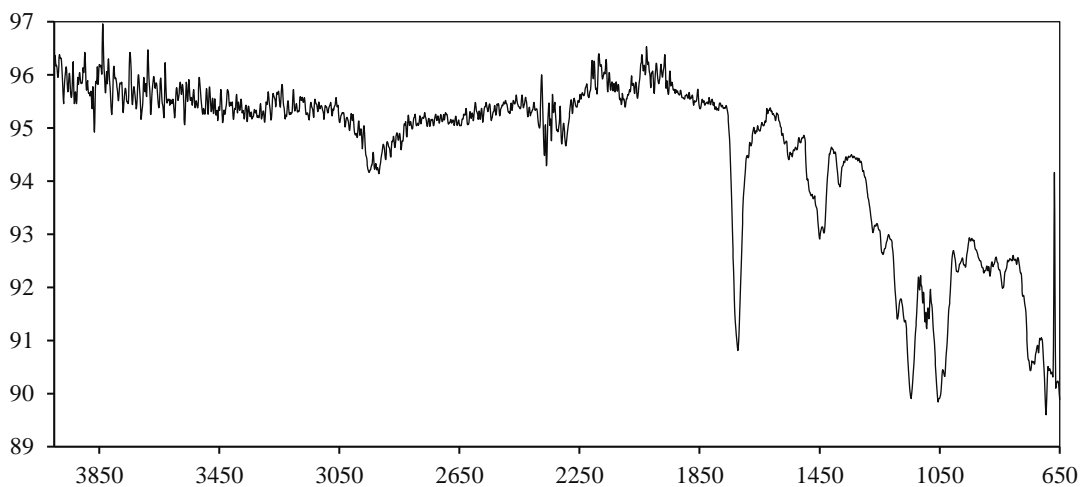


Figure 5-6. Infrared spectrum from ZnP/Pyr polymer. The polymer was electro-deposited on a gold surface.

To identify the ZnP/Pyr polymer structure, the infrared spectrum was analysed. The spectra present mainly characteristic bands from pyrrole and porphyrin (Figure 5-6). The C=C stretch and C=C in-plane bending vibrations from pyrrole ring were observed at 1553 and 991-964 cm^{-1} respectively.^{173,175} Bands from C-H deformation vibrations and C-N stretching vibrations were displayed at 1055 and 1146 cm^{-1} .¹⁷³ Aromatic porphyrin bands were at 2952-2918 cm^{-1} .¹⁷⁶ Also, vibration from porphyrin skeleton was revealed

at 1382 cm^{-1} .¹⁷⁷ The characteristic vibrational band from Zn(II)porphyrin was observed at 1723 cm^{-1} .¹⁷⁷

5.3.2 Immobilisation of nanoMIPs on ZnP/Pyr/Pt electrode

Covalent immobilisation of nanoMIPs on ZnP/Pyr polymer was performed using carbodiimide via phosphate and amine groups.¹⁷⁸ A schematic representation was inspired by Xu *et al.* research for this reaction shown in Figure 5-7.¹⁷⁹ Primary amine groups displayed from nanoMIPs prompt coordination interactions with the ZnP. To summarised both binding forces drive the immobilisation of nanoMIPs on the ZnP/Pyr polymer surface.

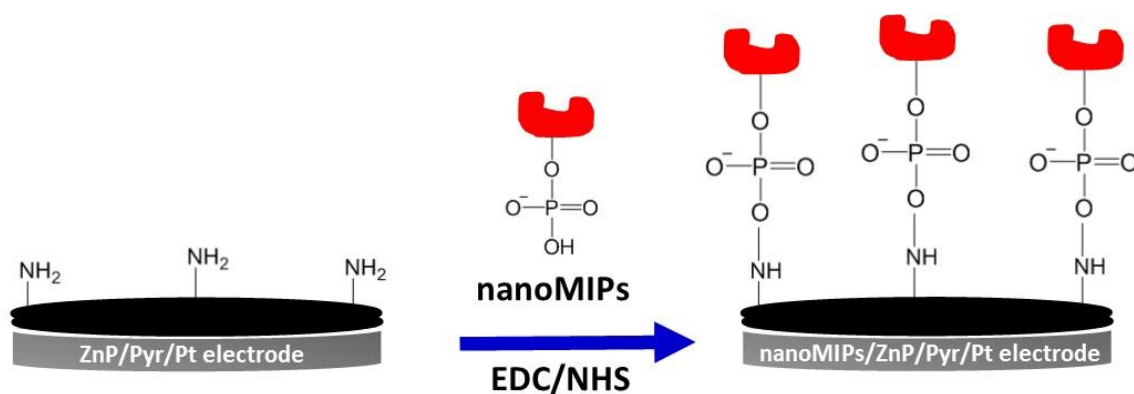


Figure 5-7. Schematic representation from nanoMIPs immobilisation on ZnP/Pyr/Pt electrode via carbodiimide chemistry.

The nanoMIPs immobilised ZnP/Pyr polymer is imaged using AFM (Figure 5-8). AFM images display topography changes between ZnP/Pyr polymer surface before (Figure 5-10 (a and a')) and after nanoMIPs immobilisation (Figure 5-8 (b and b')). The ZnP/Pyr polymer surface is highly granular and present aggregates. The roughness was found 20.4 nm and the average grain size was 230 nm. The morphology and structure of ZnP/Pyr polymer are affected by the polymerisation conditions such as nature of the metal centre, monomer concentration, solvent, current density, and electrode surface etc.¹⁸⁰ After nanoMIPs immobilisation, the roughness and average grain size decreased at 7.7 and 110 nm respectively.

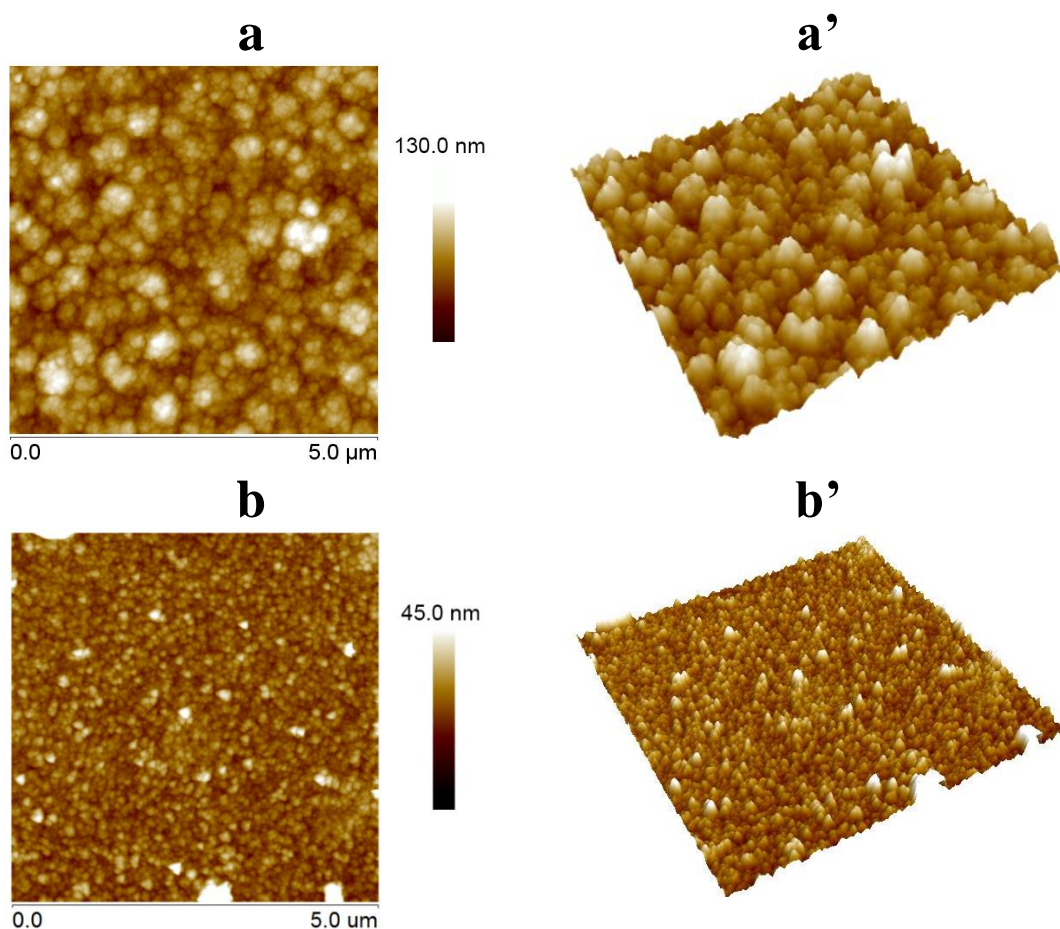


Figure 5-8. AFM images for (a and a') ZnP/Pyr polymer surface. (b and b') nanoMIPs immobilised on ZnP/Pyr polymer surface. The measured area was $5 \times 5 \mu\text{m}^2$.

5.3.3 Determination of FB1 using MINES

Determination of FB1 using DPV technique

The nanoMIPs appropriately recognised FB1 and successfully employed for DPV determination. During DPV measurements, the $[\text{Fe}(\text{CN})_6]^{4-/3-}$ was employed as a redox label. Thus, the current intensity response was correlated to the FB1 concentration. To demonstrate the nanoMIPs specificity as a recognition element, their DPV response compared to the nonimprinted polymer nanoparticles (nanoNIPs) as shown Figure 5-9. The response from the nanoNIPs was low and non-specific to FB1. Thus, the specificity of the nanoMIPs to FB1 was validated. Additionally, the ZnP/Pyr polymer was tested and a negligible response was observed (Figure 5-9). Seemingly, there is a nanoMIPs actuation between FB1 and the redox label $[\text{Fe}(\text{CN})_6]^{4-/3-}$.¹⁸¹ Therefore, nanoMIPs

specific actuation affects the DPV current response. The redox label current response increase proportionally to FB1 concentration. Notably, no changes in current response were observed when nanoNIPs or ZnP/Pyr polymer were employed as recognition elements (Figure 5-9).

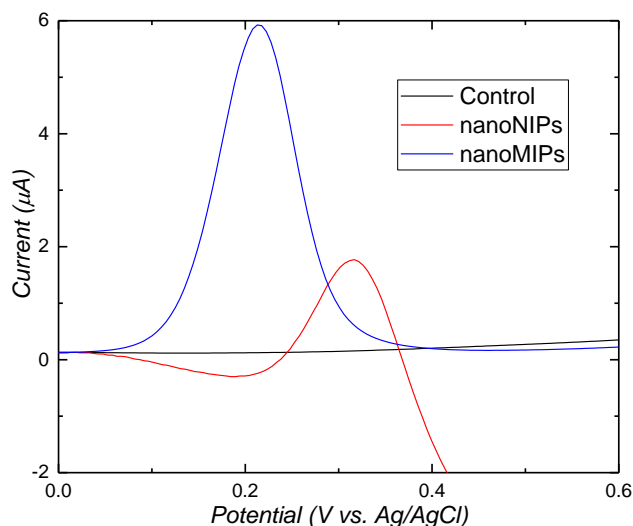


Figure 5-9. DPV response for a solution 100 fM FB1 standard in control using as recognition element ZnP/Pyr polymer, nanoNIPs and nanoMIPs. All the measurements were carried out in 0.01 M PBS buffer and 0.005 M $[\text{Fe}(\text{CN})_6]^{4-/3-}$, recorded at the potential range -0.25 to +1.10 V vs. Ag/AgCl and 5 min previous incubation.

The material actuation using redox labels such as $[\text{Fe}(\text{CN})_6]^{4-/3-}$ was previously observed in aptamers for DNA sensors.¹⁸² The nanoMIP actuation is related to the DPV current response generated by $[\text{Fe}(\text{CN})_6]^{4-/3-}$ electron transfer at the electrode surface. The electron transfer was observed only when FB1 was present in solution. A possible hypothesis of the actuation mechanism is as follow: in the absence of FB1, the redox label $[\text{Fe}(\text{CN})_6]^{4-/3-}$ is excluded from the nanoMIPs surface and the charge transfer did not take place. Conversely, the presence of FB1 can increase the porosity and permeability nanoMIPs. These changes, allow the redox label charge transfer at the electrode surface as illustrated in Figure 5-10.

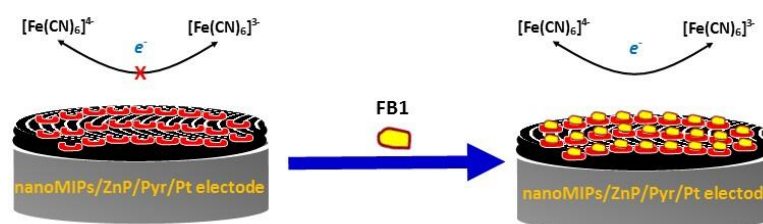


Figure 5-10. The schematic diagram of redox activity of $[\text{Fe}(\text{CN})_6]^{4-/3-}$ on nanoMIPs/ZnP/Pyr/Pt electrode because of interaction between FB1 and nanoMIPs (modified from Le *et al.*, 2016¹⁸²)

The MINES using DPV technique can detect FB1 in a linear concentration from 10 fM to 10 pM (Figure 5-11). MINES is therefore 1000 times more sensitive than MINA. The DPV response increases when the concentration of FB1 rises. There is a linear correlation between the current and FB1 concentration. Conversely, the DPV response is negligible when the control electrode (nanoNIPs electrode) was used (Figure 5-12).

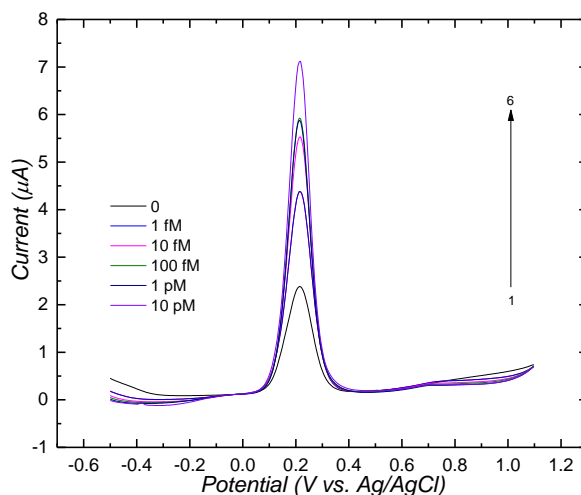


Figure 5-11. Differential pulse voltammetry response for (1) 0, (2) 1 fM, (3) 10 fM, (4) 100 fM, (5) 1 pM, and (6) 10 pM FB1. All the measurements were carried out in 0.01 M PBS and 0.005 M $[\text{Fe}(\text{CN})_6]^{4-/3-}$, recorded at the potential range -0.25 to +1.10 V (vs. Ag/AgCl).

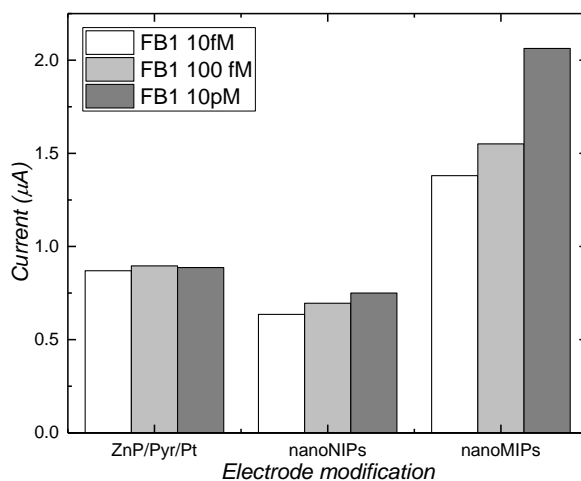


Figure 5-12. DPV calibration curve for FB1 (10 fM, 100 fM and 10 pM) in ZnP/Pyr/Pt (control), nanoNIPs and nanoMIPs. All measurements were carried out in 0.01 M PBS and 0.005 M $[\text{Fe}(\text{CN})_6]^{4-/3-}$.

The calibration curve for FB1 using DPV measurements in concentration range 1 fM to 10 pM is shown in Figure 5-13. The sensor presents a sensitivity of 0.281 $\mu\text{A}/\text{M}$ ($R^2=0.96$) and a LoD of 0.03 fM. The cross-reactivity for the FB1 sensor was evaluated

for other mycotoxins (FB2, AFB1, CTT, DON and ZEA). The sensor does not expose specific response to other mycotoxins. The sensitivity for other mycotoxins displayed values lower than $0.061 \mu\text{A}/\text{M}$ (Table 5-1). To summarise, the sensor response suggested that there is no cross-reactivity.

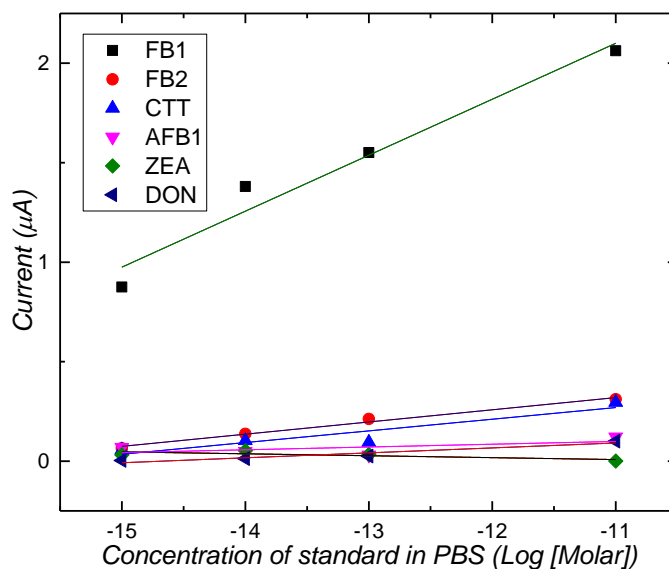


Figure 5-13. DPV calibration curve for FB1 and other mycotoxins (FB2, AFB1, CTT, DON and ZEA). All the measurements were carried out using a nanoMIPs sensor in 0.01 M PBS and 0.005 M $[\text{Fe}(\text{CN})_6]^{4-/3-}$ in a mycotoxin concentration range from 1fM – 10 pM.

Table 5-1. NanoMIPs sensor response comparison and linear equation values for DPV calibration curves for mycotoxins

Target compounds	$\Delta I (\mu\text{A}) = \text{slope} \times \text{Log } C (\text{Molar}) + \text{intercept}$		
	Slope	Intercept	R ²
FB1	0.281	5.195	0.962
FB2	0.061	0.994	0.989
AFB1	0.014	0.253	0.377
CTT	0.059	0.914	0.869
DON	0.025	0.365	0.915
ZEA	-0.0097	-0.0987	0.584

Determination of FB1 using a free label impedimetric sensor

MINES was tested using electrochemical impedance spectroscopy (EIS) in a label free mode (without ferricyanide and ferrocyanide redox label, $[\text{Fe}(\text{CN})_6]^{4-/3-}$). Previously impedimetric sensors have been successfully used for aflatoxin M1 determination.¹⁷⁸ The nanoMIPs sensor was tested using EIS in a linear concentration range of FB1 from 1 fM to 10 pM in PBS at potential +0.5 V (vs Ag/AgCl), AC amplitude 25 mV, and frequency 50 mHz to 200 kHz and 35s/scans. The interaction between nanoMIPs and FB1 was followed by measuring the impedance at the surface electrode and represented as Nyquist plots. This interaction can be seen as semicircle signals (Figure 5-14).¹⁷⁰ Apparently, the interaction between nanoMIPs and FB1 causes an increase in the resistance at the electrode surface.

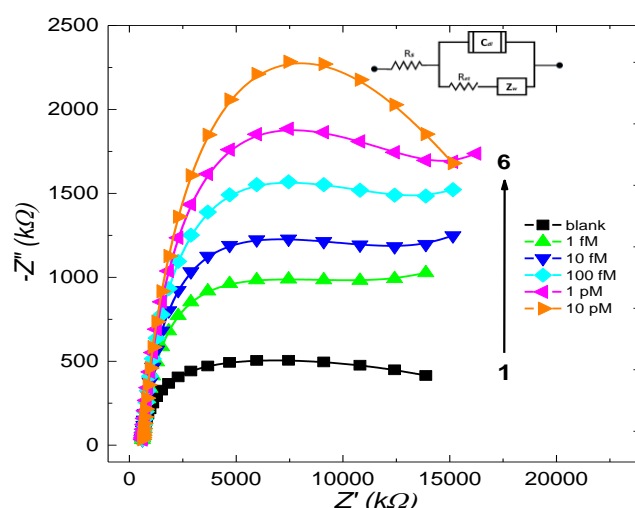


Figure 5-14. Nyquist plot for EIS determination of FB1 using a nanoMIPs sensor for concentrations at (1) 0 M, (2) 1 fM, (3) 10 fM, (4) 100 fM, (5) 1 pM, and (6) 10 pM. All the measurements were carried out in 0.01 M PBS buffer, recorded at the frequency range 400 mHz - 200 kHz and at potential +0.35 V (vs. Ag/AgCl). Inset is the equivalent circuit where R_s is the solution-phase resistance, R_{et} is the electron transfer resistance, C_{dl} is the double-layer capacitance, and Z_w is the Warburg impedance.

The label-free nanoMIPs impedimetric sensor for FB1 present sensitivity of 0.442 kΩ/M ($R^2=0.98$) and LoD of 0.7 fM in a linear concentration range from 1 fM to 10 pM (Figure 5-15). No cross-reactivity was observed for other mycotoxins (AFB1, CTT, DON and ZEA) as shown in Table 5-2.

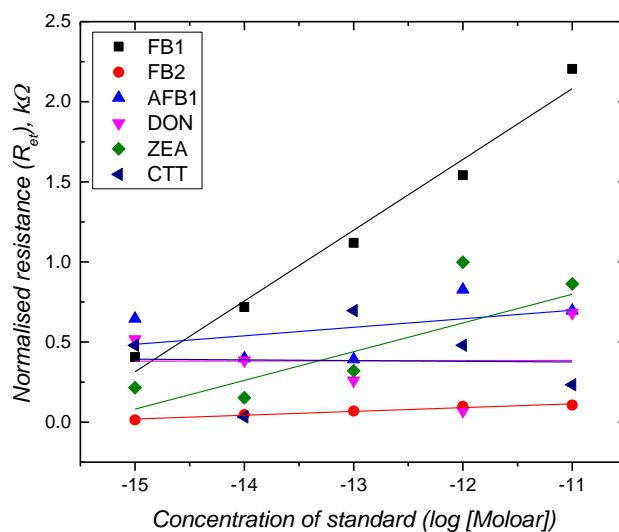


Figure 5-15. EIS calibration curve for FB1 and other mycotoxins (FB2, AFB1, CTT, DON and ZEA). All the measurements were carried in 0.01 M PBS buffer, in mycotoxins concentration from 0 – 10 pM, recorded at the frequency range 400 mHz - 200 kHz and at potential +0.35 V (vs. Ag/AgCl).

Table 5-2. FB1 Impedimetric sensor response for EIS measurements.

Linear equation parameters for the calibration curve for mycotoxins

Target compounds	ΔR (kΩ) = slope × Log C (Molar) + intercept		
	Slope	Intercept	R ²
FB1	0.442	6.944	0.980
FB2	0.024	0.375	0.971
AFB1	0.053	1.283	0.193
CTT	-0.004	0.326	<0.001
DON	0.001	0.398	<0.001
ZEA	0.179	2.770	0.748

5.4 Conclusion

Development of electrochemical sensor based on molecularly imprinted nanoparticles (MINES) has been demonstrated successfully for determination of fumonisin B1 (FB1). The sensor was tested using DPV (redox labelled sensor) and EIS (free labelled sensor). Both methods showed high sensitivity and selectivity to FB1.

MINES were fabricated by immobilising nanoMIPs on a Zinc(II)porphyrin-pyrrole (ZnP/Pyr) polymer surface on platinum electrodes. The nanoMIP sensor displayed higher response than control ZnP/Pyr polymer and nanoNIP.

The EIS ($0.442 \text{ k}\Omega/\text{M}$) is two times more sensitive than DPV ($0.281 \mu\text{A}/\text{M}$). The linearity and LoD from EIS ($R^2 = 0.98$, LoD = 0.7 fM) and DPV ($R^2 = 0.96$, LoD = 0.03 fM) demonstrated the excellent sensor performance.

CHAPTER 6 GENERAL CONCLUSION AND FUTURE WORK

6.1 Conclusions

Development of detection techniques for mycotoxins especially for fumonisins in food and animal feed has advanced rapidly. Many technologies have been manufactured for analysis of the carcinogenic fumonisins. Sophisticated instruments, such as HPLC and LCMS/MS, have been created for quantitative observation. The rapid tests, such as ELISA, immunostrip, and sensor, have been produced to analyse a number of samples in one measurement. However, the methods are expensive and challenging to be produced and applied in the developing world.

In this work, the molecularly imprinted polymer nanoparticles (nanoMIPs) were synthesised using a relatively robust and new method from Canfarotta and colleagues.¹¹⁸ However, the methods need more optimisation to obtain the nanoMIPs more precisely on both the quantitative and qualitative properties.

A novel evolution of the ELISA method, called nanoMIPs based assay (MINA), was developed for determination of fumonisin B1 (FB1) in food and animal feed. The MINA method is based on plastic antibodies called nanoMIPs. MINA minimises the chemicals used and is affordable and reliable. The sensitivity of MINA is higher than conventional ELISA based on monoclonal antibody that are in use and commercially available. No significant response from other mycotoxins can be attributed that MINA has high selectivity and sensitivity for determination of FB1. When compared to commercial ELISA kits and HPLC, MINA performance is superior. The limit of detection of MINA is lower than ELISA. However, the correlation of fumonisins analysis in real samples is lower than 90 %. and further optimisation in other aspects and validation are still required.

A nanoMIPs-based sensor (MINES) was also developed in this study. MINES can reduce the detailed protocols of MINA use. MINES uses the electrochemical properties for determination of fumonisin B1 so that the chemicals would be more efficient than MINA. The obtained label and free label MINES show an excellent response to fumonisin B1. No cross-reactivity with other mycotoxins was observed. However, the validation method

and comparative study are necessary to obtaining information about the robustness of MINES.

Overall, the nanoMIPs for fumonisin B1 have been developed and applied successfully in MINA and MINES as innovative approaches for determination of fumonisins and can lead the way in the successful development of a commercial device that can be used by government and industry and stakeholders.

6.2 Future work

The further research will be useful for enhancing the performance of nanoMIPs-based assay and sensor.

Potentially, the obtained MINA in this study will become a commercial MINA. More validation data should be achieved. The stability of MINA will be tested in different pH condition although the application has been tested in relatively neutral condition (water or PBS, pH~7). Also, the stability of the nanoMIPs coated microplate will be investigated for packaging purposed as previous commercial ELISA kit. Finally, the proficiency test involving different testing laboratory will be needed to find the quality and reliable of MINA analysis.

Although the detection limit of MINES is lower than MINA, the performance of MINES will be validated especially for testing on real samples, such as corn. These become a challenge to find the most straightforward and rapid extraction method of sample preparation for MINES. The application of MINES will be tried to the screen print electrode (SPE) instead of the glass electrode. The robustness of MINES will be evaluated by testing on different pH, solvent, temperature and storage time.

REFERENCES

1. Norred WP, Voss KA. Toxicity and role of fumonisins in animal diseases and human esophageal cancer. *J Food Prot.* 1994;57(6):522-527.
2. Zain ME. Impact of mycotoxins on humans and animals. *Journal of Saudi Chemical Society.* 2011;15(2):129-144.
3. Ostry V, Malir F, Toman J, Grosse Y. Mycotoxins as human carcinogens—the IARC monographs classification. *Mycotoxin research.* 2017;33(1):65-73.
4. IARC Working Group on the Evaluation of Carcinogenic Risks to Humans, World Health Organization, International Agency for Research on Cancer. *Some traditional herbal medicines, some mycotoxins, naphthalene and styrene.* World Health Organization; 2002.
5. Food and Drug Administration. Guidance for industry: Fumonisin levels in human foods and animal feed. <https://www.fda.gov/Food/GuidanceRegulation/GuidanceDocumentsRegulatoryInformation/ChemicalContaminantsMetalsNaturalToxinsPesticides/ucm109231.htm>. Updated 2017. Accessed June 6, 2001.
6. The commission of the european communities. The presence of deoxynivalenol, zearalenone, ochratoxin A, T-2 and HT-2 and fumonisins in products intended for animal feeding. *Official Journal of the European Union.* 2006;02/01/2018.
7. National Standardization Agency of Indonesia. Mycotoxin maximum level content on food . . 2009;SNI 7385:2009.
8. Krska R, Welzig E, Boudra H. Analysis of fusarium toxins in feed. *Anim Feed Sci Technol.* 2007;137(3):241-264.
9. Smith GW. Fumonisin. In: *Veterinary toxicology (second edition).* Elsevier; 2012:1205-1219.
10. Ali N, Sardjono, Yamashita A, Yoshizawa T. Natural co- occurrence of aflatoxins and fusarium mycotoxins (fumonisins, deoxynivalenol, nivalenol and zearalenone) in corn from indonesia. *Food Additives & Contaminants.* 1998;15(4):377-384.
11. Tangendjaja B, Rachmawati S, Wina E. Mycotoxin contamination on corn used by feed mills in indonesia. *Indonesian Journal of Agricultural Science.* 2016;9(2):68-76.
12. Yamashita A, Yoshizawa T, Aiura Y, et al. Fusarium mycotoxins (fumonisins, nivalenol, and zearalenone) and aflatoxins in corn from southeast asia. *Biosci Biotechnol Biochem.* 1995;59(9):1804-1807.
13. Martindah E, Bahri S. Mycotoxin contamination in the food chain. *WARTAZOA. Indonesian Bulletin of Animal and Veterinary Sciences.* 2017;26(3):115-124.
14. Maryam R. Contamination of fumonisins on raw materials and chicken feed in west java. . 2000:538-542.
15. Miller JD. Factors that affect the occurrence of fumonisin. *Environ Health Perspect.* 2001;109 Suppl 2:321-324.

16. Marín S, Magan N, Bellí N, Ramos AJ, Canela R, Sanchis V. Two-dimensional profiles of fumonisin B1 production by fusarium moniliforme and fusarium proliferatum in relation to environmental factors and potential for modelling toxin formation in maize grain. *International Journal of Food Microbiology*. 1999;51(2):159-167. doi: [https://doi.org/10.1016/S0168-1605\(99\)00115-4](https://doi.org/10.1016/S0168-1605(99)00115-4).
17. Belajová E, Rauová D. Single laboratory-validated HPLC methods for determination of ochratoxin A, fumonisin B1 and B2, zearalenone and deoxynivalenol in cereals and cereal-based foods. *J Food Nutr Res*. 2010;49(2):57-68.
18. Hopmans EC, Murphy PA. Detection of fumonisins B1, B2, and B3 and hydrolyzed fumonisin B1 in corn-containing foods. *J Agric Food Chem*. 1993;41(10):1655-1658.
19. Kaltner F, Rampl C, Rychlik M, Zimmermann T, Rohe A. Development and validation of a cost-effective HPLC-FLD method for routine analysis of fumonisins B1 and B2 in corn and corn products. *Food Anal Methods*. 2017;10(5):1349-1358.
20. Kawashima LM, Vieira AP, Valente Soares LM. Fumonisin B1 and ochratoxin A in beers made in Brazil. *Cienc Tecnol Aliment*. 2007;27(2):317-323.
21. Liu F-, Chen P-, Fu Y-, Shih DY-. Determination of fumonisin B1 and B2 in corn products. *J Food Drug Anal*. 2005;13(3):273-278.
22. Martins HML, Almeida IFM, Camacho CRL, Santos SMO, Costa JMG, Bernardo FMA. Occurrence of fumonisins in feed for swine and horses. *Rev Iberoam Micol*. 2012;29(3):175-177.
23. Czerwiecki L. Determination of selected mycotoxins in food. II. selection of optimal conditions for the determination of fumonisin B1 and B2 in corn products using high performance liquid chromatography. *Rocz Panstw Zakl Hig*. 1998;49(1):13-24.
24. Dilkin P, Mallmann CA, De Almeida CAA, Corrêa B. Robotic automated clean-up for detection of fumonisins B1 and B2 in corn and corn-based feed by high-performance liquid chromatography. *J Chromatogr A*. 2001;925(1-2):151-157.
25. Duncan K, Kruger S, Zabe N, Kohn B, Prioli R. Improved fluorometric and chromatographic methods for the quantification of fumonisins B1, B2 and B3. *J Chromatogr A*. 1998;815(1):41-47.
26. Kosoglu I, Aksoy U, Pehlivan R. Fumonisin B1 and B2 occurrence in dried fig fruits (*Ficus carica* L.) under meander valley's climatic conditions and relationship with fruit quality. *Food Addit Contam Part A Chem Anal Control Exposure Risk Assess*. 2011;28(11):1569-1577.
27. Lino CM, Silva LJG, Pena ALS, Silveira MI. Determination of fumonisins B1 and B2 in Portuguese maize and maize-based samples by HPLC with fluorescence detection. *Anal Bioanal Chem*. 2006;384(5):1214-1220.
28. Ma L, Xu W, He X, Huang K, Wang Y, Luo Y. Determination of fumonisins B1 and B2 in Chinese rice wine by HPLC using AQC precolumn derivatisation. *J Sci Food Agric*. 2013;93(5):1128-1133.

29. Ndube N, van der Westhuizen L, Green IR, Shephard GS. HPLC determination of fumonisin mycotoxins in maize: A comparative study of naphthalene-2,3-dicarboxaldehyde and o-phthalaldehyde derivatization reagents for fluorescence and diode array detection. *J Chromatogr B Anal Technol Biomed Life Sci.* 2011;879(23):2239-2243.
30. Scarano G, Grasso L, Arace O, Oliviero G, Serpe L. Use of semiautomatic equipment for the determination of fumonisin B1 in milk. *Ind Aliment.* 2001;40(401):257-260.
31. Soleimany F, Jinap S, Rahmani A, Khatib A. Simultaneous detection of 12 mycotoxins in cereals using RP-HPLC-PDA-FLD with PHRED and a post-column derivatization system. *Food Addit Contam Part A Chem Anal Control Exposure Risk Assess.* 2011;28(4):494-501.
32. Solfrizzo M, De Girolamo A, Visconti A. Determination of fumonisins B1 and B2 in cornflakes by high performance liquid chromatography and immunoaffinity clean-up. *Food Addit Contam.* 2001;18(3):227-235.
33. Tardieu D, Bailly J-, Skiba F, Grosjean F, Guerre P. Toxicokinetics of fumonisin B1 in turkey poult and tissue persistence after exposure to a diet containing the maximum european tolerance for fumonisins in avian feeds. *Food Chem Toxicol.* 2008;46(9):3213-3218.
34. Ye H, Lai X, Liu C. Determination of fumonisin B1 and B2 in corn using matrix-phase dispersion coupled to high performance liquid chromatography. *Asian J Chem.* 2013;25(12):6807-6810.
35. Spanjer MC, Rensen PM, Scholten JM. LC-MS/MS multi-method for mycotoxins after single extraction, with validation data for peanut, pistachio, wheat, maize, cornflakes, raisins and figs. *Food Addit Contam.* 2008;25(4):472-489.
36. Andersen AJC, De Medeiros LS, Binzer SB, et al. HPLC-HRMS quantification of the ichthyotoxin karmitoxin from karlodium armiger. *Mar Drugs.* 2017;15(9).
37. Bansal J, Pantazopoulos P, Tam J, et al. Surveys of rice sold in canada for aflatoxins, ochratoxin a and fumonisins. *Food Addit Contam Part A Chem Anal Control Exposure Risk Assess.* 2011;28(6):767-774.
38. Faberi A, Foglia P, Pastorini E, Samperi R, Laganà A. Determination of type B fumonisin mycotoxins in maize and maize-based products by liquid chromatography/tandem mass spectrometry using a QqQ linear ion trap mass spectrometer. *Rapid Commun Mass Spectrom.* 2005;19(2):275-282.
39. Kong W, Xie T, Li J, et al. Analysis of fumonisins B1 and B2 in spices and aromatic and medicinal herbs by HPLC-FLD with on-line post-column derivatization and positive confirmation by LC-MS/MS. *Analyst.* 2012;137(13):3166-3174.
40. Lukacs Z, Schaper S, Herderich M, Schreier P, Humpf H-. Identification and determination of fumonisin FB1 and FB2 in corn and corn products by high-performance liquid chromatography - electrospray-ionization tandem mass spectrometry (HPLC-ESI-MS-MS). *Chromatographia.* 1996;43(3-4):124-128.
41. Plattner RD. HPLC/MS analysis of fusarium mycotoxins fumonisins and deoxynivalenol. *Nat Toxins.* 1999;7(6):365-370.

42. Plattner RD, Weisleder D, Poling SM, eds. *Analytical determination of fumonisins and other metabolites produced by fusarium moniliforme and related species on corn.* ; 1996Advances in Experimental Medicine and Biology; No. 392.
43. Wang Y, Xiao C, Guo J, et al. Development and application of a method for the analysis of 9 mycotoxins in maize by HPLC-MS/MS. *J Food Sci.* 2013;78(11):M1752-M1756.
44. Xie T-, Qiu F, Yang M-, Qi A-. Simultaneous determination of fumonisins B1 and B2 in traditional chinese medicines by high-performance liquid chromatography-tandem mass spectrometry. *Yaoxue Xuebao.* 2011;46(7):822-827.
45. Zhao H, Chen X, Shen C, Qu B. Determination of 16 mycotoxins in vegetable oils using a QuEChERS method combined with high-performance liquid chromatography-tandem mass spectrometry. *Food Addit Contam Part A Chem Anal Control Exposure Risk Assess.* 2017;34(2):255-264.
46. Ghali R, Ghorbel H, Hedilli A. Fumonisin determination in tunisian foods and feeds. ELISA and HPLC methods comparison. *J Agric Food Chem.* 2009;57(9):3955-3960.
47. Yeung JM, Prelusky DB, Savard ME, Dang BD, Robinson LA. Sensitive immunoassay for fumonisin B1 in corn. *J Agric Food Chem.* 1996;44(11):3582-3586.
48. Shu M, Xu Y, Wang D, et al. Anti-idiotypic nanobody: A strategy for development of sensitive and green immunoassay for fumonisin B1. *Talanta.* 2015;143:388-393.
49. Shu M, Xu Y, Liu X, et al. Anti-idiotypic nanobody-alkaline phosphatase fusion proteins: Development of a one-step competitive enzyme immunoassay for fumonisin B1 detection in cereal. *Anal Chim Acta.* 2016;924:53-59.
50. Shiu C, Wang J, Yu F. Sensitive enzyme- linked immunosorbent assay and rapid one- step immunochromatographic strip for fumonisin B1 in grain- based food and feed samples. *J Sci Food Agric.* 2010;90(6):1020-1026.
51. Peltomaa R, Benito-Peña E, Barderas R, Sauer U, González-Andrade M, Moreno-Bondi MC. Microarray-based immunoassay with synthetic mimotopes for the detection of fumonisin B1. *Anal Chem.* 2017.
52. Maragos CM, Plattner RD, Miklasz SD. Determination of hydrolysed fumonisin B1 (HFB1) in corn by competitive direct enzyme- linked immunosorbent assay. *Food additives & contaminants.* 1996;13(1):105-113.
53. Li Y, Zhang J, Wang Y, et al. Immunity theory-based high-specific monoclonal antibody preparation and application of fumonisin B1. *Food Analytical Methods.* 2017;10(10):3361-3367.
54. Lamberti I, Tanzarella C, Solinas I, Padula C, Mosiello L. An antibody-based microarray assay for the simultaneous detection of aflatoxin B 1 and fumonisin B 1. *Mycotoxin research.* 2009;25(4):193.
55. Deng G, Xu K, Sun Y, Chen Y, Zheng T, Li J. High sensitive immunoassay for multiplex mycotoxin detection with photonic crystal microsphere suspension array. *Anal Chem.* 2013;85(5):2833-2840.

56. Castells M, Marín S, Sanchis V, Ramos AJ. Distribution of fumonisins and aflatoxins in corn fractions during industrial cornflake processing. *Int J Food Microbiol.* 2008;123(1-2):81-87.
57. Ono EY, Kawamura O, Ono MA, Ueno Y, Hirooka EY. A comparative study of indirect competitive ELISA and HPLC for fumonisin detection in corn of the state of paraná, brazil. *Food Agric Immunol.* 2000;12(1):5-14.
58. YU F, Chu FS. Production and characterization of antibodies against fumonisin B1. *J Food Prot.* 1996;59(9):992-997.
59. Lin X, Guo X. Advances in biosensors, chemosensors and assays for the determination of fusarium mycotoxins. *Toxins.* 2016;8(6):161.
60. Masikini M, Mailu SN, Tsegaye A, et al. A fumonisins immunosensor based on polyanilino-carbon nanotubes doped with palladium telluride quantum dots. *Sensors.* 2014;15(1):529-546.
61. Sewram V, Mshicileli N, Shephard GS, et al. Production of fumonisin B and C analogues by several fusarium species. *J Agric Food Chem.* 2005;53(12):4861-4866.
62. Sydenham EW, Shephard GS, Stockenström S, Rheeder JP, Marasas WF, van der Merwe, Marthinus J. Production of fumonisin B analogues and related compounds by fusarium globosum, a newly described species from corn. *J Agric Food Chem.* 1997;45(10):4004-4010.
63. Rheeder JP, Marasas WF, Vismar HF. Production of fumonisin analogs by fusarium species. *Appl Environ Microbiol.* 2002;68(5):2101-2105.
64. Stępień Ł, Koczyk G, Waśkiewicz A. FUM cluster divergence in fumonisins-producing fusarium species. *Fungal biology.* 2011;115(2):112-123.
65. National Center for Biotechnology Information. PubChem compound database; CID=2733487. <https://pubchem.ncbi.nlm.nih.gov/compound/2733487>. Updated 2016. Accessed October/30, 2017.
66. National Center for Biotechnology Information. PubChem compound database; CID=62314. <https://pubchem.ncbi.nlm.nih.gov/compound/62314>. Updated 2016. Accessed Nov/20, 2017.
67. Kalsi PS., ed. *Stereochemistry : Conformation and mechanism.* 7th ed. Anshan: Tunbridge Wells; 2009.
68. Author A. On the issue of enantioselectivity of chiral pesticides: A green chemistry opportunity. *Green Chem.* 2004;6(12):G77-G78.
69. Gelderblom WC, Jaskiewicz K, Marasas WF, et al. Fumonisins--novel mycotoxins with cancer-promoting activity produced by fusarium moniliforme. *Appl Environ Microbiol.* 1988;54(7):1806-1811.
70. Fatma A M Abu-Hassan, Riad H Khalil, Talaat T Saad, Mahmoud T Amer, Hany M R Abdel-Latif. Histopathological outcomes designating the toxicological aspects of fumonisin B1 on cultured Nile tilapia, *Oreochromis niloticus*. *International Journal of Fisheries and Aquatic Studies.* 2016;4(3):52-60.

71. Abu-Hassan FA, Khalil RH, Saad TT, Amer MT, Abdel-Latif HM. Histopathological outcomes designating the toxicological aspects of fumonisin B1 on cultured Nile tilapia, *Oreochromis niloticus*. . 2016.
72. Voss KA, Riley RT, Snook ME, Waes JG. Reproductive and sphingolipid metabolic effects of fumonisin B1 and its alkaline hydrolysis product in LM/bc mice: Hydrolyzed fumonisin B1 did not cause neural tube defects. *Toxicological sciences*. 2009;112(2):459-467.
73. Kellerman TS, Marasas WFO, Thiel P, Gelderblom W, Cawood M. Leukoencephalomalacia in two horses induced by oral dosing of fumonisin B₁ . . 1990.
74. Osweiler GD, Ross P, Wilson T, et al. Characterization of an epizootic of pulmonary edema in swine associated with fumonisin in corn screenings. *Journal of Veterinary Diagnostic Investigation*. 1992;4(1):53-59.
75. Haschek WM, Gumprecht LA, Smith G, Tumbleson ME, Constable PD. Fumonisin toxicosis in swine: An overview of porcine pulmonary edema and current perspectives. *Environ Health Perspect*. 2001;109 Suppl 2:251-257.
76. Merrill Jr A, Wang E, Vales T, et al. Fumonisin toxicity and sphingolipid biosynthesis. In: *Fumonisin in food*. Springer; 1996:297-306.
77. Stockmann-Juvala H, Savolainen K. A review of the toxic effects and mechanisms of action of fumonisin B1. *Hum Exp Toxicol*. 2008;27(11):799-809.
78. Alexander C, Andersson HS, Andersson LI, et al. Molecular imprinting science and technology: A survey of the literature for the years up to and including 2003. *Journal of molecular recognition*. 2006;19(2):106-180.
79. Andersson HS, Nicholls IA, eds. *Chapter 1 A historical perspective of the development of molecular imprinting*. ; 2000 *Techniques and Instrumentation in Analytical Chemistry*; No. 23.
80. Shen F, Ren X. Covalent molecular imprinting made easy: A case study of mannose imprinted polymer. *RSC Advances*. 2014;4(25):13123-13125.
81. Matsui J, Miyoshi Y, Doblhoff-Dier O, Takeuchi T. A molecularly imprinted synthetic polymer receptor selective for atrazine. *Anal Chem*. 1995;67(23):4404-4408.
82. Qi P, Wang J, Wang L, et al. Molecularly imprinted polymers synthesized via semi-covalent imprinting with sacrificial spacer for imprinting phenols. *Polymer*. 2010;51(23):5417-5423.
83. Prasad BB, Kumar D, Madhuri R, Tiwari MP. Metal ion mediated imprinting for electrochemical enantioselective sensing of l-histidine at trace level. *Biosensors and Bioelectronics*. 2011;28(1):117-126.
84. Piletska EV, Guerreiro AR, Romero-Guerra M, Chianella I, Turner AP, Piletsky SA. Design of molecular imprinted polymers compatible with aqueous environment. *Anal Chim Acta*. 2008;607(1):54-60.
85. Steinke J, Sherrington D, Dunkin I. Imprinting of synthetic polymers using molecular templates. In: *Synthesis and photosynthesis*. Springer; 1995:81-125.

86. Karim K, Breton F, Rouillon R, et al. How to find effective functional monomers for effective molecularly imprinted polymers? *Adv Drug Deliv Rev.* 2005;57(12):1795-1808.
87. Andersson HS, Karlsson JG, Piletsky SA, Koch-Schmidt A, Mosbach K, Nicholls IA. Study of the nature of recognition in molecularly imprinted polymers, II: Influence of monomer-template ratio and sample load on retention and selectivity. *Journal of Chromatography A.* 1999;848(1):39-49.
88. Yu C, Mosbach K. Influence of mobile phase composition and cross-linking density on the enantiomeric recognition properties of molecularly imprinted polymers. *Journal of Chromatography A.* 2000;888(1):63-72.
89. Mayes A, Whitcombe M. Synthetic strategies for the generation of molecularly imprinted organic polymers. *Adv Drug Deliv Rev.* 2005;57(12):1742-1778.
90. Mijangos I, Navarro-Villoslada F, Guerreiro A, et al. Influence of initiator and different polymerisation conditions on performance of molecularly imprinted polymers. *Biosensors and Bioelectronics.* 2006;22(3):381-387.
91. Turner NW, Piletska EV, Karim K, et al. Effect of the solvent on recognition properties of molecularly imprinted polymer specific for ochratoxin A. *Biosensors and Bioelectronics.* 2004;20(6):1060-1067.
92. Gladis JM, Rao TP. Effect of porogen type on the synthesis of uranium ion imprinted polymer materials for the preconcentration/separation of traces of uranium. *Microchimica Acta.* 2004;146(3):251-258.
93. Cormack PA, Elorza AZ. Molecularly imprinted polymers: Synthesis and characterisation. *Journal of Chromatography B.* 2004;804(1):173-182.
94. Yilmaz E, Mosbach K, Haupt K. Influence of functional and cross-linking monomers and the amount of template on the performance of molecularly imprinted polymers in binding assays. *Analytical Communications.* 1999;36(5):167-170.
95. Wong RSH, Ashton M, Dodou K. Effect of crosslinking agent concentration on the properties of unmedicated hydrogels. *Pharmaceutics.* 2015;7(3):305-319.
96. Mayes AG, Mosbach K. Molecularly imprinted polymer beads: Suspension polymerization using a liquid perfluorocarbon as the dispersing phase. *Anal Chem.* 1996;68(21):3769-3774.
97. Mane S, Ponrathnam S, Chavan N. Effect of chemical cross-linking on properties of polymer microbeads: A review. *Can.Chem.Trans.* 2015;3(4):473-485.
98. Gruber H. Photoinitiators for free radical polymerization. *Progress in polymer Science.* 1992;17(6):953-1044.
99. Moad G, Solomon DH. *The chemistry of radical polymerization.* Elsevier; 2006.
100. Piletsky SA, Mijangos I, Guerreiro A, et al. Polymer cookery: Influence of polymerization time and different initiation conditions on performance of molecularly imprinted polymers. *Macromolecules.* 2005;38(4):1410-1414.

101. Turner NW, Piletska EV, Karim K, et al. Effect of the solvent on recognition properties of molecularly imprinted polymer specific for ochratoxin A. *Biosens Bioelectron.* 2004;20(6):1060-1067.
102. Baggiani C, Giraudi G, Vanni A. A molecular imprinted polymer with recognition properties towards the carcinogenic mycotoxin ochratoxin A. *Bioseparation.* 2001;10(6):389-394.
103. Sellergren B, Hall AJ. *Molecularly imprinted polymers.* Wiley Online Library; 2012.
104. Beyazit S, Bui BTS, Haupt K, Gonzato C. Molecularly imprinted polymer nanomaterials and nanocomposites by controlled/living radical polymerization. *Progress in Polymer Science.* 2016;62:1-21.
105. Challa G. *Polymer chemistry: An introduction.* Prentice Hall; 1993.
106. Poma A, Guerreiro A, Whitcombe MJ, Piletska EV, Turner AP, Piletsky SA. Solid- Phase synthesis of molecularly imprinted polymer nanoparticles with a reusable Template-“Plastic antibodies”. *Advanced functional materials.* 2013;23(22):2821-2827.
107. Smolinska-Kempisty K, Guerreiro A, Canfarotta F, Cáceres C, Whitcombe MJ, Piletsky S. A comparison of the performance of molecularly imprinted polymer nanoparticles for small molecule targets and antibodies in the ELISA format. *Sci Rep.* 2016;6.
108. Chianella I, Karim K, Piletska EV, Preston C, Piletsky SA. Computational design and synthesis of molecularly imprinted polymers with high binding capacity for pharmaceutical applications-model case: Adsorbent for abacavir. *Anal Chim Acta.* 2006;559(1):73-78.
109. Yañez F, Chianella I, Piletsky SA, Concheiro A, Alvarez-Lorenzo C. Computational modeling and molecular imprinting for the development of acrylic polymers with high affinity for bile salts. *Anal Chim Acta.* 2010;659(1-2):178-185.
110. Piletska EV, Guerreiro AR, Romero-Guerra M, Chianella I, Turner APF, Piletsky SA. Design of molecular imprinted polymers compatible with aqueous environment. *Anal Chim Acta.* 2008;607(1):54-60.
111. Cáceres C, Canfarotta F, Chianella I, et al. Does size matter? study of performance of pseudo-ELISAs based on molecularly imprinted polymer nanoparticles prepared for analytes of different sizes. *Analyst.* 2016;141(4):1405-1412.
112. Subrahmanyam S, Karim K, Piletsky SA. Computational approaches in the design of synthetic receptors. In: *Designing receptors for the next generation of biosensors.* Springer; 2012:131-165.
113. Cowen T, Karim K, Piletsky S. Computational approaches in the design of synthetic receptors—A review. *Anal Chim Acta.* 2016;936:62-74.
114. Leach AR. *Molecular modelling: Principles and applications.* Pearson education; 2001.
115. Chianella I, Lotierzo M, Piletsky SA, et al. Rational design of a polymer specific for microcystin-LR using a computational approach. *Anal Chem.* 2002;74(6):1288-1293.
116. Canfarotta F, Poma A, Guerreiro A, Piletsky S. Solid-phase synthesis of molecularly imprinted nanoparticles. *Nature protocols.* 2016;11(3):443-455.

117. Lakshmi D, Akbulut M, Ivanova-Mitseva PK, et al. Computational design and preparation of MIPs for atrazine recognition on a conjugated polymer-coated microtiter plate. *Ind Eng Chem Res.* 2013;52(39):13910-13916.
118. Alvira E. Molecular dynamics study of the influence of solvents on the chiral discrimination of alanine enantiomers by β -cyclodextrin. *Tetrahedron: Asymmetry.* 2013;24(19):1198-1206.
119. Alvira E. Theoretical study of the separation of valine enantiomers by β -cyclodextrin with different solvents: A molecular mechanics and dynamics simulation. *Tetrahedron: Asymmetry.* 2015;26(15-16):853-860.
120. ChemAxon's. 116355-83-0. <https://chemicalize.com/#/calculation>. Updated 2016. Accessed November/1, 2016.
121. De Smet D, Dubrue P, Van Peteghem C, Schacht E, De Saeger S. Molecularly imprinted solid-phase extraction of fumonisin B analogues in bell pepper, rice and corn flakes. *Food Addit Contam.* 2009;26(6):874-884.
122. Bakas I, Oujji NB, Moczko E, et al. Computational and experimental investigation of molecular imprinted polymers for selective extraction of dimethoate and its metabolite omethoate from olive oil. *Journal of Chromatography A.* 2013;1274:13-18.
123. Jackson LS, Hlywka JJ, Senthil KR, Bullerman LB, Musser SM. Effects of time, temperature, and pH on the stability of fumonisin B1 in an aqueous model system. *J Agric Food Chem.* 1996;44(3):906-912.
124. Koroleva LF, Larionov L, Gorbunova N. Biomaterial based on doped calcium carbonate-phosphate for active osteogenesis. *Journal of Biomaterials and Nanobiotechnology.* 2012;3(2):226-237.
125. Wang X, Gao Y, Wang W, Qin A, Sun JZ, Tang BZ. Different amine-functionalized poly(diphenylsubstituted acetylenes) from the same precursor. *Polymer Chemistry.* 2016;7(33):5312-5321.
126. Chianella I, Guerreiro A, Moczko E, et al. Direct replacement of antibodies with molecularly imprinted polymer nanoparticles in ELISA - development of a novel assay for vancomycin. *Anal Chem.* 2013;85(17):8462-8468.
127. O'Shannessy DJ, Andersson LI, Mosbach K. Molecular recognition in synthetic polymers. enantiomeric resolution of amide derivatives of amino acids on molecularly imprinted polymers. *J Mol Recogn.* 1989;2(1):1-5.
128. O'Shannessy DJ, Ekberg B, Andersson LI, Mosbach K. Recent advances in the preparation and use of molecularly imprinted polymers for enantiomeric resolution of amino acid derivatives. *J Chromatogr A.* 1989;470(2):391-399.
129. Piletsky SA, Piletskaya EV, El'skaya AV, Levi R, Yano K, Karube I. Optical detection system for triazine based on molecularly-imprinted polymers. *Anal Lett.* 1997;30(3):445-455.
130. Kriz D, Mosbach K. Competitive amperometric morphine sensor based on an agarose immobilised molecularly imprinted polymer. *Anal Chim Acta.* 1995;300(1-3):71-75.

131. Vlatakis G, Andersson LI, Müller R, Mosbach K. Drug assay using antibody mimics made by molecular imprinting. *Nature*. 1993;361(6413):645.
132. Bedwell TS, Whitcombe MJ. Analytical applications of MIPs in diagnostic assays: Future perspectives. *Analytical and bioanalytical chemistry*. 2016;408(7):1735-1751.
133. Poma A, Turner AP, Piletsky SA. Advances in the manufacture of MIP nanoparticles. *Trends Biotechnol*. 2010;28(12):629-637.
134. Alghamdi EM, Whitcombe MJ, Piletsky SA, Piletska EV. Solid phase extraction of a-tocopherol and other physiologically active components from sunflower oil using rationally designed polymers. *Anal Methods*. 2018;10(3):314-321.
135. Garcia Y, Smolinska-Kempisty K, Pereira E, Piletska E, Piletsky S. Development of competitive 'pseudo'-ELISA assay for measurement of cocaine and its metabolites using molecularly imprinted polymer nanoparticles. *Anal Methods*. 2017;9(31):4592-4598.
136. Moczko E, Mirkes EM, Cáceres C, Gorban AN, Piletsky S. Fluorescence-based assay as a new screening tool for toxic chemicals. *Sci Rep*. 2016;6.
137. Smolinska-Kempisty K, Ahmad OS, Guerreiro A, Karim K, Piletska E, Piletsky S. New potentiometric sensor based on molecularly imprinted nanoparticles for cocaine detection. *Biosens Bioelectron*. 2017;96:49-54.
138. Moczko E, Guerreiro A, Piletska E, Piletsky S. PEG-stabilized core-shell surface-imprinted nanoparticles. *Langmuir*. 2013;29(31):9891-9896.
139. Wang XC, Bao M, Li FH, et al. Development of a sensitive, competitive, indirect ELISA for the detection of fumonisin B1 in corn originating from anhui province, china. *Journal of Environmental Science and Health, Part B*. 2016;51(2):107-112.
140. Ono EY, Kawamura O, Ono MA, Ueno Y, Hirooka EY. A comparative study of indirect competitive ELISA and HPLC for fumonisin detection in corn of the state of paraná, brazil. *Food Agric Immunol*. 2000;12(1):5-14.
141. Azevedo AM, Martins VC, Prazeres DM, Vojinović V, Cabral JM, Fonseca LP. Horseradish peroxidase: A valuable tool in biotechnology. *Biotechnol Annu Rev*. 2003;9:199-247.
142. Garcia D, Gomez-Caballero A, Guerreiro A, Goicolea MA, Barrio RJ. Molecularly imprinted polymers as a tool for the study of the 4-ethylphenol metabolic pathway in red wines. *J Chromatogr A*. 2015;1410:164-172.
143. Tang S-, Canfarotta F, Smolinska-Kempisty K, Piletska E, Guerreiro A, Piletsky S. A pseudo-ELISA based on molecularly imprinted nanoparticles for detection of gentamicin in real samples. *Anal Methods*. 2017;9(19):2853-2858.
144. Bird CB, Malone B, Rice LG, Ross PF, Eppley R, Abouzied MM. Determination of total fumonisins in corn by competitive direct enzyme-linked immunosorbent assay: Collaborative study. *J AOAC Int*. 2002;85(2):404-410.
145. Visconti A, Solfrizzo M, Girolamo AD. Determination of fumonisins B1 and B2 in corn and corn flakes by liquid chromatography with immunoaffinity column cleanup: Collaborative study. *J AOAC Int*. 2001;84(6):1828-1837.

146. De Girolamo A, Fauw DP, Sizoo E, et al. Determination of fumonisins B1 and B2 in maize-based baby food products by HPLC with fluorimetric detection after immunoaffinity column clean-up. *World Mycotoxin Journal*. 2010;3(2):135-146.
147. Ling S, Pang J, Yu J, et al. Preparation and identification of monoclonal antibody against fumonisin B1 and development of detection by ic-ELISA. *Toxicon*. 2014;80:64-72.
148. Azcona-Olivera JI, Abouzied MM, Plattner RD, Pestka JJ. Production of monoclonal antibodies to the mycotoxins fumonisins B1, B2, and B3. *J Agric Food Chem*. 1992;40(3):531-534.
149. Maragosl CM, Miklasz SD. Monoclonal antibody-based competitive enzyme-linked immunosorbent assays for the hydrolysis product of fumonisin B. . 1996.
150. Christensen HR, Yu F, Chu FS. Development of a polyclonal antibody-based sensitive enzyme-linked immunosorbent assay for fumonisin B4. *J Agric Food Chem*. 2000;48(5):1977-1984.
151. Savard M, Sinha R, Lau R, Seguin C, Buffam S. Monoclonal antibodies for fumonisins B1, B2 and B3. *Food Agric Immunol*. 2003;15(2):127-134.
152. Usleber E, Straka M, Terplan G. Enzyme immunoassay for fumonisin B1 applied to corn-based food. *J Agric Food Chem*. 1994;42(6):1392-1396.
153. Schneider E, Usleber E, Maertlbauer E. Rapid detection of fumonisin B1 in corn-based food by competitive direct dipstick enzyme immunoassay/enzyme-linked immunofiltration assay with integrated negative control reaction. *J Agric Food Chem*. 1995;43(9):2548-2552.
154. Elissalde MH, Kamps- Holtzapple C, Beier RC, Plattner RD, Rowe LD, Stanker LH. Development of an improved monoclonal antibody- based elisa for fumonisin b1-3 and the use of molecular modeling to explain observed detection limits. *Food Agric Immunol*. 1995;7(2):109-122.
155. Smolinska-Kempisty K, Guerreiro A, Canfarotta F, Cáceres C, Whitcombe MJ, Piletsky S. A comparison of the performance of molecularly imprinted polymer nanoparticles for small molecule targets and antibodies in the ELISA format. *Sci Rep*. 2016;6.
156. Sutikno, Abouzied MM, Azcona-olivera J, Hart LP, Pestka JJ. Detection of fumonisins in fusarium cultures, corn, and corn products by polyclonal antibody-based ELISA: Relation to fumonisin B1 detection by liquid chromatography. *J Food Prot*. 1996;59(6):645-651.
157. Yeung JM, Prelusky DB, Savard ME, Dang BDM, Robinson LA. Sensitive immunoassay for fumonisin B1 in corn. *J Agric Food Chem*. 1996;44(11):3582-3586.
158. Li C, Mi T, Oliveri Conti G, et al. Development of a screening fluorescence polarization immunoassay for the simultaneous detection of fumonisins B1 and B2 in maize. *J Agric Food Chem*. 2015;63(20):4940-4946.
159. Shu M, Xu Y, Wang D, et al. Anti-idiotypic nanobody: A strategy for development of sensitive and green immunoassay for fumonisin B1. *Talanta*. 2015;143:388-393.

160. Tang X, Li P, Zhang Z, Zhang Q, Guo J, Zhang W. An ultrasensitive gray-imaging-based quantitative immunochromatographic detection method for fumonisin B1 in agricultural products. *Food Control*. 2017;80:333-340.
161. Urusov AE, Petrakova AV, Gubaydullina MK, et al. High-sensitivity immunochromatographic assay for fumonisin B1 based on indirect antibody labeling. *Biotechnol Lett*. 2017;39(5):751-758.
162. Yao J, Sun Y, Li Q, et al. Colloidal gold- McAb probe- based rapid immunoassay strip for simultaneous detection of fumonisins in maize. *J Sci Food Agric*. 2017;97(7):2223-2229.
163. Heurich M, Kadir MKA, Tothill IE. An electrochemical sensor based on carboxymethylated dextran modified gold surface for ochratoxin A analysis. *Sensors and Actuators B: Chemical*. 2011;156(1):162-168. doi: <https://doi.org/10.1016/j.snb.2011.04.007>.
164. Castillo G, Poturnayová A, Šnejdárková M, Hianik T, Spinella K, Mosiello L. Development of electrochemical aptasensor using dendrimers as an immobilization platform for detection of aflatoxin B1 in food samples. . 2015:1-4.
165. Pemberton R, Pittson R, Biddle N, Drago G, Hart JP. Studies towards the development of a Screen- Printed carbon electrochemical immunosensor array for mycotoxins: A sensor for aflatoxin B1. *Anal Lett*. 2006;39(8):1573-1586.
166. Atar N, Yola ML, Eren T. Sensitive determination of citrinin based on molecular imprinted electrochemical sensor. *Applied Surface Science*. 2016;362:315-322. doi: <https://doi.org/10.1016/j.apsusc.2015.11.222>.
167. Rotariu L, Lagarde F, Jaffrezic-Renault N, Bala C. Electrochemical biosensors for fast detection of food contaminants – trends and perspective. *TrAC Trends in Analytical Chemistry*. 2016;79:80-87. doi: <https://doi.org/10.1016/j.trac.2015.12.017>.
168. Grieshaber D, MacKenzie R, Voeroes J, Reimhult E. Electrochemical biosensors-sensor principles and architectures. *Sensors*. 2008;8(3):1400-1458.
169. Yu L, Zhang Y, Hu C, et al. Highly sensitive electrochemical impedance spectroscopy immunosensor for the detection of AFB1 in olive oil. *Food Chemistry*. 2015;176:22-26. doi: <https://doi.org/10.1016/j.foodchem.2014.12.030>.
170. Walter MG, Wamser CC. Synthesis and characterization of electropolymerized nanostructured aminophenylporphyrin films. *The Journal of Physical Chemistry C*. 2010;114(17):7563-7574.
171. Mazzotta E, Malitesta C. Electrochemical detection of the toxic organohalide 2, 4-DB using a co-porphyrin based electrosynthesized molecularly imprinted polymer. *Sensors Actuators B: Chem*. 2010;148(1):186-194.
172. Dubal DP, Lee SH, Kim JG, Kim WB, Lokhande CD. Porous polypyrrole clusters prepared by electropolymerization for a high performance supercapacitor. *Journal of Materials Chemistry*. 2012;22(7):3044-3052.
173. Ferreira C, Aeiayach S, Delamar M, Lacaze P. Electropolymerization of pyrrole on iron electrodes: Influence of solvent and electrolyte on the nature of the deposits. *Journal of Electroanalytical Chemistry and Interfacial Electrochemistry*. 1990;284(2):351-369.

174. Lee JY, Lee JW, Schmidt CE. Neuroactive conducting scaffolds: Nerve growth factor conjugation on active ester-functionalized polypyrrole. *J R Soc Interface*. 2009;6(38):801-810.
175. Ghafari H, Mohammadi F, Rahimi R, Mohammadiyan E. Synthesis and characterization of a new magnetic nanocomposite with metalloporphyrin (co-TPyP) and sulfated tin dioxide ($\text{Fe}_3\text{O}_4/\text{SnO}_2/\text{SO}_4^{2-}$), and investigation of its photocatalytic effects in the degradation of rhodamine B. *RSC Advances*. 2016;6(87):83947-83953.
176. Guo X, Guo B, Shi T. The photochemical and electrochemical properties of chiral porphyrin dimer and self-aggregate nanorods of cobalt (II) porphyrin dimer. *Inorg Chim Acta*. 2010;363(2):317-323.
177. Smolko V, Shurpik D, Porfireva A, Evtugyn G, Stoikov I, Hianik T. Electrochemical aptasensor based on poly(neutral red) and carboxylated pillar[5]arene for sensitive determination of aflatoxin M1. *Electroanalysis*. 2018.
178. Xu Z, Zhou B, Jiang F, Dai J, Liu Y. Interaction between a cationic porphyrin and ctDNA investigated by SPR, CV and UV-vis spectroscopy. *Colloids and Surfaces B: Biointerfaces*. 2013;110:321-326. doi: <https://doi.org/10.1016/j.colsurfb.2013.04.040>.
179. Bruti EM, Giannetto M, Mori G, Seeber R. Electropolymerization of tetrakis (o-aminophenyl) porphyrin and relevant transition metal complexes from aqueous solution. the resulting modified electrodes as potentiometric sensors. *Electroanalysis*. 1999;11(8):565-572.
180. Ionov L. Polymeric actuators. *Langmuir*. 2014;31(18):5015-5024.
181. Le TH, Pham VP, La TH, Phan TB, Le QH. Electrochemical aptasensor for detecting tetracycline in milk. *Advances in Natural Sciences: Nanoscience and Nanotechnology*. 2016;7(1):015008.

APPENDIX 1: PUBLICATION IN SUPPORT OF THIS THESIS

Articles:

1. Hasim Munawar, Katarzyna Smolinska-Kempisty, Alvaro Garcia Cruz, Francesco Canfarotta, Elena Piletska, Kal Karim, and Sergey A. Piletsky. Molecularly imprinted polymer nanoparticles-based assay (MINA): application for Fumonisin B1 determination. Accepted in *Analyst* on 20 May 2018.
2. Hasim Munawar, Alvaro Garcia-Cruz, M. Majewska, P. Pieta, Kal Karim, W. Kutner, Sergey A. Piletsky. Electrochemical determination of Fumonisin B1 based on molecularly imprinted polymer nanoparticles: a flexible platform for sensors. In preparation (*Bioelectronic and Biosensor*, Elsevier)
3. Hasim Munawar, Abeer. H. M. Safaryan, Annalisa De Girolamo, Alvaro Garcia-Cruz, Pedro Marote, Kal Karim, Michelangelo Pascale, Sergey A. Piletsky. Determination of Fumonisin B1 mycotoxin on contaminated corns using a pioneering ELISA based on molecularly imprinted polymer nanoparticles. In preparation (*Analytical and Bioanalytical Chemistry*, Springer)

Conferences:

1. Poster presentation at Sensor in Food and Agriculture (SIFA), Cambridge, United Kingdom, 2016.
2. Poster presentation at International Symposium on Recent Advances in Food Analysis (RAFA), Prague, Czech Republic, 2017. Achievement : Poster Award sponsored by media partner Analytical and Bioanalytical Chemistry, Springer
3. Oral presentation at The International Conference on Agriculture and Natural Resources (ANRES), Bangkok, Thailand, April 26-28, 2018.

APPENDIX 2 CALIBRATION CURVE FOR NANOMIPS

nanoMIPs preparation

The nanoMIPs solution obtained were evaporated and weighed. Amount of nanoMIPs powder was diluted in 1 mL water and measured by UV spectrophotometry at 197 nm. This solution was then diluted two times for six nanoMIPs solution. Finally, all solutions were measured by UV spectrophotometry at 197 nm and plotted a calibration curve between concentration of nanoMIPs and absorbance.

Results

Tabel 1. The absorbance at 197 nm of the series concentration of nanoMIPs

Concentration (mg mL ⁻¹)	Absorbance
0.330	1.2406
0.167	0.6517
0.083	0.3216
0.042	0.1718
0.021	0.0764
0.011	0.0269

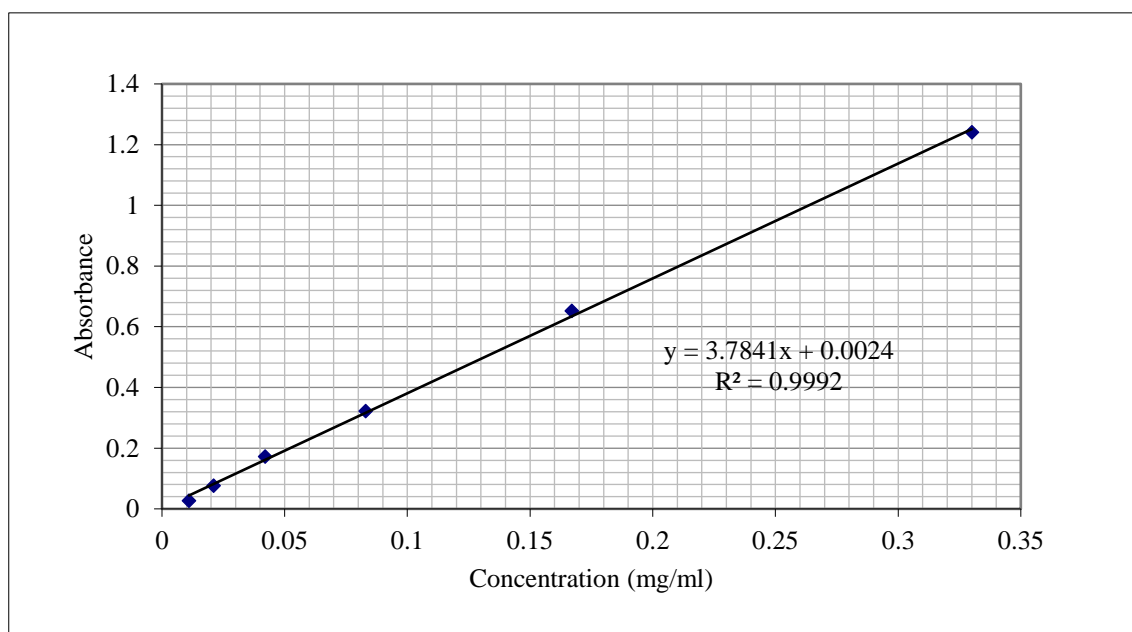


Figure 1. Calibration curve of nanoMIPs solution for FB1